UNDERSTANDING AND PREDICTION OF LIQUIDS RETENTION ON COMMONLY USED PLASTICS WITH SYMMETRICALLY ARRANGED STRUCTURE

A Dissertation

by

CHUNG-HAN CHIOU

Submitted to the Office of Graduate and Professional Studies of
Texas A&M University
in partial fulfillment of the requirements for the degree of

DOCTOR OF PHILOSOPHY

Chair of Committee,	Sheng-Jen Hsieh
Committee Members,	Hong Liang
	Xinghang Zhang
	Jun Zou
Head of Department,	Andreas A. Polycarpou

May 2016

Major Subject: Mechanical Engineering

ABSTRACT

Wetting behaviors commonly happen in the daily life and it is essential and beneficial to control solids' wettability in the industrial process. Polymers in forms of plastics have the most extensive applications in all kinds of products. This research aims to empirically study wettability of commonly used plastics with symmetrically arranged surface structure, and then proposes a methodology for solids' wettability predictions.

The research starts from studying various liquids' contact angles on plastic surfaces. It was found that surface structures within certain dimensions, in terms of liquid-solid contact length parameters, have linear relationship with liquids' contact angles. Results were found explanations by further studied the change of plastics' surface free energy due to their surface structures. Such results were used to develop empirical models for liquids' contact angles and solids' surface free energy estimations, and models were verified by liquid-solid interfacial tensions.

The extending research was investigated based on aforementioned results. Liquids' contact angle hysteresis and retentions on inclined surfaces were studied. Liquids' advancing and receding contact angles were found to maintain the same ratio on structured plastic surfaces with various dimensions and inclined angles. The new finding confirms and further extends the statement proposed in the literature. Based on liquid-solid interfacial tension and gravity effect, an empirical formula was proposed to estimate liquids' critical retention volumes on inclined plastic surfaces. Integrating the

formula with predicted advancing contact angles, the prediction of liquids' critical retention volumes on structured plastic surfaces becomes possible.

DEDICATION

This dissertation is dedicated to my family who always support and love me.

ACKNOWLEDGEMENTS

I would like to firstly thank my committee chair, Dr. Sheng-Jen Hsieh, and committee members, Dr. Hong Liang, Dr. Xinghang Zhang, and Dr. Jun Zou for their insightful advice and strong support throughout my research. Particularly, I would like to express my appreciation to Dr. Hsieh, who financially supported me and provided me an excellent TA opportunity to furnish my teaching skills while I was pursuing my PhD.

My PhD study life cannot be complete without my family. Tsai-Chien, my dear wife, is the most important person who sacrificed her musician career and wholeheartedly accompanied with me for being my spiritual pillar. Also, I would like to thank her for bringing our lovely daughter, Anna, to this world. Of course, I won't forget to mention our beloved dog, Donut. He is like our son and makes our life joyful. Besides, I sincerely appreciate my parents who raised me up and made me well educated. I also thank my parents-in-law who keep supporting us. This dissertation is dedicated to all my family.

It is never easy to study aboard without any friendship. Fortunately, I have some great friends who always bring happiness to my life. I appreciate you all making my PhD study life colorful. Particularly, I would like to thank Dr. Peter Yu and his wife, Vivian, for their truly generous help at every tough moment while we were staying in College Station.

NOMENCLATURE

CA	Contact Angle
θ	Contact Angle
CAH	Contact Angle Hysteresis
θ_A	Advancing Contact Angle
θ_R	Receding Contact Angle
V_c	Critical Retention Volume
σ	Contact Length Ratio
α	Surface Inclined Angle
SFE	Surface Free Energy
SEM	Scanning Electron Microscope
OM	Optical Microscope
R_a	Arithmetic Average Surface Roughness
H	Reduced Hysteresis
r	Correlation Coefficient

PET	Polyethylene Terephthalate
HDPE	High-Density Polyethylene
PVC	Polyvinyl Chloride
LDPE	Low-Density Polyethylene
PP	Polypropylene
ABS	Acrylonitrile Butadiene Styrene
PC	Polycarbonate
AAO	Anodic Aluminum Oxide
DI	De-ionized
EG	Ethylene Glycol
α-BN	α-Bromonaphthalene
MI	Methylene Iodide
MSE	Mean Squared Error
SEoM	Standard Error of the Mean

TABLE OF CONTENTS

Page

ABSTRACT ii

DEDICATION iv

ACKNOWLEDGEMENTS v

NOMENCLATURE vi

TABLE OF CONTENTS viii

LIST OF FIGURES xi

LIST OF TABLES xv

1 INTRODUCTION 1

1.1 Motivation 1
1.2 Research Question 2
1.3 Research Assumption 5
1.4 Research Objective 6
1.5 Material and Methods 7
1.6 Organization of the Dissertation 16

2 LITERATURE REVIEW 17

2.1 Contact Angle and Surface Free Energy 17
2.2 Contact Angle Hysteresis 19
2.3 Liquids Retention 22
2.4 Summary of Closely Related Works 25

3 SURFACE FREE ENERGY THEORY 35

3.1 The Work of Adhesion 36
3.2 One Component Theory 39
3.2.1 Zisman Plot 39
3.2.2 Equation of State 41

3.3 Two Component Theories 42
3.3.1 Owens/Wendt and Fowkes Theory 42
3.3.2 Wu Theory 44
3.4 Three Component Theory 44
3.5 Discussion 48

4 EMPIRICAL STUDY AND PREDICTION OF CONTACT ANGLE AND SURFACE FREE ENERGY OF COMMONLY USED PLASTICS WITH PILLAR-LIKE STRUCTURE 54

4.1 Material and Methods 55
4.1.1 Design of Experiments 55
4.1.2 Testing Liquid Selection 57
4.1.3 Fabrication of Solid Surfaces with Pillar-Like Structure 57
4.2 Result and Discussion 60
4.2.1 Contact Angle Analysis 60
4.2.2 Surface Free Energy Analysis 63
4.3 Summary and Conclusion 69

5 EMPIRICAL STUDY AND PREDICTION OF LIQUIDS RETENTION ON STRUCTURED POLYMER SURFACES 81

5.1 Material and Methods 82
5.1.1 Design of Experiments 82
5.1.2 Materials and Surface Fabrication 87
5.2 Model Formulation 92
5.2.1 Critical Retention Model 92
5.2.2 Liquid-Plastic Contact Line Length 98
5.3 Result and Discussion 109
5.3.1 Contact Angle Hysteresis 109
5.3.2 Critical Retention Volume 110
5.3.3 Model Evaluation 118
5.3.4 Prediction 121
5.4 Summary and Conclusion 125

6 TEST OF PROPOSED MODEL ON EXTENSIVE SOLIDS 149

6.1 Applicability of Proposed Model for Solids with Nanostructures 149
6.2 Test of Proposed Model on Various Solids 154

7 CONCLUSIONS AND FUTURE DIRECTIONS 157

7.1 Conclusion 157
7.2 Future Work 159

REFERENCES 162

LIST OF FIGURES

Page

Figure 1. Research process chart. 7

Figure 2. Digital microscope Keyence VHX-2000 VH-Z500. 9

Figure 3. Derivation of the center line. Within the evaluation length, the center line is the line which cuts the shape into upper and lower parts, where the total area of upper parts equals to the total area of lower parts. (i.e. Area of A+D+F = Area of B+C+E) 11

Figure 4. Derivation of R_a within a sampling length 12

Figure 5. A self-built goniometer system. The sample platform can move in 3 axis (upper figure) and tilt up to 90° (lower figure). 14

Figure 6. Illustration of advancing and receding contact angles due to expanding and contracting the liquid. [22] 20

Figure 7. Illustration of contact angle hysteresis happens on an inclined surface. 21

Figure 8. Young's energy balance model. 35

Figure 9. Process of (a) adhesion and (b) cohesion. 38

Figure 10. The Zisman plot for LDPE's surface energy. Ten liquids were used and the critical surface energy was approached to 22.8mJ/m^2. High correlation coefficient proves the accuracy. [69] 40

Figure 11. The Zisman plot for poly(methyl methacrylate) surface energy. The critical surface energy was approached as 22.8mJ/m^2. However, its correlation coefficient is not as high as LDPE has. [69] 52

Figure 12. The Zisman plot (solid line) of a solid which surface free energy is 35 mN/m. Theoretical values (dash line) were obtained from Equation (34). 53

Figure 13. Image of plastic sample with symmetrically arranged structure. (a) Scanning electron micrograph of HDPE surface in top view. The 2-D groove structure in top view was made by pressing a metal mesh fully embed into the plastic surface, which results in the pillar-like structure in (b) side view. 59

Figure 14. A liquid droplet sits on (a) a non-structured surface. (b) A structured surface which cause a change in its contact length and (c) circumference.....59

Figure 15. Liquids' contact angles on (a) PET (b) PP (c) HDPE (d) LDPE (e) PVC. White and black symbols stand for actual and predicted values respectively. 62

Figure 16. Apolar, polar, and total surface free energy of (a) PET (b) PP (c) HDPE (d) LDPE (e) PVC. White and black symbols stand for experiment and predicted values respectively. 67

Figure 17. Lewis acid and base components of (a) PET(b) PP (c) HDPE (d) LDPE (e) PVC. White and black symbols stand for experiment and predicted values respectively. 68

Figure 18. The symmetric square frustum-like structure was found on PETE surfaces (a) top view (b) side view (c) 3-D model. 88

Figure 19. DI water's droplet was found staying in the Wenzel state on ABS surface with frustum-like structure in hundred-micrometer scale. 89

Figure 20. Dimensions of the frustum-like structure. The contact length ratio σ is in terms of W, L, and G. 90

Figure 21 (a) The free body diagram of a rigid body, where N is the normal force and μ is the coefficient of friction. (b) The force balance diagram of a droplet sitting on the inclined surface. Gravity effect makes its profile asymmetric in the x-z plane. 93

Figure 22. A spherical-cap-shaped droplet.....95

Figure 23. A DI water droplet attaches on a structured and vertical ABS surface. The contour displays front-to back asymmetry when the droplet is (a) just dispensed (b) reaching the critical retention volume (c) sliding down. 99

Figure 24. A droplet's asymmetric profile in the front view, composed by blue and red arcs, can be approximated by two circles. [40] The advancing contact angle exists in between the intersection of smaller arc (in blue) and the horizontal line, while the receding contact angle exists in between the intersection of larger arc (in red) and the horizontal line. 102

Figure 25. (a) A droplet's contour can be approximated by rotating its profile from the x-z plane to the x-y plane. (b) In the x-y plane, the contour displays the front-to back asymmetry. 102

Figure 26. Continuing from Figure 25, a droplet's volume can be approximated by the solid of revolution, where the plane curve is its profile and the center line is the truncate line. The larger arc is formulated as Equation (45) and the center line is formulated as Equation (44). Hatched portion stands for the result of the solid of revolution. 103

Figure 27. For the purpose of simple calculation, the droplet's profile is mirrored by the y-axis. Similar with Figure 26, hatched portion stands for the result of the solid of revolution, in which the plane curve is the smaller arc. 103

Figure 28. A droplet's volume can be obtained by summation of two hatched portions V1 and V2 shown in Figure 26 and Figure 27. 104

Figure 29. The original two-circle method proposed by ElSherbini and Jacobi. [40] ... 107

Figure 30. (a) The front view and (b) top view of a droplet which is coordinated and modeled for two-circle method. [40] 108

Figure 31. Critical retention volume (a) DI Water on HDPE (b) EG on ABS versus surface at 45° ,60° ,75°, and 90° inclined angles. 112

Figure 32. Liquids' critical retention volume on (a) PETE at 90° inclined angle (b) ABS at 60° inclined angle. White and black symbols stand for experimental values and estimation values from Equation (13) respectively. 113

Figure 33. Liquids' critical retention volumes decay as advancing contact angle increased. (a) PP at 45° and 90° inclined angles, (b) PETE at 45° and 75° inclined angles. White and black symbols stand for DI water and EG respectively. 116

Figure 34. DI water's (a) critical retention volumes and (b) advancing contact angles on structured HDPE (solid line) and PP (dash line) surfaces. 117

Figure 35. Liquids' advancing contact angles on structured ABS (triangle), LDPE (square), and PP (circle) surfaces at 90° inclined angle. White and black symbols stand for DI water and EG respectively. 123

Figure 36. Predicted (lines) and experiment (scatter dots) critical retention volume on structured ABS (dot line, triangle), LDPE (dash line, square), and HDPE (solid line, circle) surfaces at 90° inclined angle. White and black symbols stand for DI water and EG respectively. 124

Figure 37. SEM images of (a) AAO barrier layer and (b) bottom view, which shows AAO barrier layer is composed of hexagonally packed structures. [91] 152

Figure 38. DI water's contact angle on polished aluminum surface and AAO barrier layer. Nanostructures decrease the contact angle, however, roughness effect could alter the changing trend.....154

LIST OF TABLES

Page

Table 1. Surface free energy, polarity, and density of selected probed liquids. (Note, at 20ºC).....15

Table 2. Roughness parameters of all plastic samples. (Unit in nm) Sampling length 500μm 15

Table 3. Summary of closely related studies and comparisons with the author's present study.....32

Table 4. Variable lists of contact angle experiments.....56

Table 5. Surface free energy of testing liquids.....70

Table 6. Specifications of plastics' surface structures. The surface of Sample I is non-structured. 70

Table 7. Liquids' contact angles (CA) on structured plastics. *Predicted Value.....71

Table 8. Correlation coefficient (r) of liquids' contact angles and contact length ratio σ.....72

Table 9. Plastics' surface free energy. *Predicted Value. 72

Table 10. Correlation coefficient (r) of plastics' $\gamma_S^{TOT}, \gamma_S^{LW}, \gamma_S^{AB}, \gamma_S^+, \gamma_S^-$ and contact length ratio σ. 74

Table 11. Plastics' surface free energy. *Obtained from van Oss-Chaudhury-Good equation by applying predicted contact angles. 75

Table 12. Plastic-liquid interaction. *Calculated from predicted plastics' surface free energy. 78

Table 13. Variable lists of contact angle hysteresis experiments.....85

Table 14. Variable lists of liquids' critical retention volume experiments. 86

Table 15. Specifications of square frustum-like structures on polymers' surfaces and their corresponding contact length ratio σ, where G, L, and W are illustrated in Figure 20. 126

Table 16. Surface free energy of testing liquids and their polarity. 126

Table 17. DI water's (ρ=1000 kg/m^3) critical retention volumes (µL) on ABS (H=0.6) surface at 90° surface inclined angle. Units of θ_A and γ_{LS} are ° and mN/m, respectively. 127

Table 18. Liquids' critical retention volumes, advancing and receding contact angles on polymers with various conditions. 128

Table 19. Reduce hysteresis H and θ_R / θ_A of various liquid-polymer combinations. ...133

Table 20. Liquids' critical retention volumes on polymers with various conditions. Comparisons of experiment data with the present and previous models. 135

Table 21. Average liquid-solid surface tension, unit in mN/m. 140

Table 22. MSE of proposed model for all plastics-α-σ combinations: [unit in µL] 140

Table 23. MSE of proposed and previous models in overall. [unit in µL].....140

Table 24. Liquids' advancing contact angles on structured polymers at various inclined angles. Comparisons of experiment with predicted values. 141

Table 25. Liquids' critical retention volumes on polymers with various conditions. Comparisons of experiment data with predicted values. 146

Table 26. DI water's contact angle on polished aluminum surface and AAO barrier layer. 153

Table 27. Various solid-liquid combinations for proposed methodology evaluations. .156

1 INTRODUCTION

1.1 Motivation

Controlling solids wettability is essential and beneficial to the industry and human life because the wetting behavior commonly happens in the daily life. The research of wetting behavior can be wildly applied to several industrial processes which include water condensation of turbine blades, parts painting and drying, chemical adhesion and coating, oil extraction, and even cleaning, sanitizing, and anti-bacterial storage in the food industry. In daily life applications, pesticide spraying on the wood floor and self-cleaning glass windows are also such applications. All these examples have different liquid and solid combination but they all relate to wetting behaviors. Due to various applications, one might expect a hydrophilic or a hydrophobic solid surface to fulfill the requirement. For example, the surfaces of aluminum cans are expected to be hydrophilic during the painting process. This is because manufacturers expect to see the surfaces being painted uniformly and tightly attached to the paint. On the other hand, a hydrophobic surface is required for self-cleaning glass windows and turbine blades because water droplets are expected not to residue on surfaces of windows and blades, and therefore keep them clean and enhance the cooling effect.

While driving in the raining day, the raindrop falls onto the car's windshield. Some bigger droplets soon slide down however some smaller droplets slide slowly or even stick on the windshield. For the driving safety, the driver expects the view as clear as possible; even wipers are used to clean the windshield, it is still better to have the water

or any liquid droplet residues on the windshield as less as possible. The similar scenario happens at buildings' construction; e.g. the roof structure design. In order to alleviate the water and snow loadings of the buildings, the roof is usually designed to be inclined; however, it is always better that the raindrop and snow can slide down to the ground instead of staying on the roof. The demand of a hydrophobic surface shows in both examples listed above. The contrary demand happens at painting job during the assembly process. A part or a product needs to be painted uniformly. It is usually better the paint or vanish can stay on the products' surfaces without rolling off. The similar scenario also happens at bug spray, cleaning, and sterilization process. These examples show that a hydrophilic surface is required for liquids attaching and storing on products' surfaces. There is a common property of aforementioned applications and demands, which is that surfaces where wetting behaviors happened are not necessarily horizontal. Therefore, the research on liquids' wetting behaviors and controlling the wettability on inclined surfaces caught the author's attention.

1.2 Research Question

As the dissertation title, the present study focuses on liquids' sliding onset on commonly used plastics. Liquids' sliding onset is also known as liquids' retentions. Because liquids' sliding behavior occurs on an inclined surface, this behavior must occur along with liquid droplets displaying contact angle hysteresis phenomenon. Therefore, to investigate liquids' retentions, it is inevitably to do research on contact angle hysteresis. Researches on liquids' retentions and contact angle hysteresis have applications on

coating procedures, digital micro-fluidics, droplet evaporation, ink-jet printing, and pesticides spraying. For some case, contact angle hysteresis is a problem, such as immersion lithography; however, it is essential for coating and spraying. [1], [2] In addition, these researches are also crucial in development of superhydrophobic and water repellent surfaces. Although liquids' sliding behavior includes the onset of droplets' movement, droplets' moving velocity and acceleration, the present study will only focus on the onset of droplets' movement. This is because the author intends to induce the research to the application of liquid storage on structured surfaces.

Based on the author's research motivations and objectives, the research problems can be formulated as:

1. What is the effect of surface structures on liquids' contact angles?

   To be more specific, the surface structure with various specifications (height, length, width, pitch) can induce the change on liquid's contact angles. The first research question is to understand the relation in between these parameters and contact angles.

2. What is the effect of surface structures on solids' surface free energy?

   Contact angles change could originate from solids' surface free energy change due to surface structures. The second research question is to study the math in between structure' parameters and solids' surface free energy.

3. What is the effect of surface structures on liquids' contact angle hysteresis?

   When the solid surface is inclined, the liquid droplet would display contact angle hysteresis phenomenon. Extending from the first research question, the third question is to understand the relation in between contact angle hysteresis and parameters which include structures' specifications, liquids' volumes, and surface inclined angles. The relation could be linear or non-linear. If it is non-leaner, then which mathematical model can be applied closely? (polynomial, exponential or sinusoidal)

4. What is the link between liquids' contact angle hysteresis and retentions on inclined solid surfaces?

   A droplet displays contact angle hysteresis phenomenon when it stays on an inclined solid surface. A droplet would slide down if its volume reaches a critical value. Although several models have been proposed to link liquids' contact angle hysteresis and retentions, which model can best fit the measurement data? Can we formulate an empirical model which best fit the measurement data?

5. Can we control liquids' retentions by designing surfaces' specifications?

   This is an extending question from question 3 and question 4, after the effect of surface structures on liquids' contact angle hysteresis and the link between liquids' contact angle hysteresis and retentions on inclined solid surfaces are figured out. While applying estimated contact angle hysteresis obtained from

question 3, can the empirical model built in the question 4 successfully predict liquids' retentions?

1.3 Research Assumption

The present research is studied under following assumptions:

1. The research target is to develop empirical models which best fit contact angle, contact angle hysteresis, solids' surface free energy, and critical retention volume results obtained from selected liquids and solids. Selections of liquids and solids are reported in the section 1.5 and repeated in sections 4.1.2 and 5.1.2.

2. Due to fabrication methods and plastics' properties, the pillar-like structure and the square frustum-like structure are representatives of symmetrically arranged structure.

3. Symmetrically arranged structure is defined as the structure which has grooves with the same size orthogonally intersecting in the same pitch.

4. The present study only considers surface structures' effects on aforementioned research questions, although those results are also affected by surface roughness. In the present study, plastics have surface structures in the hundred-micrometer scale and arithmetic average surface roughness R_a in the hundred-nanometer

scale. Therefore, the effect of surface roughness is neglected.

5. It is assumed that liquid droplets stay in the Wenzel state when droplets are dispensed on structured surfaces. This assumption implies that liquid-solid three phase contact line would change due to structure effect.

6. It is assumed that droplets' shapes are symmetrical no matter dispensed on structured or non-structured surfaces. The symmetric shape means that a droplet's profile can be mirrored by a line which passes upper and lower ends in the top view. An example of the symmetric shape is shown in Figure 25 (b).

1.4 Research Objective

The research objectives are listed below:

- Being able to quantitatively characterize of changes in liquid's contact angle and contact angle hysteresis due to solids' surface structures and other parameters.
- Understanding how a solid's surface free energy is changed due to its surface structure.
- Being able to conclude empirical formulas to predict a liquid's contact angle and contact angle hysteresis on structured solid surfaces.
- Being able to conclude an empirical formula to estimate a liquid's retention on an inclined surface.

- Being able to predict and control a liquid's retention by using research outcomes.

1.5 Material and Methods

This research firstly determines the surface structure effect on liquids' contact angles, contact angle hysteresis, retentions, and solids' surface free energy, and then endeavors in empirical models formulation. To determine the surface structure effect, experiments are designed following the process chart illustrated in the Figure 1.

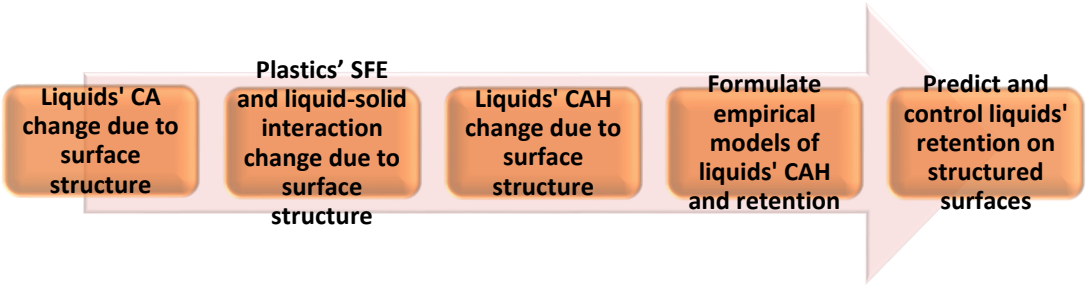

Figure 1. Research process chart.

Materials selection includes testing liquid materials and plastics selections. Probed liquids using in the present study includes de-ionized (DI) water, formamide (also known as methanamide), ethylene glycol (EG), α-Bromonaphthalene (α-BN), and methylene iodide (MI). This choice was made based on their accessibility and diverse polarities. DI water is a good representatives of bipolar liquids. EG and formamide are monopolar liquids with strong base component. MI and α-BN are commonly used apolar

liquids. Diverse polarities of selected probed liquids are desired for solids' surface free energy characterizations. The detail would be addressed in section 3 and section 4. All testing liquids' surface free energy, polarity, and their density are listed in Table 1.

Selections of polymers are based on their commonly usage in the industrial. Polyethylene terephthalate (PET), High-density polyethylene (HDPE), Low-density polyethylene (LDPE), Polyvinyl chloride (PVC), Polypropylene (PP), and Acrylonitrile Butadiene Styrene (ABS) were selected as representatives of commonly used plastics. PET has its best application in bottle production. HDPE has applications of plastic bags, 3-D printer filament, and food storage containers. LDPE has its well-known application in plastic wraps. PVC is the material of pipes, insulation on electrical cables, and clothes. PP has applications in plastic cups, prescription bottles, and furniture. ABS has applications in keyboards, toys, and automotive industry. The application list of among commonly used plastics is just the tip of the iceberg. However, it demonstrates the diversity of these plastics' application, no matter in the industry or daily life. Considering the accessibility, these polymers were selected.

There are many methods of surface structure fabrications, such as coating, etching, crystallization, and deposition, pressing, and cutting. Considering the efficiency of machining process, the last two fabrication methods were adopted in the present study, although these methods cause the deformation of plastics and reduce the sharpness of structures. The detail of each method is addressed in the beginning of section 4 and section 5 respectively. Therefore, it is necessary to characterize samples' surface

morphology. In the present study, optical microscope (OM), scanning electron microscope (SEM), and profilometer were used for surface measurements.

In the present study, a digital optical microscope (Keyence VHX-2000) with lens having highest resolution of 5000x was used, shown in Figure 2. An OM has optical and illumination systems which enables users to study microstructure. Since selected polymer surfaces are opaque to visible light, the reflecting mode was used. Microstructures were shown in the different contrasts which were imaged by various reflections from different regions. [3] The microscope used for this study has a large depth-of-field, ability to observe an image from any angle, and an easy to use system with the ability to save captures images to a hard disk drive. Images taken from OM are shown in section 5.

Figure 2. Digital microscope Keyence VHX-2000 VH-Z500.

A 3-D image of the microstructure was obtained by scanning electron microscope. The principle of SEM is to use an electron beam to scan the sample surface. The electron beam interacts with atoms on the sample surface. Secondary electrons (SE) or back-scattered electrons (BSE) are collected by electron collectors installed within SEM. SE can be used to generate images of sample surfaces in three dimensions, while BSE can be used to analyze the sample's material composition which were differentiated by the intensity of BSE signals. [3], [4] To use SEM for surface characterization, the specimen surface must be electrically conductive. Therefore, the platinum coating in nanoscale thickness was applied onto plastics' surfaces. In the present study, a field emission scanning electron microscope (FEI Quanta 600 FE-SEM) was used and images of plastics' surface structures are shown in section 4 and section 5.

Surface roughness was obtained by using a profilometer. A profilometer is a mechanical instrument used to measure a surface's profile, and thus, is able to determine the surface's roughness. In case of a contact mode, profilometer has a diamond stylus which drags horizontally on the sample surface. In the present study, the profilometer (KLA-Tencor P-6 Stylus) was used and it can measure a small shape ranging in height from 10 nm to a few millimeters. While surface roughness has multiple amplitude parameters with various definitions, the arithmetic average of the absolute values R_a is the most popular one-dimensional roughness parameter. R_a is the average roughness over one sampling length. To ensure that R_a can represent the type of surface, several consecutive sampling lengths must be composed as evaluation length; and the average value of R_a obtained during each sampling length becomes the final R_a value. To calculate the

average roughness, it is necessary to define the reference line. Figure 3 illustrates the definition of the center line. Within a sampling length, the derivation of R_a is illustrated in Figure 4 and formulated in Equation (1). Listed in Table 2, R_a values of all plastic samples were obtained before surface structure fabrications, although it is assumed to neglect roughness effect in the present study.

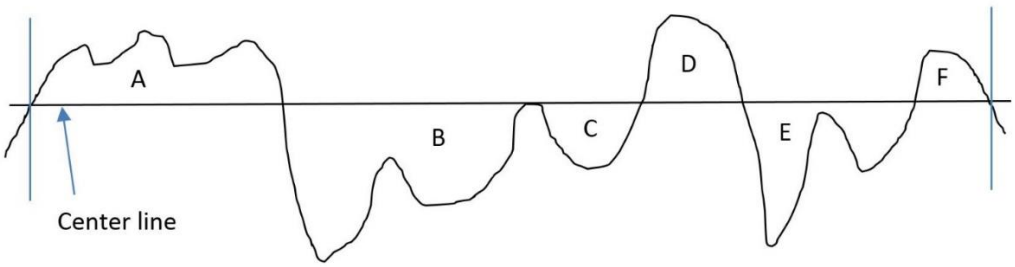

Figure 3. Derivation of the center line. Within the evaluation length, the center line is the line which cuts the shape into upper and lower parts, where the total area of upper parts equals to the total area of lower parts. (i.e. Area of A+D+F = Area of B+C+E)

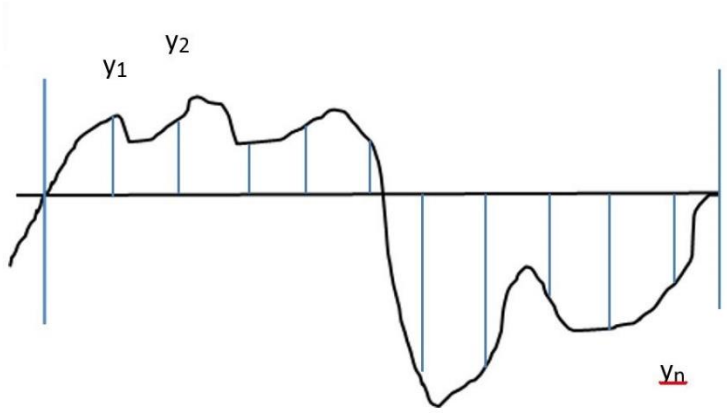

Figure 4. Derivation of R_a within a sampling length.

$$\mathbf{R_a} = \frac{|\mathbf{y_1}| + |\mathbf{y_2}| + \cdots + |\mathbf{y_n}|}{\mathbf{n}} \quad (1)$$

Contact angle measurement is essential to understanding the wettability of solid surfaces. Current contact angle measure instrument setting can be traced back to the design of Bigelow et al. [5] The measurement needs to be accomplished by two steps, images capture and contact angles acquisition. In the present study, the author used a self-built goniometer system, shown in Figure 5, and contact angle of each plastic-liquid combination was obtained by taking 25 measurements. Syringes and needles made by Hamilton Company are used to control the volume of testing liquids as 10 μL for each droplet. The testing liquids were dispensed onto sample surfaces in the normal direction. Droplet images were captured by the high performance CCD camera (VH-310G2-M/C 264) made by Vieworks with 640×480 resolution and 264 fps frame rate. Ideally, the profile of the droplet is an arc, and the line passing the very left and right ends of the arc

forms a baseline. Angles between baselines and tangent lines to the arc at two ends are called contact angles. Captured images are then analyzed by the self-design program, which does two three-point circle fittings and slope calculation at intersections of the arc and the baseline. The acquired data is then processed by taking average and standard deviation.

Measurements of contact angle hysteresis and liquids' critical retention volume were processed at the same goniometer system mentioned above. Detailed measurement process is described in section 5. Note that there are two definitions of contact angle hysteresis, and the present study discusses the contact angle hysteresis happens on inclined surfaces only.

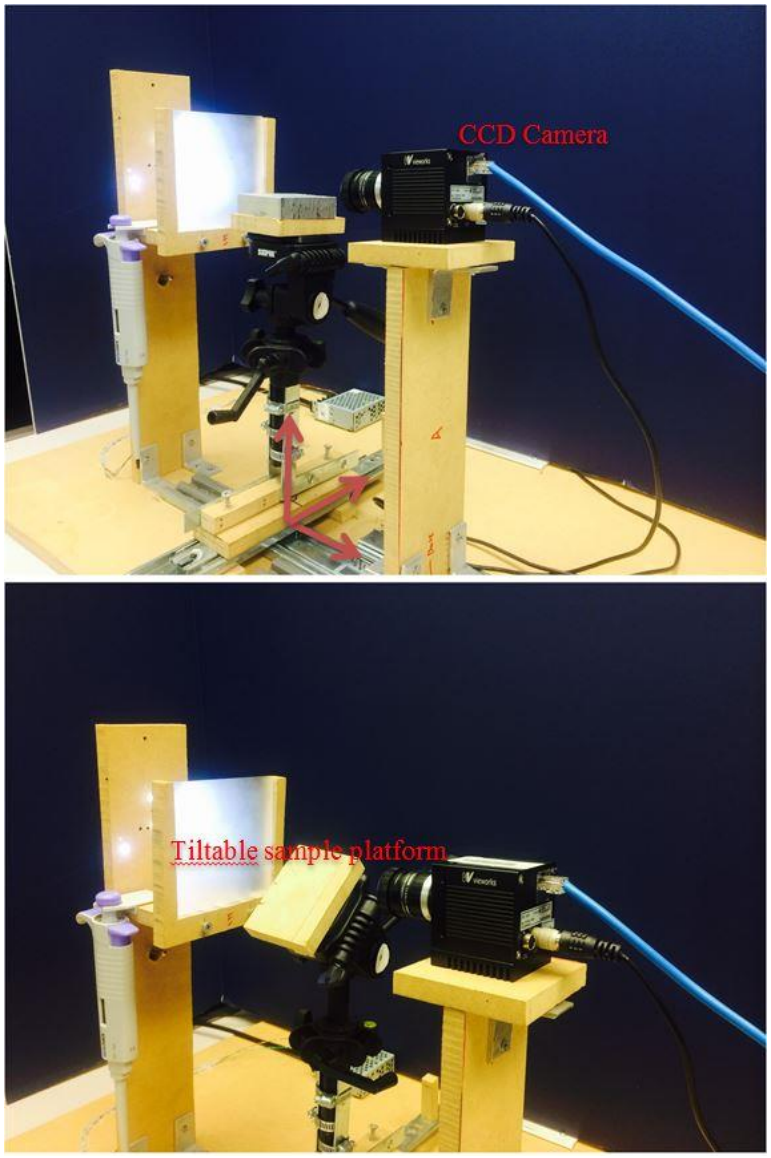

Figure 5. A self-built goniometer system. The sample platform can move in 3 axis (upper figure) and tilt up to 90° (lower figure).

Table 1. Surface free energy, polarity, and density of selected probed liquids. (Note, at 20ºC)

Testing liquids	Total γ^{Total} (mN/m)	Apolar γ^{LW} (mN/m)	Lewis Acid γ^{+} (mN/m)	Lewis Base γ^{-} (mN/m)	Polarity	Density (g/cm^3)
De-ionized (DI) Water	72.8	21.8	25.5	25.5	Bipolar	1
Formamide	58	39	2.28	39.6	Monopolar	1.133
Ethylene glycol (EG)	48	29	1.92	47	Monopolar	1.113
α-Bromonaphthalene (α-BN)	44.4	44.4	0	0	Apolar	1.484
Methylene iodide (MI)	50.8	50.8	0	0	Apolar	3.325

Table 2. Roughness parameters of all plastic samples. (Unit in nm) Sampling length 500µm

	PET	HDPE	PVC	LDPE	PP
Average roughness R_a	242.9	111.7	243.4	42.9	341.2
Max R_a	339.1	224.1	208.9	77.9	493.5
Root mean square R_q	330.6	184.7	294.0	68.3	446.6
Peak R_p	778.4	599.4	568.9	510.4	1408
Valley R_v	1601	873.5	867.2	215.8	1193
	ABS	**PC**	**Al (polished)**	**AAO 300nm**	**AAO 70nm**
Average roughness R_a	205.2	4.4	154.7	97.8	57.0
Max R_a	313.5	3.2	151.2	25.2	11.9
Root mean square R_q	278.1	5.3	189.2	119.1	73.2
Peak R_p	953.7	14.5	250.5	275.6	167.8
Valley R_v	824.5	11.9	656.8	332.3	129.0

1.6 Organization of the Dissertation

This dissertation consists of seven sections. Section 1 describes research motivation, research objective and question, followed by research assumptions. The research methodology part includes designs of experiments and material and method. Section 2 is the literature review. The author surveyed the previous studies in the field of contact angle, theory of surface free energy, contact angle hysteresis, liquids' retentions and closely related works. Section 3 introduces several theories of surface free energy calculations. At the end of this section, theories were summarized and compared with each other. Section 4 talks about the result and discussion of the empirical study and prediction of contact angle and surface free energy of commonly used plastics with pillar-like structure. Extending study from Section 4, Section 5 talks about the result and discussion of the empirical study and prediction of contact angle hysteresis and liquids' retention on structured polymer surfaces. Section 6 is the comprehensive experiment evaluation on proposed methodologies. The author attempts to evaluate proposed empirical models while applying to materials other than polymers. Section 7 concludes the present study and provides directions of future works.

2 LITERATURE REVIEW*

2.1 Contact Angle and Surface Free Energy

Understanding and controlling solids' wettability has caught people's attention for hundreds of years, and contact angle is the most intuitive parameter to understand and quantify liquids' wetting behaviors and surface wettability. Young [6] was the first person to quantitatively describe the liquid-solid contact angle. He proposed a surface free energy model and a so called Young's Equation to demonstrate the relationship of surface free energy between solid, liquid, and vapor, Equation (2). Within Young's Equation, θ is the contact angle, γ_{SV}, γ_{LS}, and γ_{LV} stand for solid-vapor, liquid-solid, and liquid-vapor surface free energy respectively.

$$\boldsymbol{\gamma_{SV} = \gamma_{LS} + \gamma_{LV}\cos\theta} \quad (2)$$

Young's model (Figure 8) simply demonstrates the contact angle is influenced by the energy balance along the three faces contact line. Cohesive and adhesive energies are the foundation of surface free energy theory. They also play a role in determine wetting behaviors. [7], [8] In fact, the shape of a liquid droplet on a solid surface relates to interfacial attractions and repulsion. However, this concept was not clear at the beginning of theory development. Zisman proposed a so-called Zisman method to obtain

* Part of this section is reprinted with permission from "Empirical Study and Prediction of Contact Angle and Surface Free Energy of Commonly Used Plastics with Pillar-like Structure by Chung-Han Chiou, Sheng-Jen Hsieh, Surface and Interface Analysis, 47, 1, 45-55, Copyright (2015) by Wiley and "Empirical study and prediction of liquids retention on structured polymer surfaces" by Chung-Han Chiou, Sheng-Jen Hsieh, Surface and Interface Analysis, 48, 3, 146-163, Copyright (2016) by Wiley.

the solids' critical surface free energy by extrapolating the surface free energy at $\cos\theta=1$ on the Zisman plot. He used several liquids which surface tensions have been well-characterized to measure their contact angles. Zisman plot is then generated by a series of liquids' surface tensions versus cosine of liquids' contact angles. Within his theory, Zisman considers that surface free energy of a substance has only one component. Neumann et al [9] empirically studied contact angle, adhesion energy, and modified Berthelot's rule. They proposed the concept of equation of state (EOS) from extensive experiment results. However, theories proposed by Zisman and Neumann are both one component theories, which have their application limit and were challenged by later studies. Fowkes [10] considered that surface free energy is composed by multiple components which include dispersion γ^d, polar γ^p, hydrogen γ^h, induction γ^i, acid-base γ^{ab}, and all remaining γ^o. Owen and Wendt [11] adopted Fowkes' concept and simplified the all components to two categories: dispersion γ^d and polar γ^p. They proposed so-called OWRK theory which can be used to obtain the solid's dispersion γ^d and polar γ^p surface free energy by solving OWRK equation. Similar with OWRK theory, Wu [12], [13] proposed his theory and he also considers that surface free energy is composed by dispersion and polar components. van Oss et al., [7], [8] proposed the acid-base theory. They mentioned that only van der Waals-London interactions are important for macroscopic bodies in condensed system investigation. [14], [15] Lifshitz [16] proposed Lifshitz's theory, and the formula was derived to calculate the free energy of interaction of two phases. van Oss et al. [7] pointed out only Lifshitz-van der Waals interaction (denoted as LW in the following) can be accurately estimated, and polar interactions of

the hydrogen-bonding type often occur. van Oss et al. [17] also pointed out that polar interactions are asymmetrical. Since the hydrogen-bonding relates to electron acceptor (Lewis Acid) and electron donor (Lewis base) interactions, the polar interaction is also called acid-base interaction (denoted as AB), and acid and base components are expressed as γ^+ and γ^-. [18], [19] van Oss et al. [7] applied Good-Girifalco-Fowkes combining rule [20] and Dupre equation to calculate the apolar interaction between two materials. Since polar interactions are not symmetric, they proposed the corresponding asymmetric combining equation to calculate polar interaction between two materials. In addition, van Oss et al. [8] also claimed that apolar and polar surface free energy are additive. However, Lewis acid and Lewis base components are not additive. They also discussed the interfacial attractions and interfacial repulsion which relate to apolar cohesion, polar cohesion, and polar adhesion between two materials' compounds. The acid-base considers the surface free energy composed by three components. This theory and the van Oss-Chaudhury-Good equation are complete and adopted by many current scholars.

2.2 Contact Angle Hysteresis

Contact angle hysteresis is a physical phenomenon which often occurs in the daily life, such as raindrop sliding, bug spray retention, and coffee stain. It is also essential in the industrial process, such as coating, printing, and immersion lithography. [21] There are several expressions of contact angle hysteresis mentioned in the literatures. One major manifestation is that contact angle hysteresis happens on horizontal surfaces. In this

scenario, shown in Figure 6, contact angles formed by expanding and contracting the liquid are referred to as the advancing contact angle θ_A and the receding contact angle θ_R, respectively.

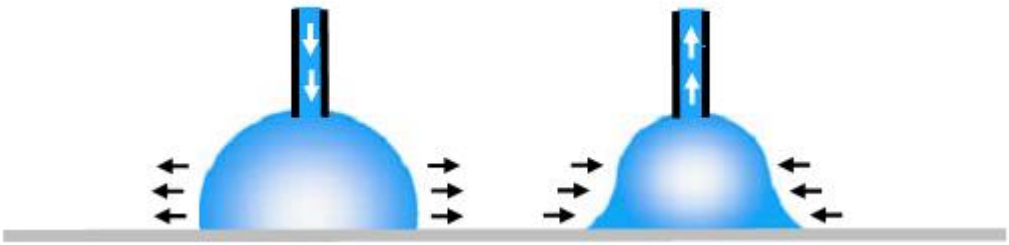

Figure 6. Illustration of advancing and receding contact angles due to expanding and contracting the liquid. [22]

When a droplet stays on an inclined surface, its profile is no more symmetrical. Due to the gravity effect, the contact angle at the lower end is greater than the contact angle at the upper end. This phenomenon is another major expression of contact angle hysteresis, where contact angles at the lower and upper ends stand for advancing contact angle θ_A and the receding contact angle θ_R, respectively, Figure 7.

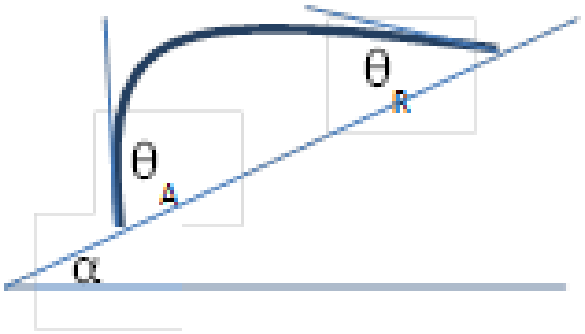

Figure 7. Illustration of contact angle hysteresis happens on an inclined surface.

For all expressions, contact angle hysteresis θ_{CAH} can be quantitatively defined as the difference between θ_A and θ_R as:

$$\theta_{CAH} = \theta_A - \theta_R \tag{3}$$

The research of contact angle hysteresis can be traced back to Johnson and Dettre. They claimed contact angle hysteresis is caused by surface heterogeneity, and the phenomenon is a metastable state which the vibrational energy of a drop and the heights of the energy barriers keep balance. [23] They also measured the water wettability of titania-coated glass as a function of the number of coating treatments to investigate the contact angle hysteresis under various surface heterogeneities. [24] Extrand and Kumagai measured θ_A and θ_R of four organic liquids and water on silicon wafers and a variety of polymer surfaces using an inclinable plane. [25] They claimed contact angle hysteresis is not an extensive property. According to the experimental result, every solid surface has its unique reduced hysteresis H, which is defined as:

$$H = (\theta_A - \theta_R)/\theta_A \quad (4)$$

Their finding leads a conclusion which links the relationship between θ_A and θ_R, regardless of contacting liquids. Their conclusion agrees with Johnson and Dettre [23] that hysteresis is dominated by chemical interactions or heterogeneities. However, they also concluded that structures play a minor role of contact angle hysteresis which might be controversial in micrometer scale. McHale et al. [26] discussed theoretically on Wenzel [27] and Cassie-Baxter [28] models. They predicted that Wenzel-type surface would become sticky, while Cassie-Baxter-type surface would become slippy. The sticky or slippy surface description could be referred to Quéré et al. [29] No matter a structured surface belongs to which type, their research results both conclude that surface structure does affect contact angle and therefore affects contact angle hysteresis. Gao and McCarthy [30] stated that contact angle hysteresis is attributed to three-phase contact line change, which indicates that contact angle hysteresis is a 1-D issue. Based on aforementioned studies, the author has proposed contact length ratio σ as a parameter which quantifies the three-phase contact line change due to surface structures. [31]

2.3 Liquids Retention

Liquid droplets' sliding is always associated with contact angle hysteresis phenomenon. Therefore, contact angle hysteresis plays an important role in understanding droplets' motion, design of a liquid repellent surface, and in research on superhydrophobicity. [32], [33], [34] Research on liquid sliding behaviors includes the criteria of sliding onset

(i.e. break the barrier of the metastable state), and the droplet' performances (velocity, acceleration, and deformation) while it is moving. Bouteau et al. [35] investigated the droplets' sliding onset on inclined Langmuir–Blodgett surfaces. Their findings argued that a single ellipse can fit whole contour of the droplet. They analyzed the relationship of dimensionless retentive force and contact angle hysteresis and claimed that the model of parallel-sided elongated drops agrees with the measurements. Their result indicates that the main influence of the capillary forces at the rear and front edges of the drop is more obvious than that at the lateral sides. In fact, the contour of the droplet on inclined surfaces could have various shapes. Extrand and Kumagai [25] proposed the droplet's contour could be a circular drop, a parallel-sided drop, or a drop with front-to back asymmetry. Research on liquid sliding behaviors can extend to investigation of sliding velocity and acceleration. Kim et al. [36] studied the sliding velocity of drops of three liquids on smooth polycarbonate (PC) surfaces. They constructed a scaling law that predicts the sliding velocity; however, its correctness might be in a limit range. Sakai et al. [37] studied sliding acceleration of water droplets on commercial polytetrafluoroethylene (PTFE) plates and silicon wafers coated by octadecyltrimethoxysilane (ODS) and heptadecafluorodecyltrimethoxysilane (FAS). When the solid samples are tilted at 35°, they claimed sliding actions could be sorted into three categories: constant accelerated motion, constant velocity (no acceleration) motion, and stasis which depend on the contact radius or injection–suction rate in dynamic contact angle hysteresis.

The present study focuses on the onset of liquids' sliding behavior on commonly used plastics with surface structures. The study can be applied to the investigation of the liquid storage and repellency on structured surfaces. It was aforementioned that research on liquids' sliding behavior would definitely couple with contact angle hysteresis. Therefore, the present study started from the investigation of contact angle hysteresis at various critical conditions (onset of liquids' sliding), and then induced to the research on droplets' critical retention volumes.

Droplets' critical retention volumes have been studied for decades. Several models for estimation of the maximum retention volume have been reported. Dussan [38] analyzed the retention volume of small drops under the assumption of small contact angle hysteresis and proposed the maximum retention volume as:

$$\mathbf{V_{max}} = \frac{\mathbf{1}}{\mathbf{2}}\left(\frac{\boldsymbol{\gamma_L}}{\boldsymbol{\rho g \sin\alpha}}\right)^{\mathbf{3/2}} \times \left(\frac{\mathbf{96}}{\boldsymbol{\pi}}\right)^{\mathbf{1/2}} \times (\mathbf{\cos\theta_{min} - \cos\theta_A})^{\mathbf{3/2}}\,(\mathbf{1 + \cos\theta_A})^{\mathbf{3/4}} \times (\mathbf{2 - 3\cos\theta_A + \cos^3\theta_A}) \times (\mathbf{2 + \cos\theta_A})^{\mathbf{-3/2}} \times (\mathbf{1 - \cos\theta_A})^{\mathbf{-9/4}} \quad (5)$$

where γ_L is liquid's surface tension, ρ is liquid's density, and α is surface inclined angle.

Extrand and Gent [39] studied the retention of ethylene glycol, glycerol, and water on several polymers. They proposed the ratio F/R of critical force to contact area radius, which can derive the critical retention volume as Equation (6), and claimed the ratio is a characteristic value of each liquid-solid combination. Their conclusions stated that the

force F is proportional to the radius R of contact circle. They also tested the ability of droplet's retention on rough surfaces and found it is better because of the greater θ_{CAH}.

$$\mathbf{V} = \frac{\mathbf{8\sqrt{3}}}{\boldsymbol{\pi}^{\mathbf{2}}} \frac{(\boldsymbol{\gamma}_{\mathbf{L}} \mathbf{sin}\boldsymbol{\theta}_{\mathbf{av}}(\mathbf{cos}\boldsymbol{\theta}_{\mathbf{min}} - \mathbf{cos}\boldsymbol{\theta}_{\mathbf{A}}))^{3/2}}{(\boldsymbol{\rho}\mathbf{g}\,\mathbf{sin}\boldsymbol{\alpha})^{3/2}(\mathbf{2} - \mathbf{3cos}\boldsymbol{\theta}_{\mathbf{av}} + \mathbf{cos}^{\mathbf{3}}\boldsymbol{\theta}_{\mathbf{av}})^{1/2}} \tag{6}$$

where $\theta_{av} = (\theta_A + \theta_{min})/2$.

ElSherbini and Jacobi [40] investigated retention forces and drop parameters on vertical and inclined surfaces, expressed in Equation (7). They used two-circle method for approximating shapes of drops to predict the maximum drop size.

$$\mathbf{V} = \frac{\mathbf{576}}{\boldsymbol{\pi}^{\mathbf{5}}} \frac{(\boldsymbol{\gamma}_{\mathbf{L}} \mathbf{sin}\boldsymbol{\theta}_{\mathbf{av}}(\mathbf{cos}\boldsymbol{\theta}_{\mathbf{min}} - \mathbf{cos}\boldsymbol{\theta}_{\mathbf{A}}))^{3/2}}{(\boldsymbol{\rho}\mathbf{g}\,\mathbf{sin}\boldsymbol{\alpha})^{3/2}\,(\mathbf{2} - \mathbf{3cos}\boldsymbol{\theta}_{\mathbf{av}} + \mathbf{cos}^{\mathbf{3}}\boldsymbol{\theta}_{\mathbf{av}})^{1/2}} \tag{7}$$

They proposed the bond number B_0 to estimate the θ_R and the critical drop size when using θ_A as input. In the conclusion, they stated the bond number B_0 is constant for a given θ_A, which allows predicting maximum drop diameters and volumes at various surface inclinations and for different liquid–surface combinations having the same θ_A.

2.4 Summary of Closely Related Works

Solids' surface structure is known to affect liquids' contact angle performances. Wenzel [27], Cassie and Baxter [28] are pioneers who proposed their own models to predict liquids contact angles on rough solid surfaces. Dettre and Johnson [41] first proposed the observation that the transition between Wenzel and Cassie states exists. This transition is

important because of its application on superhydrophobic surface design. However, the transition between two states will not be possible without overcoming the energy barrier. Based on energy balance, Patankar [42] proposed a methodology to determine the possibility of a drop state transition from Cassie to Wenzel. Patankar [42] and Marmur [43] also mentioned that the energy barrier might not exist between two states for certain structure geometries. This conclusion confirms that surface structure is a key factor to control surface wettability. Patankar [44] even proposed a theory that multiple structure structures are appropriate to develop self-cleaning surfaces, which have excellent water repellent properties. Nakajima, in his review paper [45], reinforced the importance of surface structure for wettability control in microscopic system. He pointed out that nano-level structure and chemical composition affect macroscopic surface hydrophobicity. On the premise that solid surfaces maintain their compositions, producing surface structure by all means becomes an important path to control solids' wettability. However, Gao and McCarthy [46] claimed there exists flaws in both models of Wenzel and Cassie-Baxter because they both emphasized the concept of liquids' contact area due to surface structure. All of the data that Gao and McCarthy proposed indicates that it is liquid-solid interactions at the three-phase contact line to determine liquid droplets' profiles. Their conclusion is consistent with Bartell [47] and Extrand's [48]. In addition to dimension issue, Wenzel and Cassie-Baxter models ignore the effect of structure shape which is also a key factor that affects liquids' contact angle behavior. [45] Typical surface morphologies include one and two dimensions structures. Sasaki et al. [49] proposed their study of hydrophobicity which was enhanced by rough surface with repetition of a

one-dimensional groove structure on it. Patankar [44] manufactured the pillar geometry on paraffin wax to fabricate self-cleaning surfaces. Yoshimitsu et al. [50] also investigated hydrophobicity of silicon wafers with various pillar-like and groove structures on surfaces. Promraksa and Chen [51] used the Surface Evolver to determine contact angles of liquid droplets sitting on a cosine wave-like pattern surface. Zhu et al. [52] designed micro square pillar arrays on silicon surfaces to tune water contact angles. They claimed that their experiment results are close to Cassie–Baxter theoretical predictions. Kang et al. [53] fabricated rough nickel surfaces with micro arrays and found they were superhydrophilic. Most of aforementioned studies endeavored to alter water's contact angle and make solids become either hydrophobic or hydrophilic. Due to various applications, the industry also cares about all kinds of liquids' contact angles in addition to water's. Liquid-solid interaction has been known to determine liquids' contact angles on solids. [7], [8] Therefore, it is necessary to investigate solids' surface free energy variations after any treatments or surface modifications. Based on previous studies [54], [55], [56], [57] and the industry's needs, an effective approach was proposed to estimate contact angles of liquids with various polarity on commonly used plastics with pillar-like structure. These plastics include Polyethylene terephthalate (PET), High-density polyethylene (HDPE), Low-density polyethylene (LDPE), Polyvinyl chloride (PVC), and Polypropylene (PP). Predictions of surface free energy of these plastics were also proposed.

Eral et al. [1] listed a series of studies related to liquids' sliding behavior and contact angle hysteresis in their In the following of this section, the author will briefly mention

the most closely related studies, and eventually formulate his own specific research questions. Extrand and Kumagai [58] studied the contact angle hysteresis, drop shape, and drop retention with a tiltable plane. They concluded contact angle hysteresis depends on the nature of the liquids and substrates. In their study, water and ethylene glycol were used as testing liquids and four polymers and silicon were used as substrates. All substrates have nanoscale roughness and even atomically smooth. They formulated the retentive force of an elliptically shared drop. Although this study neither mentioned the surface free energy, nor been processed on substrates with pillar-like structure, their result could be the foundation of the present study. ElSherbini and Jacobi [59] investigated retention forces and drop parameters on vertical and inclined surfaces. They used two-circle method for approximating shapes of drops to predict the maximum drop size. They proposed the Bond number to estimate the receding contact angle and the critical drop size when using advancing contact angle as input. In the conclusion, they stated the Bond number is constant for a given advancing contact angle, which allows predicting maximum drop diameters and volumes at various surface inclinations and for different liquid–surface combinations having the same advancing contact angle. Their research results are strong; however, they left a question and future research direction. First, the Bond number was proposed to estimate the critical drop size for different liquid–surface combinations. However, the Bond number consists of liquid-vapor interaction which might ignore the important interaction between liquid and solid surface. Second, the solid substrates used in their research have smooth surfaces, which might lead to a totally different result on the structured surfaces. Ahmed et al. [60]

investigated the different stages involved in the motion of droplets down inclined surfaces in the lubrication approximation framework. They proposed a numerical model which can be implemented to investigate the effect of contact angle hysteresis on the motion of the droplets as they slide down the incline. They also proposed a simple analytical model to predict the dynamics of the sliding motion of the droplet. In their research, they used glass as solid substrates without surface roughness and water as the testing liquid, which are the major difference from the author's research materials. Hirvi and Pakkanen [61] used molecular dynamics simulations to study the impact and sliding of a nanosized water droplet on nanostructured polyethylene (PE) and poly(vinyl chloride) (PVC) polymer surfaces. Although they used same materials with similar structures, their research direction and target are different from the author's. Yeh et al. [62] studied contact angle hysteresis on regular pillar-like hydrophobic surfaces. Xiu et al. [63] derived a relationship between the surface work of adhesion and the dynamic contact angle hysteresis. Although their research seems closer to the author's, there is something different from two researches. First, they used silicon and water as solid substrate and testing liquid respectively, which are different from the author's research material. Second, their experiments were processed on horizontal surfaces, which is different from the author's experiment setting. Third, they applied Wenzel and Cassie models to analyze the effect of surface roughness on contact angle hysteresis, in other words, they treated the roughness effect as a 2-D issue. However, such a perspective is debatable. Gao and McCarthy [46] has indicated that the roughness effect should be a 1-D issue. Marmur and Bittoun [64] argued Gao and McCarthy's conclusion and stated

that the 1-D or 2-D perspective should depend on the drop size and roughness level. The author's previous research [65] has adopted the perspective of contact line change to investigate the roughness effect on contact angle and surface free energy. Therefore the author will keep using 1-D perspective in the present study.

Models proposed by Dussan [38], Extrand and Gent [39], and ElSherbini and Jacobi [40] have similar terms although built up based on different assumptions. One common point is that they all adopted liquid's surface tension γ_L as the source of retention force, which might ignore the important interaction between liquid and solid surface. van Oss et al. [7], [8] have derived a simultaneous equation to calculate solid's Lifshitz-vander Waals (γ^{LW}) and Lewis acid-base components ($\gamma^+$and γ^-). Their conclusion stated that liquids' contact angles are determined by liquid-solid interaction. Therefore, it is reasonable to believe liquid-solid surface tension (γ_{LS}) plays an important role on contact angle hysteresis. Aforementioned studies were processed on non-structured surfaces, which left the uncertainty of these models' availability to structured surfaces. The authors' previous study indicated that liquids' contact angles could be affected by structures of contacting surfaces. The authors measured contact angles of de-ionized water, ethylene glycol, and α-Bromonaphthalene when they were dispensed on five commonly used plastics with pillar-like structures. The results showed that contact angles and contact length ratio σ have linear relationship. Based on the conclusion, we can deduce that θ_A and θ_R would also be affected by structures of contacting surfaces. This deduction implies that surface structures would also affect liquids' critical retention volumes.

Therefore, in the present study, the authors would investigate how θ_A and θ_R change corresponding to various contact length ratio σ, and then attempt to predict them. In addition, the authors would derive their own model for liquids' critical retention volume estimation. The model and predicted θ_A and θ_R would be examined their correctness by comparing with previous studies and experiment data. *Table 3* was generated to summarize main results of closely related works; also, this table can be used to compare the difference from the author's and previous studies.

Table 3. Summary of closely related studies and comparisons with the author's present study.

	Dussan [38] (1985)	**Extrand. [39] (1995)**	**Elsherbini [40] (2006)**	**Yoshimitsu et al. [50] (2002)**
CAH horizontal				
CAH inclined	V	V	V	
Drop sliding onset	Retentive force	Retentive force	Retentive force	Sliding angle
Surface free energy			V	
Surface structure	Smooth	Smooth	Smooth	Pillar-like groove structures
Chemical heterogonous				
Use Wenzel (W) or Cassie (C) model (2-D perspective)				W & C
Use contact line motion (1-D perspective)				
Prediction or modeling	Calculate retention force	Calculate retention force	Predict receding CA	
Use water or another liquids	Water	Water EG	Water EG	Water only
Polymers or another solids		Polymer & Silicon	Unspecified	Silicon

Table 3. Continued

	Kus. [66] (2007)	**Yeh et al. [62] (2008)**	**Xiu et al. [63] (2008)**	**Hirvi [61] (2008)**
CAH horizontal	V	V	V	
CAH inclined				V 45°, 90°
Drop sliding onset				
Surface free energy				
Surface structure		V pillar	V pillar	V pillar
Chemical heterogonous				
Use Wenzel (W) or Cassie (C) model (2-D perspective)	V	W & C	C	
Use contact line motion (1-D perspective)	C			
Prediction or modeling		Use W&C model	V	Simulation
Use water or another liquids	V	Water only	Water only	Water only
Polymers or another solids	Water only	Silicon	Silicon	PE & PVC

Table 3. Continued

	Ahmed [2] (2014)	**Chiou [31] (2014)**	**Montes. [67] (2014)**	**Present study**
CAH horizontal			V	
CAH inclined	V 10°-70°		V	V
Drop sliding onset				Critical retention volume
Surface free energy		V		V
Surface structure	V	Pillar-like structure with various specifications		Pillar-like and square frustum-like structure with various specifications
Chemical heterogonous				
Use Wenzel (W) or Cassie (C) model (2-D perspective)				
Use contact line motion (1-D perspective)		V		V
Prediction or modeling	V	Predict CA and SFE	Most stable CA	Predict advancing CA and critical retention volume
Use water or another liquids	Analytical model	Water, EG & α-BN	Water only	Water & EG
Polymers or another solids		Five commonly used plastics	polymer	Five commonly used plastics

3 SURFACE FREE ENERGY THEORY*

In this section, the author aims to introduce various methods and theories of surface free energy characterization. Theory of surface free energy can be traced back to Young [6] who firstly proposed a well-known Young's Equation, Equation (2) ,which describes the relationship between contact angle and surface interactions at three phase contact line. Theories of surface free energy have been developed ever since Young's Equation was proposed.

$$\gamma_{SV} = \gamma_{LS} + \gamma_{LV}\, cos\theta \tag{8}$$

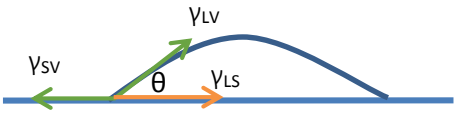

Figure 8. Young's energy balance model.

Figure 8 illustrates Young's Equation in which γ_{SV} is solid's surface free energy, γ_{LV} is liquid's surface tension, and γ_{LS} is the liquid-solid interfacial tension. Surface free energy has the unit as mJ/m^2, however, this unit can be simplified as mN/m or dynes/cm.

* Part of this section is reprinted with permission from "Empirical Study and Prediction of Contact Angle and Surface Free Energy of Commonly Used Plastics with Pillar-like Structure by Chung-Han Chiou, Sheng-Jen Hsieh, Surface and Interface Analysis, 47, 1, 45-55, Copyright (2015) by Wiley.

The main application of surface free energy theory is to explain the specific wetting behavior of a liquid-solid combination. A solid's surface free energy characterization relies on contact angle measurements, however, the number of testing liquids depend on which surface free energy theory is applied. In this section, the number of components of surface free energy would be used to classify those theories. The works of adhesion and cohesion are necessary to be mentioned which are the fundamental of surface free energy theory.

3.1 The Work of Adhesion

The work of adhesion is the work to separate the adjacent surfaces of substance A and B and generate a new surface, which can be illustrated in Figure 9(a) and formulated as

$$W_A = \gamma_A + \gamma_B - \gamma_{AB} \tag{9}$$

where γ_A and γ_B stand for surface tension of substance A and B, and γ_{AB} stands for interfacial tension between A and B. When the substance A and B represent a solid and a liquid respectively, rewriting Equation (2) and Equation (9) would result Young-Dupre equation as

$$W_{SL} = \gamma_{LV} + \gamma_{SV} - \gamma_{LS} = \gamma_{LV}(1 + \cos\theta) \tag{10}$$

Figure 9(b) illustrates the cohesion process which is similar with adhesion process when A and B are the same substance. The work of cohesion is expressed as

$$W_C = \gamma_A + \gamma_A - 0 = 2\gamma_A \quad (11)$$

Good and Girifalco [20] proposed the work of adhesion between the solid and the liquid is the geometric mean of the solid's and the liquid's work of cohesion, expressed as Equation (12).

$$W_{SL} = \sqrt{W_{SS} W_{LL}} \quad (12)$$

According to Equation (11), W_{SS} equal to $2\gamma_{SV}$ and W_{LL} equal to $2\gamma_{LV}$. Therefore, Equation (10) can be rewritten as

$$W_{SL} = \sqrt{2\gamma_{SV} \times 2\gamma_{LV}} = 2\sqrt{\gamma_{SV}\gamma_{LV}} = \gamma_{LV}(1 + \cos\theta) \quad (13)$$

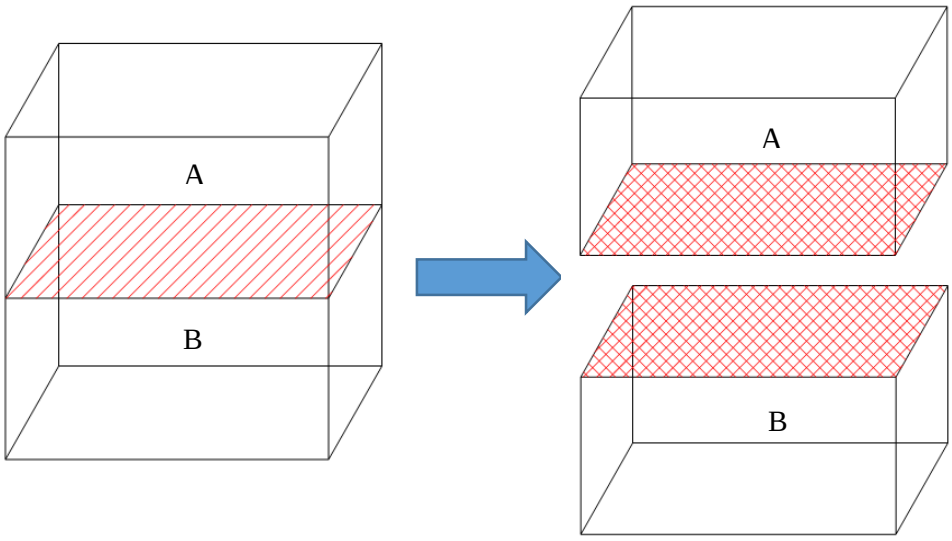

(a)

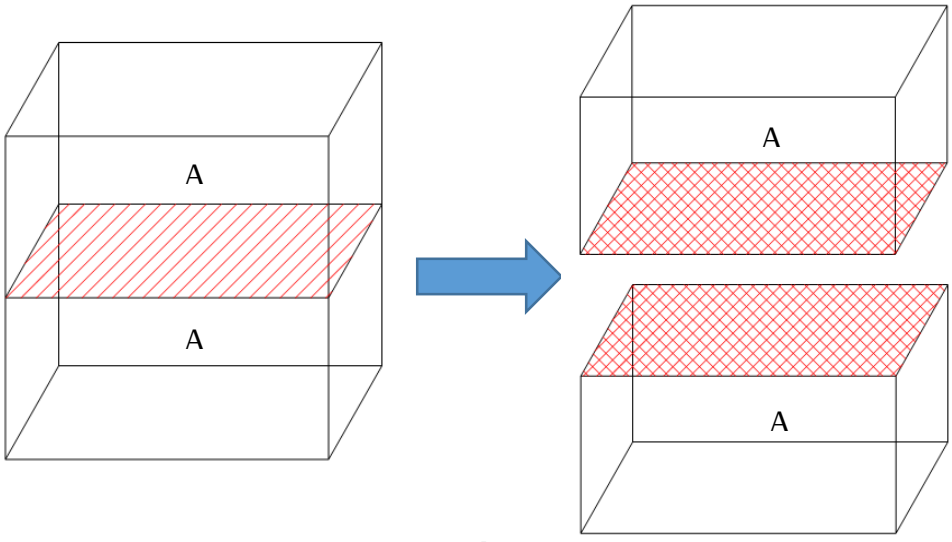

(b)

Figure 9. Process of (a) adhesion and (b) cohesion.

3.2 One Component Theory

3.2.1 Zisman Plot

The most famous one component theory was proposed by Zisman. [68] He proposed so-called critical surface tension which was obtained empirically by a series of liquids' contact angles. Zisman plot was hence generated which displays the connection in between cosine of contact angles and liquids' surface tensions. Figure 10 demonstrates the Zisman plot of LDPE surfaces. Ten liquids were used and each data point reflects a liquid's surface tension and cosine of its contact angle on a LDPE surface. A fitting line was generated by the data points with non-zero contact angles (i.e. $\cos\theta \neq 1$). By extrapolating the fitting line at $\cos\theta=1$, the critical surface tension was obtained. In this case, the intersection of the horizontal and the vertical dot lines is the extrapolated value which represents the critical surface tension of the LDPE surface. This method is simple but controversial because it relies on sufficient testing liquids to generated data points with non-zero contact angles. However, even if data points are sufficient, the fitting line is not necessary a straight line with high correlation coefficient r^2. When a fitting line has low correlation coefficient r^2 to data points, the extrapolation would lead to incorrect value of critical surface tension of the solid, or even worse, a negative number. According to Equation (10), the critical surface tension is valid only if γ_{LS} equals to 0, which means that Zisman method neglects the interfacial surface tension. From the perspective of multiple component theories, introduced in later of this section, Zisman method can only get the correct result for an apolar surface which polar component is zero.

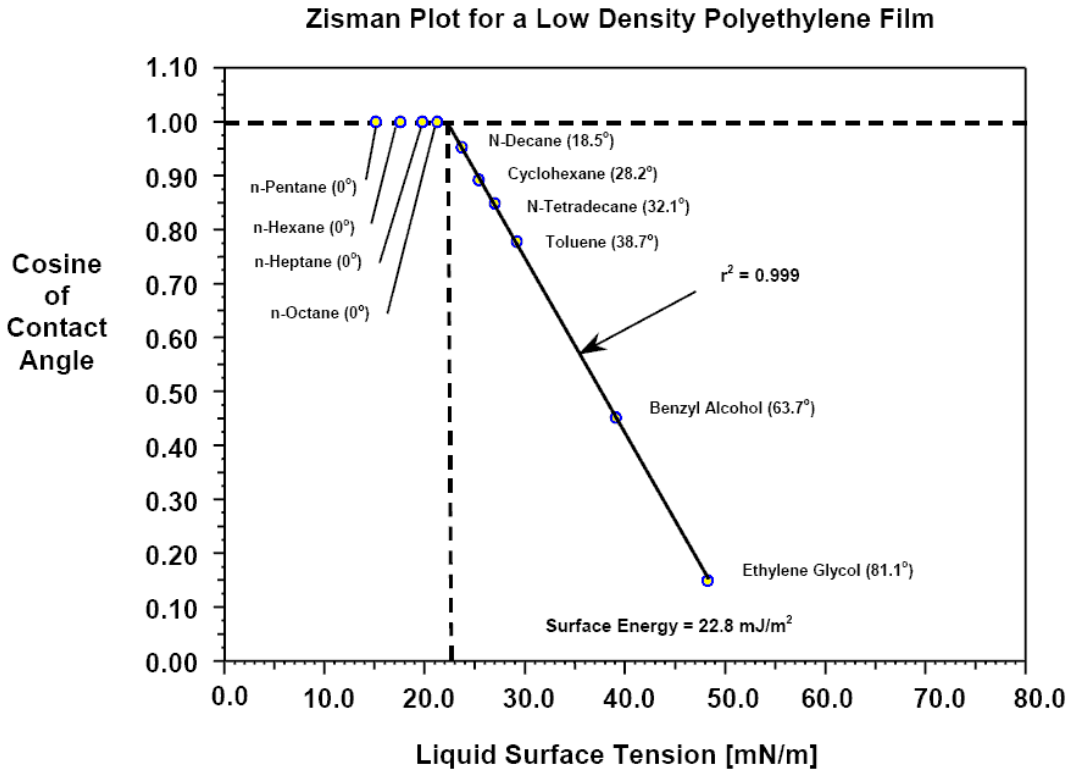

Figure 10. The Zisman plot for LDPE's surface energy. Ten liquids were used and the critical surface energy was approached to 22.8mJ/m^2. High correlation coefficient proves the accuracy. [69]

3.2.2 Equation of State

The other one component theory originates from equation of state. Kwok and Neumann [70] proposed the analytical expression of equation of state of Φ by modifying Berthelot's rule together with experimental data, where Φ stands for interaction parameter and expressed as

$$\Phi = e^{\beta(\gamma_1-\gamma_2)^2} \tag{14}$$

where β is an empirical constant and Φ can be also expressed from Young-Dupre equation as

$$\Phi = \frac{\gamma_1(1+\cos\theta)}{2\sqrt{\gamma_1\,\gamma_2}} \tag{15}$$

When substance 1 and 2 represent liquid and solid, combining Equation (14) and (15) would get

$$\cos\theta = -1 + 2\sqrt{\frac{\gamma_{SV}}{\gamma_{LV}}}\,e^{-\beta(\gamma_{LV}-\gamma_{SV})^2} \tag{16}$$

Equation (16) describes the relationship between the contact angle, liquid's and solid's surface tensions. It assumes that surface free energy of the solid has only one component which can be determined by one testing liquid. After extensive measurements, Kwok and Neumann concluded that the constant β is 0.0001247 $(m^2/mJ)^2$. The conclusion brings the debates that whether the β is universal for all liquid-solid combinations or not.

3.3 Two Component Theories

Two component theories are based on dividing the surface tension into dispersive (also called as apolar) and polar components. These theories can be classified by using either geometric or harmonic mean in the expression of liquid-solid interfacial tension.

3.3.1 Owens/Wendt and Fowkes Theory

Fowkes [10] claimed that surface energy of a substance is composed by the dispersion γ^d, polar γ^p, hydrogen γ^h, induction γ^i, acid-base γ^{ab}, and all remaining γ^o components, expressed as Equation (17).

$$\gamma = \gamma^d + \gamma^p + \gamma^h + \gamma^i + \gamma^{ab} + \gamma^o \tag{17}$$

Owen and Wendt [71] adopted Fowkes' concept and modified the all components in Equation (17), except of dispersion γ^d, are classified as polar term. Therefore, Equation (17) is simplified as

$$\gamma = \gamma^d + \gamma^p \tag{18}$$

Equation (17) and (18) show that the surface free energy is additive for each component. Therefore, the work of adhesion should be the sum of both components as well. According to Equation (13), works of adhesion of each component are

$$W_{SL}{}^d = 2\sqrt{\gamma_{SV}{}^d \gamma_{LV}{}^d} \tag{19}$$

and

$$W_{SL}{}^{p} = 2\sqrt{\gamma_{SV}{}^{p}\gamma_{LV}{}^{p}} \tag{20}$$

Combining Equation (19) and (20) to replace W_{SL} term within Young-Dupre equation (Equation (10)) results

$$\gamma_{LS} = \gamma_{LV} + \gamma_{SV} - 2\sqrt{\gamma_{SV}{}^{d}\gamma_{LV}{}^{d}} - 2\sqrt{\gamma_{SV}{}^{p}\gamma_{LV}{}^{p}} \tag{21}$$

Combining the above equation with Young's equation (Equation (2)), the so-called OWRK (Owens, Wendt, Rabel, and Kaelble) equation is expressed as

$$\sqrt{\gamma_{SV}{}^{d}\gamma_{LV}{}^{d}} + \sqrt{\gamma_{SV}{}^{p}\gamma_{LV}{}^{p}} = \frac{\gamma_{LV}(1+\cos\theta)}{2} = \frac{(\gamma_{LV}{}^{d} + \gamma_{LV}{}^{p})}{2}(1+\cos\theta) \tag{22}$$

Since the surface free energy of a solid is composed by two components, above equation contains two unknowns while solving $\gamma_{SV}{}^{d}$ and $\gamma_{SV}{}^{p}$. Therefore, it is necessary to use two testing liquids which lead above equation to 1st order simultaneous equations with two unknowns, Equation (23). In practice, one polar liquid, such as water and formamide, and one apolar liquid, such as diiomethane and α-BN are chosen for surface free energy characterization. This choice can avoid infinite solutions while the simultaneous equations are linearly dependent.

$$\begin{aligned}
&\sqrt{\gamma_{L_1V}{}^{d}}\sqrt{\gamma_{SV}{}^{d}} + \sqrt{\gamma_{L_1V}{}^{p}}\sqrt{\gamma_{SV}{}^{p}} = \frac{\gamma_{L_1V}(1+\cos\theta_1)}{2} = \frac{(\gamma_{L_1V}{}^{d} + \gamma_{L_1V}{}^{p})}{2}(1+\cos\theta_1) \\
&\sqrt{\gamma_{L_2V}{}^{d}}\sqrt{\gamma_{SV}{}^{d}} + \sqrt{\gamma_{L_2V}{}^{p}}\sqrt{\gamma_{SV}{}^{p}} = \frac{\gamma_{L_2V}(1+\cos\theta_2)}{2} = \frac{(\gamma_{L_2V}{}^{d} + \gamma_{L_2V}{}^{p})}{2}(1+\cos\theta_2)
\end{aligned} \tag{23}$$

3.3.2 Wu Theory

Following Owen and Wendt, Wu [13], [72], [73] divided the surface free energy of a substance into dispersive and polar components. However, Wu claimed that the work of adhesion should be calculated as the harmonic mean of surface tensions, which leads the work of adhesion expressed as

$$W_{SL} = \frac{4\gamma_S{}^d\gamma_L{}^d}{\gamma_S{}^d + \gamma_L{}^d} + \frac{4\gamma_S{}^p\gamma_L{}^p}{\gamma_S{}^p + \gamma_L{}^p} \tag{24}$$

Following the same procedure of OWRK method, the Wu theory leads to

$$\frac{\gamma_S{}^d\gamma_L{}^d}{\gamma_S{}^d + \gamma_L{}^d} + \frac{\gamma_S{}^p\gamma_L{}^p}{\gamma_S{}^p + \gamma_L{}^p} = \frac{(\gamma_{LV}{}^d + \gamma_{LV}{}^p)(1 + \cos\theta)}{4} \tag{25}$$

Similar to the OWRK method, it is necessary to collect contact angle data from two liquids while using above equation for surface free energy characterization.

3.4 Three Component Theory

The three component theory is also known as the acid-base theory which was proposed by van Oss, Chaudhury, and Good. [7], [8], [19] This theory is currently the most precise surface free energy discussion, and hence adopted in the present study.

The surface free energy of a solid or a liquid is composed of apolar γ^{LW}, and polar terms γ^{AB}. The γ^{LW} term is Lifshitz-van der Waals interaction and also called non-polar surface tension. The γ^{AB} term can further divide into Lewis acid γ+, and Lewis base γ-, components, where γ+ and γ- stand for electron acceptor and donor capacity

respectively. γ^{AB} is also called acid-base component, which is two times geometric mean of acid and base components, Eq. (26).

$$\gamma_i^{AB} = 2\sqrt{\gamma_i^+ \gamma_i^-} \tag{26}$$

Some substances might only have apolar property, while most substances have both polar and apolar ones. For most cases, γ^+ and γ^- components of a material are not equal. [7], [8] Many polar substances are strong electron donors but have very little or even no capability to be electron acceptors. On the contrary, rare polar substances are electron acceptors but have no capability to be electron donors. In other words, for those polar substances, either one of Lewis acid or base surface free energy is zero. Such polar substances are described as monopolar whereas the rest are bipolar. [7]

A plastic's apolar γ^{LW}, Lewis acid $\gamma+$, and Lewis base $\gamma-$ surface free energy can be obtain by solving simultaneous van Oss-Chaudhury-Good equations, Eq. (27).

$$\begin{aligned}
\gamma_{L1}(1 + cos\theta_1) &= 2\left(\sqrt{\gamma_S^{LW}\gamma_{L1}^{LW}} + \sqrt{\gamma_S^+\gamma_{L1}^-} + \sqrt{\gamma_S^-\gamma_{L1}^+}\right) \\
\gamma_{L2}(1 + cos\theta_2) &= 2\left(\sqrt{\gamma_S^{LW}\gamma_{L2}^{LW}} + \sqrt{\gamma_S^+\gamma_{L2}^-} + \sqrt{\gamma_S^-\gamma_{L2}^+}\right) \\
\gamma_{L3}(1 + cos\theta_3) &= 2\left(\sqrt{\gamma_S^{LW}\gamma_{L3}^{LW}} + \sqrt{\gamma_S^+\gamma_{L3}^-} + \sqrt{\gamma_S^-\gamma_{L3}^+}\right)
\end{aligned} \tag{27}$$

Where θ is the acquired contact angle, γ_L is the total surface free energy of the testing liquid. Subscripts S, L, 1, 2, and 3 represent solid (in this study, most solids are

plastics), liquid, and three testing liquids respectively. Since contact angles data might carry error which originates from measuring and acquiring steps, Monte Carlo simulation needs to be applied into the calculation to estimate errors of γ_S^{LW}, γ_S^+, and γ_S^- . While processing Monte Carlo simulation, the average of contact angles is set as the mean value, and its standard deviation is set to be normal distribution. The mean value and standard deviation of plastics' surface free energy and plastic-liquid interaction can be obtained after thousands of iterations.

van Oss et al. [8]claimed that Lifshitz-vander Waals γ^{LW} and Lewis acid-base γ^{AB} surface free energy terms are additive, and the total surface free energy of a material or interaction between two materials is the sum of its apolar and polar surface free energy terms, Eq. (28).

$$\gamma^{TOT} = \gamma^{LW} + \gamma^{AB} \tag{28}$$

To investigate solids wettability, liquid-solid interaction is necessary to be mentioned because it plays an important role in forming shapes of liquid droplets on solid surfaces. Similar with surface free energy of a solid or a liquid, liquid-solid interaction also includes apolar γ^{LW}, and polar γ^{AB} terms. Cohesive and adhesive energies between two materials' compounds can be calculated by below equations. Good and Girifalco [20]proposed the combination rule of apolar γ^{LW} interaction between materials i and j as

$$\gamma_{ij}^{LW} = (\sqrt{\gamma_i^{LW}} - \sqrt{\gamma_j^{LW}})^2 = \gamma_i^{LW} + \gamma_j^{LW} - 2\sqrt{\gamma_i^{LW}\gamma_j^{LW}} \tag{29}$$

where γ_{ij}^{LW} represents the apolar cohesion.

van Oss et al. [7]proposed the polar (AB) interaction between materials i and j as:

$$\gamma_{ij}^{AB} = 2\left(\sqrt{\gamma_i^+} - \sqrt{\gamma_j^+}\right)\left(\sqrt{\gamma_i^-} - \sqrt{\gamma_j^-}\right) \\ = 2(\sqrt{\gamma_i^+\gamma_i^-} + \sqrt{\gamma_j^+\gamma_j^-} - \sqrt{\gamma_i^+\gamma_j^-} - \sqrt{\gamma_i^-\gamma_j^+}) \quad (30)$$

where the $\sqrt{\gamma_i^+\gamma_i^-} + \sqrt{\gamma_j^+\gamma_j^-}$ term represents polar cohesion and $\sqrt{\gamma_i^+\gamma_j^-} - \sqrt{\gamma_i^-\gamma_j^+}$ term represents polar adhesion.

For some special case, the polar interaction between a solid and a liquid, γ_{SL}^{AB}, reduces to polar component of a solid, γ_S^{AB}. This special case happens at the interaction between a solid and an apolar liquid. α-Bromonaphthalene (α-BN) and methylene iodide (MI) are such examples of the apolar liquids, which acid and base components are both zero ($\gamma_L^+ = \gamma_L^- = 0$). The polar interaction between a plastic and α-BN thus reduces to Eq. (31) as

$$\gamma_{SL}^{AB} = 2\left(\sqrt{\gamma_S^+} - \sqrt{\gamma_L^+}\right)\left(\sqrt{\gamma_S^-} - \sqrt{\gamma_L^-}\right) \\ = 2\left(\sqrt{\gamma_S^+} - 0\right)\left(\sqrt{\gamma_S^-} - 0\right) = \gamma_S^{AB} \quad (31)$$

where the polar adhesion no longer exists.

The polar interaction is not necessary positive, sometimes; it might have a negative value. From a mathematical perspective, $\gamma_{SL}^{AB} < 0$ happens at:

$$\gamma_S^+ > \gamma_L^+ \; and \; \gamma_S^- < \gamma_L^- \tag{32}$$

or

$$\gamma_S^+ < \gamma_L^+ \; and \; \gamma_S^- > \gamma_L^-$$

From the molecular interaction perspective, a negative polar interaction represents the polar cohesion is smaller than polar adhesion. This usually happens between a solid and a monopolar liquid. Ethylene glycol (EG) is such an example of the monopolar liquid, which acid component, γ_L^+, is close to zero, and its base component, γ_L^-, is relatively large. Therefore, the polar interaction between a plastic and EG is often negative, Eq. (32) and Table 12. In this study, de-ionized (DI) water was used a primary testing liquid, which has equal acid γ_L^+ and base γ_L^- components, Table 1. According to the measurement, plastics' acid and base components (

Table 9) are usually smaller than DI water's. Therefore, the polar interaction γ_{SL}^{AB} between DI water and plastics is always a positive value (Table 12).

3.5 Discussion

Several well-known surface free energy theories were introduced in this section. The comprehensive discussion of these theories would be included in the following.

All theories originate from the work of adhesion. This statement can be deduced from the mathematical format of each theory. No matter which theory, geometric mean of two substances' surface tensions always appear in the equations. Although the Wu theory

uses the harmonic mean, its formulation is still based on the work of adhesion but different mathematical approach.

The Zisman method is to find the critical surface tension of a solid. The extrapolated method is used to find the maximum of surface tension of a liquid which can fully wet (i.e. cosθ=1) the solid surface. This theory assumes there is only one component in solid's surface free energy. From the perspective of three component theory, the Zisman theory is considered as the simplification of van Oss-Chaudhury-Good equations, Eq. (20), in which acid and base components of both liquid and solid are neglected. The simplified equation is expressed as

$$\gamma_L(1 + cos\theta) = 2\left(\sqrt{\gamma_S\gamma_L}\right) \tag{33}$$

Simplifying the above equation, the surface free energy of a solid can be expressed as

$$\gamma_S = \frac{\gamma_L(1 + cos\theta)^2}{4} \tag{34}$$

Equation (34) shows that the surface free energy of a solid can be characterized by only one liquid which contact angle and surface tension are known parameters. Apparently, this is not the Zisman method which uses several liquids to approach the critical surface tension of a solid. However, it is the very reason that the Zisman method is challenged. Because the Zisman method can only apply to dispersive surfaces, such as some polymers. Indeed, all Zisman plot display that cosθ is inverse proportional to the γ_L. However, cosθ and γ_L do not necessarily have the linear relation. Figure 11 demonstrates the Zisman plot for poly(methyl methacrylate), in which the fitting line doesn't have

very high correlation coefficient. For such case, the critical surface tension obtained from extrapolation could have the error. According to Equation (34), Figure 12 illustrates the nonlinear relation between cosθ and γ_L when a solid's surface free energy is 35mN/m. However, the Zisman method, shown in the solid line, would result a smaller critical surface tension of a solid than its theoretical value. In fact, the Zisman method has its limit on solid surfaces with high surface free energy. This is because this theory has an assumption that there is no polar component of a solid's surface free energy. Therefore, it is inadequate to apply the Zisman method for all solid surfaces. [69], [74], [75]

The other one component theory, Neumann's equation of state, also has its limit applying to the solid surface which has strong interaction with a liquid. For some cases, [74], [76] this approach is impractical, although other cases can give acceptable fittings. [70], [75] The fitting constant β has been the target of arguments, which was challenged for being a constant for all solid and liquid pairs. [75] Negligence of spreading pressure contributions to surface tension is the common deficiency of both one component theories, [76] which reduces their applicability to characterize surface free energy of arbitrary solids.

Two component theory, Owens/Wendt and Fowkes theory, is apparently more reliable than Zisman and Neumann's methods. Zenkiewicz [77] reported his study on surface free energy calculations based on various theories. He indicated that surface free energy results obtained from OWRK and van Oss-Chaudhury-Good equation can have lower

than 3% difference, while results obtained from OWRK and Neumann's theory can reach the difference to at most 21%. Using multiple component theories can reach close surface free energy result is because these theories take polar and other components into consideration. However, several studies indicated that the methodology of contact angle measurement takes an important role. [69], [77], [78] For examples, a solid surface with different pH values would result in different contact angles which inevitably lead to various surface free energy results. Volpe et al. provided their practical comments that liquid-solid surface interaction calculation should be more precisely made than evaluate the surface free energy of a solid. [78] The author agrees with this perspective because interfacial tension is not directly calculated from contact angle data. Error is inevitable to appear in the contact angle measurement. An input with uncertainty will defiantly lead to the uncertain output. Therefore, surface free energy calculation cannot rely on contact angle data obtained from single test. In practical, Monte Carlo simulation is a good method to deal with input errors and return the mean value of surface free energy with standard deviation. For interfacial tension calculation, inputs are acid and base components which obtained from van Oss-Chaudhury-Good equation. Such inputs carry with errors from contact angle measurements and hence result calculation errors within interfacial tensions. Therefore, a meaningful report of surface free energy should include mean value and standard deviation. Also, the methodology of contact angle measurement should be mentioned at the same time. This criterion was followed in following sections.

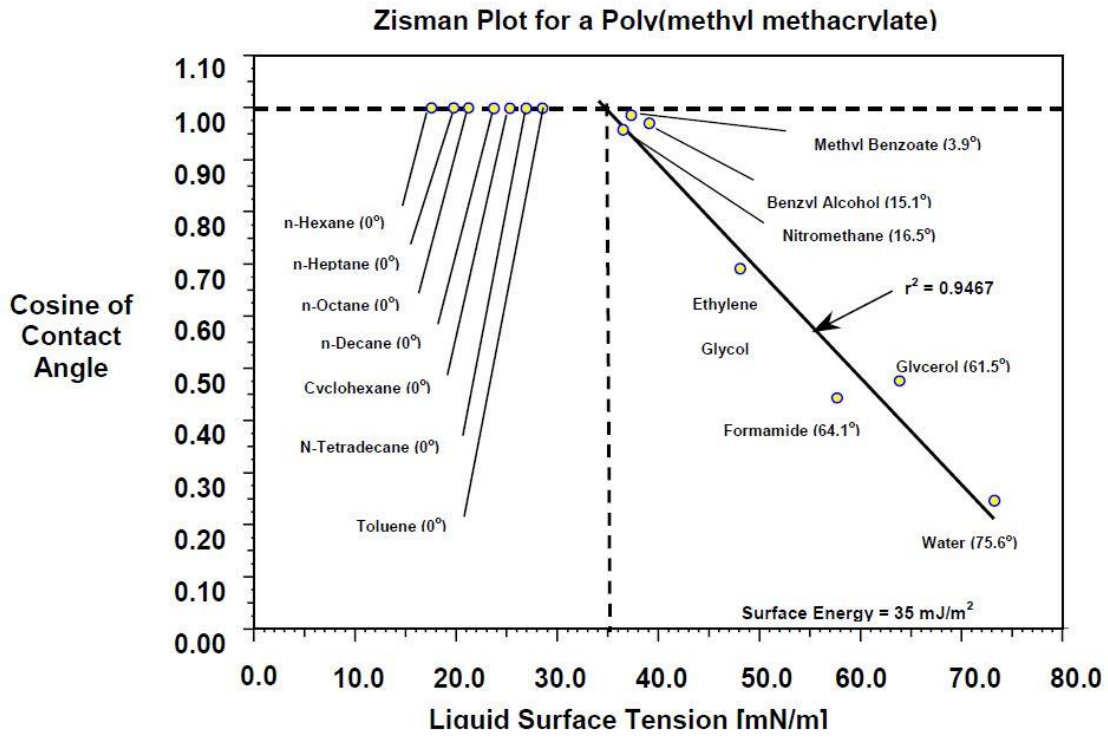

Figure 11. The Zisman plot for poly(methyl methacrylate) surface energy. The critical surface energy was approached as 22.8mJ/m^2. However, its correlation coefficient is not as high as LDPE has. [69]

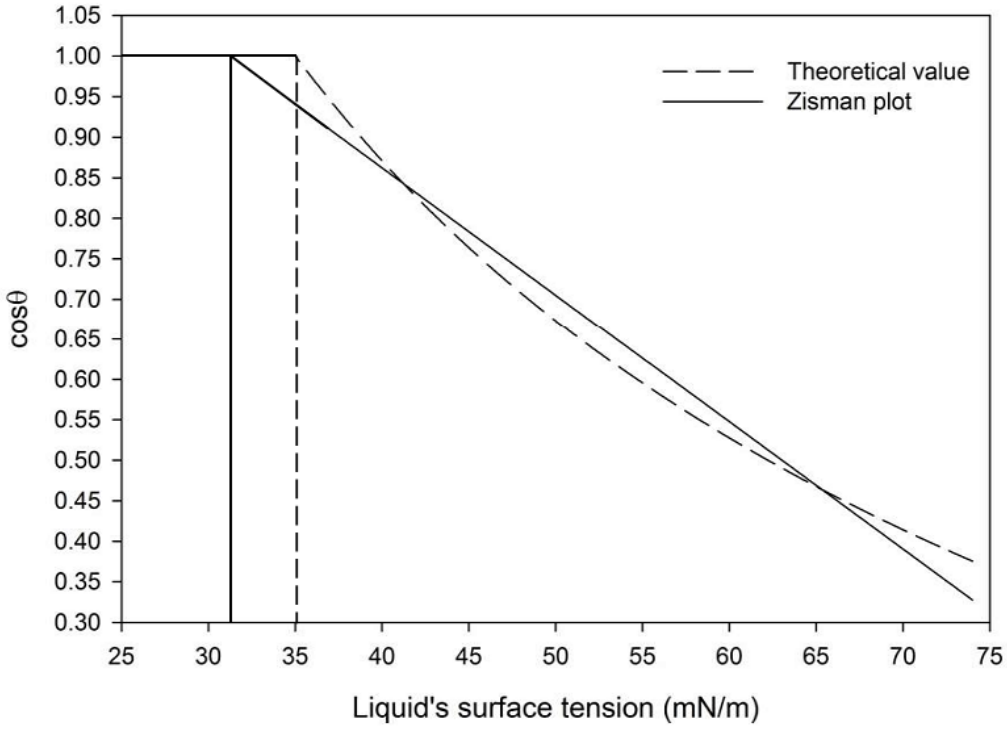

Figure 12. The Zisman plot (solid line) of a solid which surface free energy is 35 mN/m. Theoretical values (dash line) were obtained from Equation (34).

4 EMPIRICAL STUDY AND PREDICTION OF CONTACT ANGLE AND SURFACE FREE ENERGY OF COMMONLY USED PLASTICS WITH PILLAR-LIKE STRUCTURE*

In this section, the author studied contact angles of three liquids which include de-ionized (DI) water, ethylene glycol (EG), and α-Bromonaphthalene (α-BN), contacting with five commonly used plastics. These plastics include PET, PP, HDPE, LDPE, and PVC which have non-structured and structured surfaces. The author aims to understand the structure effect on liquids' contact angle and plastics' surface free energy change. Therefore, the author started from the contact angle measurement on non-structured plastic surfaces, which obtained results as the control group. These results were then compared with results from the treatment group which obtained from structured surfaces. The comparisons clarified the role what surface structures play in liquids contact angle performances. According to the result, all liquid-solid combinations have similar trends of contact angle changes on structured surfaces. The result hence implies that contact angles on structured surfaces may be predictable from data obtained from non-structured surfaces. The prediction and contact angle study were reported in section 4.2.1. As mentioned in section 3, the change of contact angle originates from the change of surface free energy. Therefore, in section 4.2.2, the author inevitably discussed how

* Part of this section is reprinted with permission from "Empirical Study and Prediction of Contact Angle and Surface Free Energy of Commonly Used Plastics with Pillar-like Structure by Chung-Han Chiou, Sheng-Jen Hsieh, Surface and Interface Analysis, 47, 1, 45-55, Copyright (2015) by Wiley.

surface structures affect plastics' surface free energy. The predictability of plastics' surface free energy on structured surfaces was mentioned and examined by liquid-solid interactions. This section starts from explanation of testing liquids' selection and fabrication of surface structures.

4.1 Material and Methods

4.1.1 Design of Experiments

There are two major experiments processed in the present study, which will be done sequentially followed the process chart. The first one is contact angle experiment, which was designed to build up the foundation of the present study. To understand how surface structures affect liquids' contact angle hysteresis and sliding behaviors on polymers, it is necessary to investigate how surface structures affect the wettability and surface free energy of plastics in advance. Measuring contact angle is the most intuitive approach to understand plastics' wettability and surface free energy. In order to understand the effect of surface structures, contact angle data obtained from non-structured plastics' surfaces was classified as the control group. On the other hand, contact angle data obtained from plastics' surfaces with surface structures was classified as the treatment group. For each plastic-liquid combination, the surface structure was the only independent variable, and the contact length ratio σ, was the parameter of the surface fraction. For cross-materials comparisons, plastics and testing liquids could be independent variables. All contact angle data was obtained from surfaces of plastic samples which were placed

horizontally, i.e. the tilting angle of testing rig was 0º. While measuring contact angles, the volume of each liquid droplet dispensed onto plastics' surfaces was controlled to be 10μL. Therefore, the droplet volume and tilting angle of testing rig were control variables. Measured contact angles and calculated surface free energy were dependent variables of preliminary experiments. Overall, there were fifteen plastic-liquid combinations composed by five plastics and three testing liquids. For each plastic-liquid combination, contact angle and surface free energy were measured and calculated at four surface fractions. By such experiment designs, outcomes could be compared at various surface fractions for the same plastic-liquid combination. In addition, outcomes could also be compared cross-materials. All experiment variables are listed in Table 4.

Table 4. Variable lists of contact angle experiments.

Variable	**Value**	**Type**
Plastics	PET, PP, HDPE, LDPE, PVC	Dependent variable / Control variable
Testing liquids	DI Water, Ethylene Glycol, α-Bromonaphthalene	Dependent variable / Control variable
Tilting angle of testing rig	0º, horizontal	Control variable
Droplet volume	10μL / ea.	Control variable
Surface structure parameter	σ=1, flat surface (Control group)	Independent variable
	σ=1.64, 1.80, 1.96 structured surface (Treatment group)	
Contact angle	0º ~ 90º	Dependent variable
Surface free energy	-30 mN/m^2 ~ 70 mN/m^2	Dependent variable

4.1.2 Testing Liquid Selection

According to the van Oss-Chaudhury-Good equation, Equation (27), apolar, Lewis acid, and Lewis base surface free energy of a plastic are able to be characterized only if a plastic's contact angles are collected from three testing liquids. Besides, at least two testing liquids must be polar. For this purpose, three well-characterized liquids, de-ionized (DI) water, ethylene glycol (EG, $C_2H_4(OH)_2$), and α-Bromonaphthalene (α-BN, $C_{10}H_7Br$), are selected as testing liquids in the present study. The polarities of selected testing liquids are bipolar, monopolar, and apolar, which makes the van Oss-Chaudhury-Good equation solvable. The surface free energy and polarity of selected testing liquids are shown in Table 5.

$$\gamma_L(1+cos\theta) = 2(\sqrt{\gamma_S^{LW}\gamma_L^{LW}} + \sqrt{\gamma_S^{+}\gamma_L^{-}} + \sqrt{\gamma_S^{-}\gamma_L^{+}}) \quad (27)$$

4.1.3 Fabrication of Solid Surfaces with Pillar-Like Structure

Surface structure is the key factor to affect the solids' wetting performances. Pillar-like structure, due to its symmetry, ease of fabrication, and liquids storage capability, was selected as the structure shape. Several approaches such as coating [79], etching[52], crystallization[80], and deposition[53], [81] can be utilized to fabricate surfaces with specific structures. However, these approaches are complex and time consuming. Pressing method[82] is a relatively simple, fast, and easily-control approach. It is suitable to fabricate plastics' surface structures in hundred- micro scale. The pressing approach was hence adopted in the present study, and hydraulic press machine was used

to press the mesh fully embed into plastics surfaces, see Figure 13. Three metal meshes with various specifications are used to fabricate pillar-like structures on plastics' surfaces. Each plastic then has four samples with various pillar-like structures. The specifications of pillar-like structures on each sample are listed in Table 6.

Previous studies have confirmed that surface structure affects liquids' contact angle due to a change in three-phase contact line. [46], [47], [48], [56] Liquid droplets may have longer contact length on structured surfaces which leads a change in droplets' circumferences, Figure 14. To differentiate various levels of surface structures, contact length ratio σ, was proposed as a parameter of surface fraction, which can be defined as (Note σ =1 for the flat surface)

$$\sigma = \frac{\text{Pillar Width} + 2 \times \text{Pillar Height} + \text{Grove Width}}{\text{Pillar Width} + \text{Groove Width}} \tag{35}$$

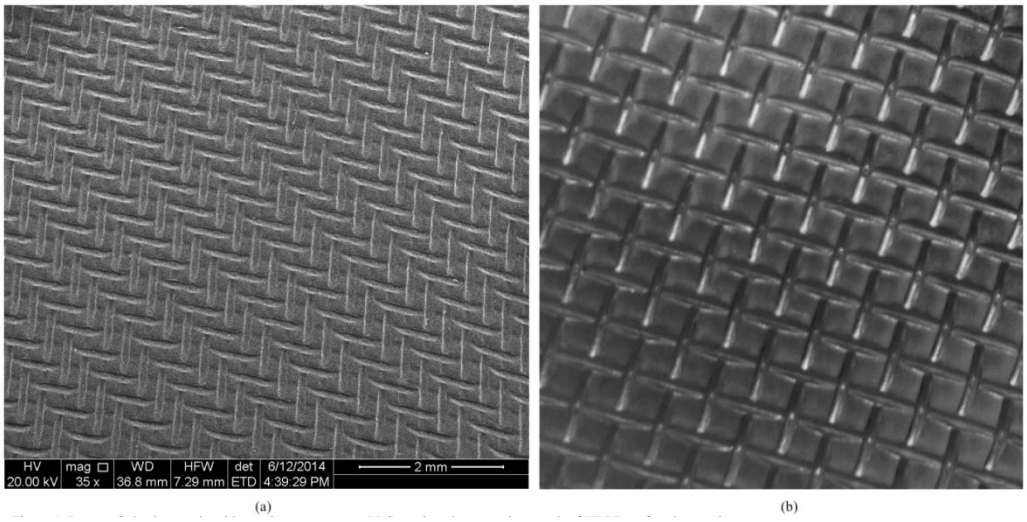

Figure 13. Image of plastic sample with symmetrically arranged structure. (a) Scanning electron micrograph of HDPE surface in top view. The 2-D groove structure in top view was made by pressing a metal mesh fully embed into the plastic surface, which results in the pillar-like structure in (b) side view.

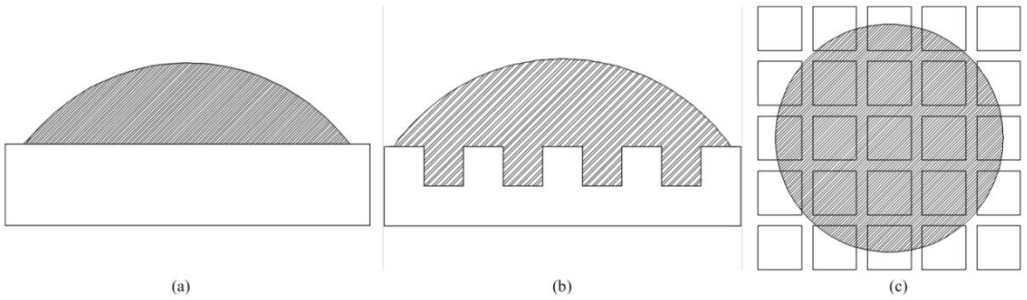

Figure 14. A liquid droplet sits on (a) a non-structured surface. (b) A structured surface which cause a change in its contact length and (c) circumference.

4.2 Result and Discussion

4.2.1 Contact Angle Analysis

The results of liquids' contact angles on plastics with various σ are shown and listed in Figure 15 and Table 7. It was found that DI water's contact angles on all five plastics increased as σ rose. However, ethylene glycol and α-BN had different contact angle performances. As σ increased, ethylene glycol had higher contact angles on PET and PP, fair performance on PVC, and lower contact angles on HDPE and LDPE. α-BN had different trends from DI water and ethylene glycol. As σ increased, its contact angles rose on PVC, remained fairly on HDPE and LDPE, and dropped on PET and PP. These results indicate that pillar-like structure changes liquids' contact angle performance. However, trends of structure effect depend on plastic-liquid combinations.

The correlation between liquids' contact angle and σ was investigated by calculation of correlation coefficient r. The results of all plastic-liquid combinations are listed in Table 8. High r values indicate the correlation between liquids contact angle and σ is leaner in the range of σ=1.0 to 1.96 for most plastic-liquid combinations. This outcome implies that liquids contact angle performance may be predicted by a linear regression model in the same range. Contact angle predictions of all liquid-solid combinations at σ=1.64, 1.8, and 1.96 are shown and listed in Figure 15 and Table 7, where predicted value was obtained from the linear regression line which best fits the other three actual values.

Table 7 also lists the error (%) of prediction to experiment values. It was found that most contact angle prediction errors are less than 6%, even for those liquid-plastic

combinations have low r values. As a consequence of low prediction errors, the linear regression model may be considered as a reliable approach to estimate liquids contact angles on these commonly used plastics in the range of σ=1.0 to 1.96. Obviously, pillar-like structure must affect plastics' surface polarity which leads a change in liquids contact angles, therefore, it is necessary to further investigate its effect on surface free energy.

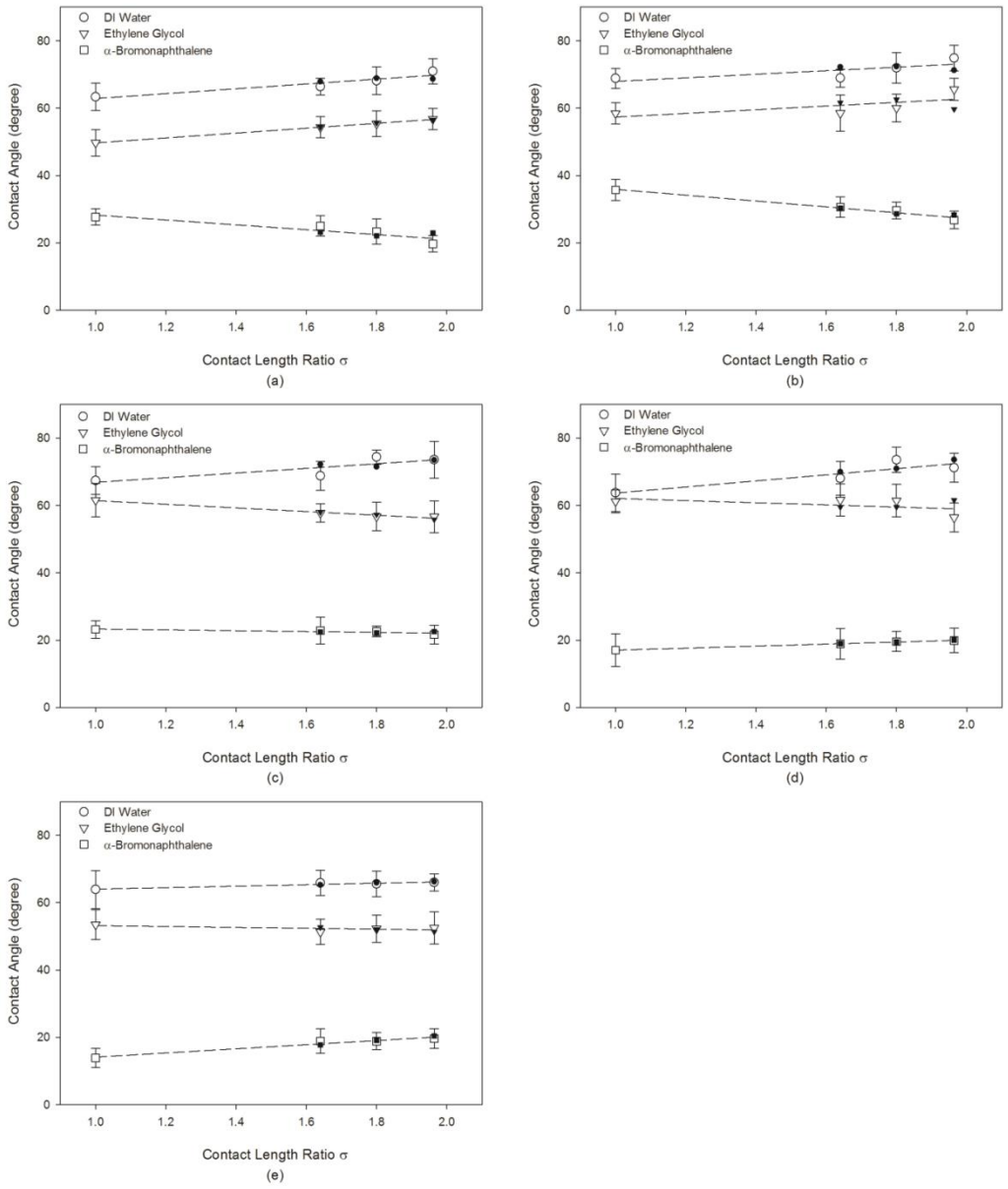

Figure 15. Liquids' contact angles on (a) PET (b) PP (c) HDPE (d) LDPE (e) PVC. White and black symbols stand for actual and predicted values respectively.

4.2.2 Surface Free Energy Analysis

Plastics' γ_S^{LW}, γ_S^+, γ_S^-, γ_S^{AB}, and γ_S^{TOT} were obtained from Equation (26), (27), and (28) and listed and illustrated in

Table 9 and Figure 16. It can be found from Figure 16 that both PET and PP had increasing trends of apolar and polar terms. This phenomenon leads to their similar trends of contact angle performances shown in Figure 15 (a) and (b). On the contrary, PVC had decreasing trends of both apolar and polar terms which results in that liquids' contact angle performances on PVC and PET are of difference. Both HDPE and LDPE had fair trends of apolar term which cause that α-BN's insignificant contact angle change. Although HDPE and LDPE had opposite trends of their polar terms at the first glance, their similar trends of contact angle performances could be explained by further discussion of Lewis acid γ_S^+ and base γ_S^- components. As shown in Figure 17 (c) and (d), both PEs had decreasing trend of γ_S^+, and increasing trend of γ_S^-. This result indicates that pillar-like structure weakens electron acceptor's capacity and enhances electron donor's capacity of both PEs. As a consequence, their polarities tend to become bipolar as σ increased. Since PEs' acid and base components had similar trends as s increased, their similar contact angle performances of polar liquids could be hence explained. The same explanation can also apply to PET and PP's contact angle performances, because they had the same trends of acid and base components. Pillar-like structure was found to enhance both acid and base components of PET and PP, and the greater enhancement of γ_S^+ leads their polarities tend to become monopolar as σ increased.

Figure 16 also displays that pillar-like structure had linear effects on plastics' γ_S^{LW}, γ_S^{AB}, and γ_S^{TOT}. This statement can be confirmed from Table 10, where correlation coefficients, r, of γ_S^{LW}, γ_S^{AB}, and γ_S^{TOT} are high. In addition, Table 10 lists correlation coefficients, r, of γ_S^+ and γ_S^-. High r of γ_S^+ indicates that pillar-like structure also has linear effects on plastics' γ_S^+. Although parts of r of γ_S^- are low, regression lines of γ_S^- shown in Figure 17 can still pass through the error bar of each data point. These outcomes arouse our speculation of plastics' surface free energy predictions by applying linear regression models.

Figure 16 and Figure 17 display predictions of plastics' surface free energy at σ=1.64, 1.8, and 1.96, where linear regression models of each plastic' surface free energy were developed by calculations of linear regression lines which best fit the other three actual values. The predicted values and errors are shown in

Table 9. It was found that linear regression models had outstanding performance of plastics' γ_S^{LW} and γ_S^{TOT} predictions. Although this approach seems to have ordinary performances on $\gamma_S^{AB}, \gamma_S^+,$ and γ_S^- numerically, the outcome can be ascribed that values of $\gamma_S^{AB}, \gamma_S^+,$ and γ_S^- are small and their errors are sensitive to slight disturbances. Although γ_S^- had the worst prediction performance, however, its predicted values illustrated in Figure 17 are located within the error range of each experiment value. Similar results happen on all plastics' γ_S^{AB} and γ_S^+ predictions which allow us to claim that the regression model is a reliable method to predict plastics' total, apolar, polar surface free energy and even acid and base components in the range of σ=1.0 to 1.96.

Results of plastics' surface free energy calculations can be used to validate liquids' contact angle predictions. The predicted values of liquids' contact angles were applied to Equation (27), and the calculated values of $\gamma_S^{LW}, \gamma_S^+,$ and γ_S^- were then applied to Equation (26) and (28) to obtain γ_S^{AB} and γ_S^{TOT}. It can be found from Table 11 that calculated values have good agreement with experiment values. This outcome validates liquids' contact angle predictions on structured plastics.

Liquids' contact angle on structured plastic surfaces can be further investigated by analyzing solid (plastic)-liquid interaction, which is the most important factor that influences shapes of liquid droplets. Since pillar-like structure has changed plastics' surface free energy, interfacial attractions and repulsions are hence altered. Experiment values of plastic-liquid apolar and polar interactions were obtained from Equation (29) and (30), and results are shown in Table 12. Aforementioned results reveal that pillar-like structure enhances electron donor's capacity of PET and PP. This consequence significantly affects PET's and PP's polar interactions with DI water (bipolar liquid) and EG (monopolar liquid). As σ increased, the difference of plastic's and DI water's electron donor's capacities γ^+ reduced, and hence causes PET's and PP's polar interactions with DI water decreased. On the contrary, the difference of plastic's and EG's γ^+ was amplified as σ increased, which makes absolute values of PET's and PP's polar interactions with EG increased. Note that the negative value comes from opposite signs of differences of plastics' and EG's γ^+ and γ^-. On the other hand, pillar-like structure makes PEs' electron donor's capacities decreased and electron acceptor's capacities increased, which consequently shrinks both differences of γ^+ and γ^- between

PEs and EG. Therefore, absolute values of polar interaction between PEs and EG decreases. Due to opposite trends of PEs' γ_S^+ and γ_S^-, their polar interactions with bipolar liquids, DI water, don't have significant change. Since apolar interactions of all plastic-liquid combinations are small, the overall interaction between a plastic and a liquid is actually dominated by their polar interaction.

Plastics' $\gamma_S^{LW}, \gamma_S^+,$ and γ_S^- predictions from linear regression approaches can be validated by calculating plastic-liquid interactions. The predicted $\gamma_S^{LW}, \gamma_S^+,$ and γ_S^- were applied to Equation (29) and (30), and results of each plastic-liquid interaction compared to experiment values are listed in Table 12. Note that since α-BN is an apolar liquid with zero value of acid and base components, its polar interaction with any plastic is actually the polar surface free energy of the plastic itself. Therefore, the predictions of plastics-α-BN polar interaction, γ_{SL}^{AB}, are identical to predictions of plastics' γ_S^{AB}. It was found that predicted plastic-liquid interactions agree with the existing experiment data. This result validates the predictions of plastics' $\gamma_S^{LW}, \gamma_S^+,$ and γ_S^-.

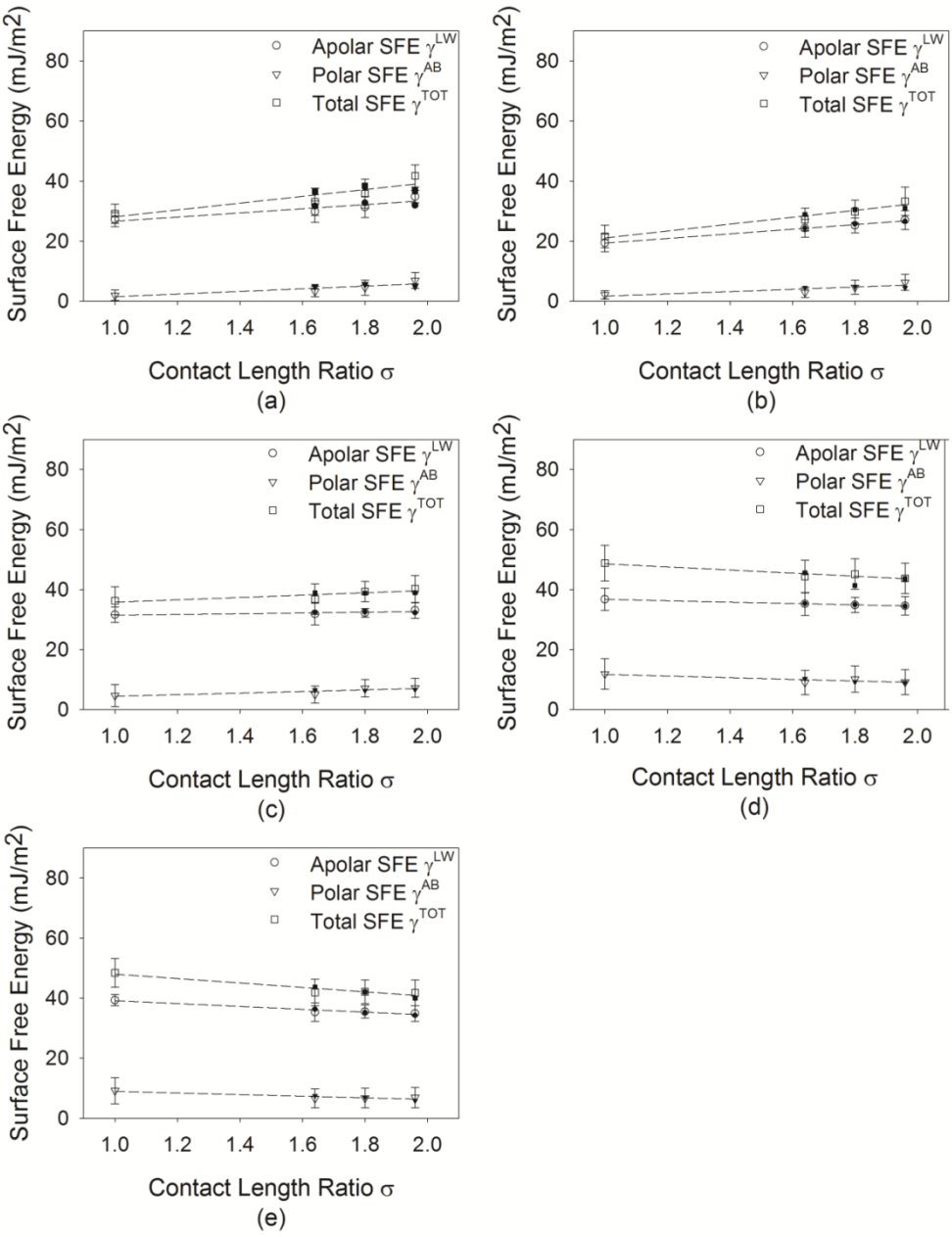

Figure 16. Apolar, polar, and total surface free energy of (a) PET (b) PP (c) HDPE (d) LDPE (e) PVC. White and black symbols stand for experiment and predicted values respectively.

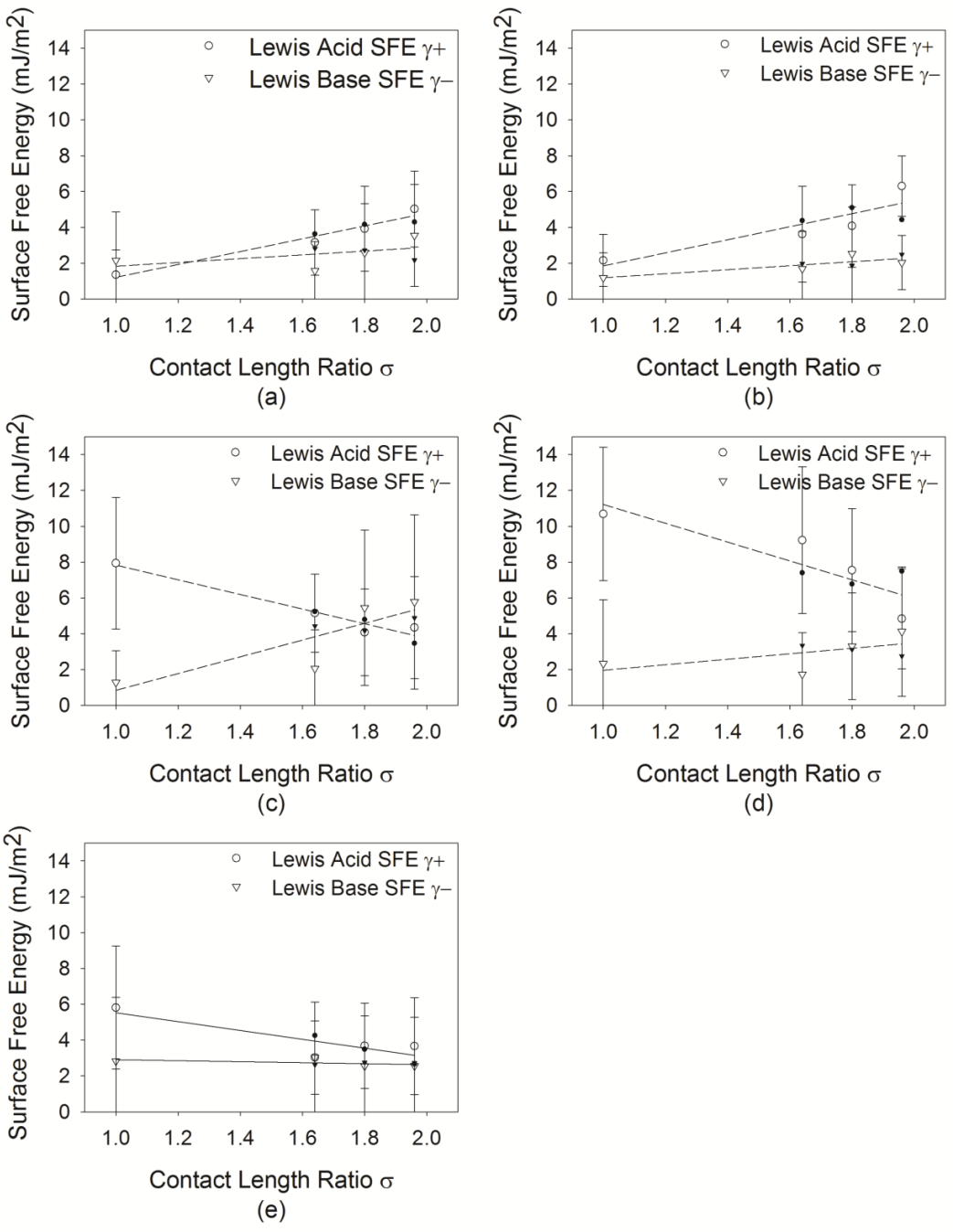

Figure 17. Lewis acid and base components of (a) PET(b) PP (c) HDPE (d) LDPE (e) PVC. White and black symbols stand for experiment and predicted values respectively.

4.3 Summary and Conclusion

Contact angles of DI water, EG, and α-BN on commonly used plastics with pillar-like structure were studied. It was found that pillar-like structure has linear effect on liquids' contact angles. The result was confirmed by high correlation coefficient, r. Due to the linear effect, liquids' contact angles may be predictable in the range of σ=1.0 to 1.96. Most of errors of contact angle predictions are less than 6% reveals the accuracy of linear regression models. Plastics' surface free energies at various σ were further studied. Predicted contact angles were also applied to surface free energy calculation. Contact angle predictions were validated by comparisons of experimental and calculated values. Furthermore, pillar-like structure also seems to have linear effect on plastics' surface free energy. High r values of σ and surface free energy indicate the existence of linear regression models. Low errors of predicted γ_S^{LW} and γ_S^{TOT} plus $\gamma_S^{AB}, \gamma_S^+,$ and γ_S^- having good agreement with the existing experiment data indicate accuracy of linear regression models. Results of surface free energy predictions were then applied to obtain plastic-liquid interactions. Outcomes were found to agree with the existing experiment data, which further validates the predictions of plastics' $\gamma_S^{LW}, \gamma_S^+,$ and γ_S^-. In addition, the empirical study of plastics' polarity change due to pillar-like structure was proposed. It was found that PET and PP tend to become monopolar, and PEs tend to become bipolar as σ increased. The research achievements provide the industry simple and rapid manufacturing approaches to control and estimate surface wettability and surface free energy of commonly used plastics. Since the structure effect has been proved to have linear relationship with liquids' contact angles, it is reasonable to investigate how

surface structure affects contact angle hysteresis when the solid surface stays no more horizontally. This study would also lead the investigation of liquids critical retention on inclined surfaces. Both studies are reported in the next section.

Table 5. Surface free energy of testing liquids.

Testing liquids	Total γ^{Total} (mN/m)	Apolar γ^{LW} (mN/m)	Lewis Acid γ^{+} (mN/m)	Lewis Base γ^{-} (mN/m)	Polarity
DI Water	72.8	21.8	25.5	25.5	Bipolar
Ethylene Glycol (EG)	48	29	1.92	47	Monopolar
α-Bromonaphthalene (α-BN)	44.4	44.4	0	0	Apolar

Table 6. Specifications of plastics' surface structures. The surface of Sample I is non-structured.

	Contact Length Ratio σ	Pillar Length / Width (μm)	Pillar Height / Groove Depth (μm)	Groove Length / Width (μm)
Sample I	1.00	-	-	-
Sample II	1.64	863	406	406
Sample III	1.80	381	254	254
Sample IV	1.96	109	101	101

Table 7. Liquids' contact angles (CA) on structured plastics. *Predicted Value.

Plastics	σ	DI Water CA (°)	DI Water CA (°)*	Error (%)	Ethylene Glycol CA (°)	Ethylene Glycol CA (°)*	Error (%)	α-BN CA (°)	α-BN CA (°)*	Error (%)
PET	1.00	63.3597± 4.0432	-	-	49.7432± 3.9141	-	-	27.6992± 2.4395	-	-
	1.64	66.3905± 2.4906	67.8825	2.2474	54.3730± 3.1079	54.3723	0.0013	25.0634± 3.0617	23.2146	7.3764
	1.80	68.1415± 4.1415	68.9036	1.1184	55.3938± 3.7859	55.6040	0.3795	23.3874± 3.7452	22.1124	5.4515
	1.96	70.9778± 3.7778	68.6627	3.2617	56.8167± 3.1357	56.5836	0.4102	19.7345± 2.4272	22.9708	16.3990
PP	1.00	68.8431± 2.9196	-	-	58.4838± 3.1725	-	-	35.7132± 3.1311	-	-
	1.64	68.9312± 2.6569	72.1829	4.7173	55.5299± 5.3521	61.6894	5.3981	30.6651± 3.0500	30.2729	1.2790
	1.80	71.9502± 4.5440	72.3274	0.5243	60.0761± 4.1411	62.5709	4.1527	29.6656± 2.4731	28.6559	3.4036
	1.96	74.8946± 3.7899	71.2586	4.8548	65.6215± 3.2593	59.7222	8.9899	26.7999± 2.6191	28.3411	5.7508
HDPE	1.00	67.3972± 4.0733	-	-	61.5861± 4.9611	-	-	23.2057± 2.6268	-	-
	1.64	68.7915± 4.3657	72.1530	4.8865	57.7912± 2.7655	58.0493	0.4466	22.8711± 3.9378	22.4129	2.0034
	1.80	74.3713± 2.1047	71.4648	3.9081	56.7484± 4.1904	57.2914	0.9569	22.6014± 1.5925	22.1838	1.8477
	1.96	73.5749± 5.4493	73.4744	0.1366	56.6584± 4.7365	55.8219	1.4764	21.6429± 2.8141	22.5622	4.2476
LDPE	1.00	63.7313± 5.5811	-	-	61.2532± 3.3803	-	-	16.9889± 4.8591	-	-
	1.64	68.0384± 5.0428	69.9657	2.8327	61.6221± 4.7758	59.5265	3.4007	18.9441± 4.5605	18.9996	0.2930
	1.80	73.5414± 3.7561	70.9248	3.5580	61.4434± 4.8163	59.5450	3.0897	19.6296± 2.9688	19.4818	0.7529
	1.96	71.1903± 4.2897	73.5643	3.3347	56.4060± 4.3181	61.6000	9.2082	19.8949± 3.6314	20.0715	0.8877
PVC	1.00	63.8714± 5.6525	-	-	53.4827± 4.4049	-	-	13.8684± 2.8163	-	-
	1.64	65.8652± 3.7616	65.2467	0.9390	51.2860± 3.7319	52.6908	2.7391	18.8878± 3.6437	17.7658	5.9403
	1.80	65.5261± 3.8281	65.8679	0.5216	52.2711± 4.0688	52.0639	0.3964	18.8636± 2.5663	19.1120	1.3168
	1.96	66.0044± 2.5269	66.2239	0.3326	52.5023± 4.8238	51.3565	2.1824	19.6198± 2.9308	20.4230	4.0938

Table 8. Correlation coefficient (r) of liquids' contact angles and contact length ratio σ.

	PET	PP	HDPE	LDPE	PVC
DI Water	0.9481	0.7707	0.8421	0.8995	0.9482
EG	0.9994	0.6777	0.9889	0.5317	0.5981
α-BN	0.9107	0.9851	0.8214	0.9970	0.9767

Table 9. Plastics' surface free energy. *Predicted Value.

Plastics	σ	γ_S^{LW}	γ_S^{LW*}	Error (%)	γ_S^{AB}	γ_S^{AB*}	Error (%)
PET	1.00	27.1964 ± 2.3876	-	-	1.9580 ± 1.7600	-	-
	1.64	29.8451 ± 3.5899	31.4934	5.5228	3.2280 ± 1.7050	4.7031	45.6978
	1.80	31.3357 ± 3.4920	32.5934	4.0137	4.5073 ± 2.5276	5.2923	17.4157
	1.96	34.8204 ± 2.0820	31.8007	8.6723	6.9197 ± 2.6700	4.5958	33.5842
PP	1.00	19.4028 ± 2.9708	-	-	2.1394 ± 1.3436	-	-
	1.64	24.2946 ± 2.9768	24.2962	0.0067	2.9117 ± 1.7449	4.5609	56.6415
	1.80	25.2407 ± 2.4722	25.6712	1.7056	4.6137 ± 2.3618	4.8205	4.4823
	1.96	27.0094 ± 3.1465	26.5296	1.7766	6.3003 ± 2.6385	4.4475	29.4075
HDPE	1.00	31.5851 ± 2.5134	-	-	4.6756 ± 3.6388	-	-
	1.64	31.8459 ± 3.5822	32.3531	1.5926	5.0180 ± 2.8365	6.5142	29.8167
	1.80	32.2397 ± 1.4570	32.5125	0.8463	7.1500 ± 2.8399	6.2899	12.0294
	1.96	33.0289 ± 2.5975	32.2267	2.4289	7.2651 ± 3.0947	6.7483	7.1132
LDPE	1.00	36.7956 ± 3.7022	-	-	11.8903 ± 5.0546	-	-
	1.64	35.2283 ± 3.8161	35.2785	0.1426	9.0060 ± 4.0390	10.2711	14.0476
	1.80	34.8352 ± 2.5510	34.9147	0.2283	10.1973 ± 4.3861	9.1885	9.8930
	1.96	34.5815 ± 3.1420	34.4438	0.3982	9.1451 ± 4.1368	9.0210	1.3574
PVC	1.00	39.3000 ± 1.8600	-	-	9.1500 ± 4.3600	-	-
	1.64	35.3400 ± 3.0700	36.2900	2.6882	6.5500 ± 3.1500	7.4172	13.2395
	1.80	35.4800 ± 2.1800	35.1957	0.8013	6.6500 ± 3.2600	6.8257	2.6423
	1.96	34.8400 ± 2.5500	34.2209	1.7769	6.8700 ± 3.3900	5.8213	15.2647

Table 9. Continued

Plastics	σ	γ_S^{TOT}	γ_S^{TOT*}	Error (%)	γ_S^{+}	γ_S^{+*}	Error (%)
PET	1.00	29.1544 ± 3.2110	-	-	1.3605 ± 1.3788	-	-
	1.64	33.0731 ± 4.5433	36.1967	9.4444	3.1596 ± 1.8272	3.6302	14.8947
	1.80	35.8430 ± 4.8895	37.8857	5.6990	3.9238 ± 2.3616	4.1625	6.0824
	1.96	41.7402 ± 3.7287	36.3964	12.8024	5.0269 ± 2.1213	4.2986	14.4875
PP	1.00	21.5422 ± 3.7223	-	-	2.1547 ± 1.4541	-	-
	1.64	27.2063 ± 3.8294	28.8569	6.0669	3.6210 ± 2.6640	4.3783	20.9146
	1.80	29.8544 ± 3.8201	30.4917	2.1347	4.0793 ± 2.2977	5.1042	25.1254
	1.96	33.3097 ± 4.6798	30.9770	7.0031	6.3082 ± 1.6857	4.4241	29.8678
HDPE	1.00	36.2608 ± 4.6389	-	-	7.9365 ± 3.6822	-	-
	1.64	36.8640 ± 5.0940	38.8672	5.4341	5.1474 ± 2.1855	5.2318	1.6388
	1.80	39.3898 ± 3.3817	38.8026	1.4906	4.0716 ± 2.4263	4.7870	17.5710
	1.96	40.2940 ± 4.4832	38.9751	3.2732	4.3424 ± 2.8535	3.4645	20.2161
LDPE	1.00	48.8368 ± 5.9493	-	-	10.6827 ± 3.7210	-	-
	1.64	44.3641 ± 5.4611	45.6497	2.8978	9.2237 ± 4.0918	7.4000	19.7715
	1.80	45.1615 ± 5.0716	41.3750	2.8764	7.5436 ± 3.4350	6.7723	10.2243
	1.96	43.7608 ± 5.1100	43.5871	0.3969	4.8364 ± 2.8067	7.4921	54.9099
PVC	1.00	48.4200 ± 4.7500	-	-	5.8100 ± 3.4300	-	-
	1.64	41.8900 ± 4.4300	43.7068	4.3370	3.0300 ± 2.0500	4.2564	40.4754
	1.80	42.1000 ± 3.9000	42.0489	0.1213	3.6800 ± 2.3900	3.4889	5.1918
	1.96	41.7600 ± 4.2500	40.0277	4.1481	3.6594 ± 2.6920	2.6647	27.1816

Table 9. Continued

Plastics	σ	γ_S^-	γ_S^{-*}	Error (%)
PET	1.00	2.1616 ± 2.7102	-	-
	1.64	1.5850 ± 1.6160	2.8294	78.5085
	1.80	2.5895 ± 2.7448	2.7300	5.4242
	1.96	3.5525 ± 2.8510	2.1718	38.8651
PP	1.00	1.1945 ± 1.3781	-	-
	1.64	1.6940 ± 2.0867	1.9830	17.0595
	1.80	2.5310 ± 2.6127	1.8748	25.9257
	1.96	2.0417 ± 1.5164	2.4863	21.7783
HDPE	1.00	1.2817 ± 1.7562	-	-
	1.64	2.0593 ± 2.1632	4.4294	115.0939
	1.80	5.4482 ± 4.3334	4.1585	23.6724
	1.96	5.7813 ± 4.8685	4.8819	15.5568
LDPE	1.00	2.3333 ± 3.5656	-	-
	1.64	1.7398 ± 2.3180	3.3402	91.9890
	1.80	3.3036 ± 2.9810	3.1208	5.5321
	1.96	4.1194 ± 3.6165	2.7476	33.2999
PVC	1.00	2.8300 ± 3.5500	-	-
	1.64	3.0300 ± 3.0800	2.6290	13.2343
	1.80	2.5500 ± 2.8000	2.7520	7.9216
	1.96	2.5560 ± 2.7300	2.7262	6.6599

Table 10. Correlation coefficient (r) of plastics' $\gamma_S^{TOT}, \gamma_S^{LW}, \gamma_S^{AB}, \gamma_S^+, \gamma_S^-$ and contact length ratio σ.

	γ_S^{TOT}	γ_S^{LW}	γ_S^{AB}	γ_S^+	γ_S^-
PET	0.9003	0.9191	0.8510	0.9772	0.5758
HDPE	0.7910	0.8388	0.7441	0.9681	0.8401
PVC	0.9548	0.9729	0.9122	0.8551	0.4997
LDPE	0.8686	0.9956	0.8676	0.8747	0.5949
PP	0.9828	0.9848	0.9832	0.8303	0.7089

Table 11. Plastics' surface free energy. *Obtained from van Oss-Chaudhury-Good equation by applying predicted contact angles.

Plastics	σ	γ_S^{LW}	γ_S^{LW*}	γ_S^{AB}	γ_S^{AB*}
PET	1.00	27.1964 ± 2.3876	-	1.9580 ± 1.7600	-
	1.64	29.8451 ± 3.5899	31.6746	3.2280 ± 1.7050	4.9263
	1.80	31.3357 ± 3.4920	32.7088	4.5073 ± 2.5276	5.7204
	1.96	34.8204 ± 2.0820	31.9053	6.9197 ± 2.6700	5.1665
PP	1.00	19.4028 ± 2.9708	-	2.1394 ± 1.3436	-
	1.64	24.2946 ± 2.9768	24.7003	2.9117 ± 1.7449	4.8168
	1.80	25.2407 ± 2.4722	26.3271	4.6137 ± 2.3618	5.0732
	1.96	27.0094 ± 3.1465	26.6430	6.3003 ± 2.6385	5.1093
HDPE	1.00	31.5851 ± 2.5134	-	4.6756 ± 3.6388	-
	1.64	31.8459 ± 3.5822	32.4291	5.0180 ± 2.8365	7.5668
	1.80	32.2397 ± 1.4570	32.6426	7.1500 ± 2.8399	7.2533
	1.96	33.0289 ± 2.5975	32.2896	7.2651 ± 3.0947	8.2249
LDPE	1.00	36.7956 ± 3.7022	-	11.8903 ± 5.0546	-
	1.64	35.2283 ± 3.8161	35.4869	9.0060 ± 4.0390	6.2059
	1.80	34.8352 ± 2.5510	35.0723	10.1973 ± 4.3861	6.9995
	1.96	34.5815 ± 3.1420	34.5570	9.1451 ± 4.1368	8.4983
PVC	1.00	39.3000 ± 1.8600	-	9.1500 ± 4.3600	-
	1.64	35.3400 ± 3.0700	36.5174	6.5500 ± 3.1500	4.3279
	1.80	35.4800 ± 2.1800	35.3908	6.6500 ± 3.2600	4.6867
	1.96	34.8400 ± 2.5500	34.2456	6.8700 ± 3.3900	4.7032

Table 11. Continued

Plastics	σ	γ_S^{TOT}	γ_S^{TOT*}	γ_S^+	γ_S^{+*}
PET	1.00	29.1544 ± 3.2110	-	1.3605 ± 1.3788	-
	1.64	33.0731 ± 4.5433	36.6009	3.1596 ± 1.8272	3.1068
	1.80	35.8430 ± 4.8895	38.4292	3.9238 ± 2.3616	3.8562
	1.96	41.7402 ± 3.7287	37.0719	5.0269 ± 2.1213	4.2434
PP	1.00	21.5422 ± 3.7223	-	2.1547 ± 1.4541	-
	1.64	27.2063 ± 3.8294	29.5171	3.6210 ± 2.6640	4.3976
	1.80	29.8544 ± 3.8201	31.4002	4.0793 ± 2.2977	5.4015
	1.96	33.3097 ± 4.6798	31.7524	6.3082 ± 1.6857	4.0761
HDPE	1.00	36.2608 ± 4.6389	-	7.9365 ± 3.6822	-
	1.64	36.8640 ± 5.0940	39.9959	5.1474 ± 2.1855	4.6576
	1.80	39.3898 ± 3.3817	39.8959	4.0716 ± 2.4263	4.3820
	1.96	40.2940 ± 4.4832	40.5145	4.3424 ± 2.8535	3.2024
LDPE	1.00	48.8368 ± 5.9493	-	10.6827 ± 3.7210	-
	1.64	44.3641 ± 5.4611	41.6928	9.2237 ± 4.0918	6.9757
	1.80	45.1615 ± 5.0716	42.0718	7.5436 ± 3.4350	6.6506
	1.96	43.7608 ± 5.1100	43.0553	4.8364 ± 2.8067	7.3861
PVC	1.00	48.4200 ± 4.7500	-	5.8100 ± 3.4300	-
	1.64	41.8900 ± 4.4300	40.8453	3.0300 ± 2.0500	3.8038
	1.80	42.1000 ± 3.9000	40.0775	3.6800 ± 2.3900	3.0877
	1.96	41.7600 ± 4.2500	38.9488	3.6594 ± 2.6920	2.4403

Table 11. Continued

Plastics	σ	γ_S^-	γ_S^{-*}
PET	1.00	2.1616 ± 2.7102	-
	1.64	1.5850 ± 1.6160	1.9529
	1.80	2.5895 ± 2.7448	2.1215
	1.96	3.5525 ± 2.8510	1.5726
PP	1.00	1.1945 ± 1.3781	-
	1.64	1.6940 ± 2.0867	1.3190
	1.80	2.5310 ± 2.6127	1.1912
	1.96	2.0417 ± 1.5164	1.6011
HDPE	1.00	1.2817 ± 1.7562	-
	1.64	2.0593 ± 2.1632	3.0732
	1.80	5.4482 ± 4.3334	3.0015
	1.96	5.7813 ± 4.8685	5.2810
LDPE	1.00	2.3333 ± 3.5656	-
	1.64	1.7398 ± 2.3180	1.3803
	1.80	3.3036 ± 2.9810	1.8417
	1.96	4.1194 ± 3.6165	2.4445
PVC	1.00	2.8300 ± 3.5500	-
	1.64	3.0300 ± 3.0800	1.2311
	1.80	2.5500 ± 2.8000	1.7784
	1.96	2.5560 ± 2.7300	2.2661

Table 12. Plastic-liquid interaction. *Calculated from predicted plastics' surface free energy.

Plastics		σ	DI Water	DI Water*
PET	γ_{SL}^{LW}	1.00	0.3454 ± 0.2507	-
		1.64	0.7251 ± 0.5049	0.9196
		1.80	0.9456 ± 0.5630	1.1027
		1.96	1.5423 ± 0.4283	0.9593
	γ_{SL}^{AB}	1.00	30.6252 ± 6.4323	-
		1.64	26.1855 ± 3.8193	24.0113
		1.80	22.6740 ± 4.7044	22.1777
		1.96	18.5667 ± 3.3311	22.6968
PP	γ_{SL}^{LW}	1.00	0.1922 ± 0.2626	-
		1.64	0.1549 ± 0.1891	0.0905
		1.80	0.1827 ± 0.1843	0.2134
		1.96	0.3624 ± 0.3232	0.2427
	γ_{SL}^{AB}	1.00	30.0666 ± 4.1496	-
		1.64	25.4540 ± 4.3115	23.0386
		1.80	22.3276 ± 4.1658	21.5779
		1.96	18.9857 ± 2.8087	22.9396
HDPE	γ_{SL}^{LW}	1.00	0.9465 ± 0.4186	-
		1.64	1.0342 ± 0.6004	1.0519
		1.80	1.0316 ± 0.2576	1.0906
		1.96	1.2042 ± 0.4775	1.0269
	γ_{SL}^{AB}	1.00	18.9264 ± 5.3203	-
		1.64	21.3295 ± 4.1472	19.0654
		1.80	17.4594 ± 4.5070	19.6146
		1.96	16.7360 ± 4.8359	17.9423
LDPE	γ_{SL}^{LW}	1.00	2.0257 ± 0.8088	-
		1.64	1.6878 ± 0.7723	1.6590
		1.80	1.5579 ± 0.5230	1.5704
		1.96	1.5258 ± 0.6272	1.4628
	γ_{SL}^{AB}	1.00	14.4552 ± 5.8196	-
		1.64	16.3570 ± 5.2686	18.6662
		1.80	15.4841 ± 2.9940	18.2482
		1.96	18.2752 ± 4.1470	16.2600
PVC	γ_{SL}^{LW}	1.00	2.5741 ± 0.4629	-
		1.64	1.6753 ± 0.6577	1.8876
		1.80	1.6781 ± 0.4602	1.6383
		1.96	1.5500 ± 0.5100	1.3993
	γ_{SL}^{AB}	1.00	16.6684 ± 5.8608	-
		1.64	21.0160 ± 5.6153	24.4247
		1.80	20.5675 ± 5.5232	24.4715
		1.96	20.4900 ± 5.6700	24.7229

Table 12. Continued

Plastics		σ	Ethylene Glycol	Ethylene Glycol*
PET	γ_{SL}^{LW}	1.00	0.0835 ± 0.1157	-
		1.64	0.1152 ± 0.1552	0.0590
		1.80	0.1409 ± 0.1712	0.1116
		1.96	0.2946 ± 0.1779	0.0693
	γ_{SL}^{AB}	1.00	3.8217 ± 6.2988	-
		1.64	-4.0060 ± 6.3975	-4.1151
		1.80	-6.0717 ± 7.2029	-6.2422
		1.96	-8.8247 ± 5.9598	-7.5545
PP	γ_{SL}^{LW}	1.00	1.1021 ± 0.7102	-
		1.64	0.3088 ± 0.3213	0.1724
		1.80	0.1958 ± 0.2065	0.0646
		1.96	0.1318 ± 0.1915	0.0499
	γ_{SL}^{AB}	1.00	-0.1922 ± 6.0907	-
		1.64	-5.0281 ± 8.7659	-8.1204
		1.80	-6.6316 ± 6.9676	-10.8192
		1.96	-12.4404 ± 4.5744	-7.0806
HDPE	γ_{SL}^{LW}	1.00	0.1036 ± 0.1151	-
		1.64	0.1022 ± 0.0858	0.0958
		1.80	0.0895 ± 0.0577	0.1077
		1.96	0.1272 ± 0.0940	0.0883
	γ_{SL}^{AB}	1.00	-16.2935 ± 8.3184	-
		1.64	-9.7306 ± 6.1660	-7.8837
		1.80	-7.9339 ± 5.7331	-7.2510
		1.96	-6.4910 ± 7.7076	-3.6816
LDPE	γ_{SL}^{LW}	1.00	0.5492 ± 0.3768	-
		1.64	0.4000 ± 0.3258	0.3271
		1.80	0.3104 ± 0.2172	0.2884
		1.96	0.3123 ± 0.2542	0.2434
	γ_{SL}^{AB}	1.00	-20.3085 ± 6.1073	-
		1.64	-18.4797 ± 8.5513	-14.2646
		1.80	-14.2783 ± 8.4341	-13.1223
		1.96	-8.0537 ± 7.6811	-14.0994
PVC	γ_{SL}^{LW}	1.00	0.8001 ± 0.2582	-
		1.64	0.3711 ± 0.2920	0.4327
		1.80	0.3551 ± 0.2059	0.3179
		1.96	0.3048 ± 0.2199	0.2179
	γ_{SL}^{AB}	1.00	-10.0249 ± 7.0418	-
		1.64	-3.5375 ± 5.5218	-6.4896
		1.80	-5.3339 ± 6.0115	-4.1033
		1.96	-5.6645 ± 6.4622	-1.8888

Table 12. Continued

Plastics		σ	α-BN	α-BN*
PET	γ_{SL}^{LW}	1.00	2.1652 ± 0.6811	-
		1.64	1.5757 ± 0.8603	1.0719
		1.80	1.2537 ± 0.7279	0.8915
		1.96	0.6168 ± 0.2849	1.0299
	γ_{SL}^{AB}	1.00	1.9580 ± 1.7600	-
		1.64	3.2280 ± 1.7050	4.9263
		1.80	4.5073 ± 2.5276	5.7204
		1.96	6.9197 ± 2.6700	5.1665
PP	γ_{SL}^{LW}	1.00	5.2753 ± 1.5675	-
		1.64	3.1327 ± 1.0784	2.8676
		1.80	2.7683 ± 0.8247	2.3481
		1.96	2.2693 ± 0.9295	2.2549
	γ_{SL}^{AB}	1.00	2.1394 ± 1.3436	-
		1.64	2.9117 ± 1.7449	4.8168
		1.80	4.6137 ± 2.3618	5.0732
		1.96	6.3003 ± 2.6385	5.1093
HDPE	γ_{SL}^{LW}	1.00	1.1484 ± 0.4896	-
		1.64	1.1623 ± 0.7112	0.9383
		1.80	0.9903 ± 0.2572	0.9024
		1.96	0.8996 ± 0.4431	0.9622
	γ_{SL}^{AB}	1.00	4.6756 ± 3.6388	-
		1.64	5.0180 ± 2.8365	7.5668
		1.80	7.1500 ± 2.8399	7.2533
		1.96	7.2651 ± 3.0947	8.2249
LDPE	γ_{SL}^{LW}	1.00	0.4630 ± 0.4611	-
		1.64	0.6503 ± 0.5681	0.4988
		1.80	0.6328 ± 0.3542	0.5493
		1.96	0.6953 ± 0.4708	0.6159
	γ_{SL}^{AB}	1.00	8.1605 ± 7.5233	-
		1.64	6.0073 ± 4.5454	6.2059
		1.80	7.7651 ± 3.0316	6.9995
		1.96	6.6652 ± 2.9490	8.4983
PVC	γ_{SL}^{LW}	1.00	0.1824 ± 0.1237	-
		1.64	0.5911 ± 0.3890	0.3849
		1.80	0.5402 ± 0.2643	0.5102
		1.96	0.6225 ± 0.3292	0.6583
	γ_{SL}^{AB}	1.00	9.1598 ± 4.4598	-
		1.64	6.5226 ± 3.1876	4.3279
		1.80	6.7240 ± 3.2818	4.6867
		1.96	6.8742 ± 3.3935	4.7032

5 EMPIRICAL STUDY AND PREDICTION OF LIQUIDS RETENTION ON STRUCTURED POLYMER SURFACES*

In this section, the author reported the study of liquids' contact angle hysteresis and critical retention volume on inclined polymer surfaces. This study is the extending research of the previous section. The author aims to understand the structure effect on liquids' contact angle hysteresis and critical retention volume change, in which the investigation of liquids' retention must couple with the study of liquids' contact angle hysteresis. Therefore, the author started from the contact angle hysteresis measurement on non-structured plastic surfaces, which were then compared with results obtained from structured surfaces.

The liquid and plastic selections and the contact angle hysteresis measurement were reported in section 5.1, which also includes the structure fabrication. As mentioned in section 1, previous researches have proved that advancing and receding contact angles on non-structured surfaces could be linked by reduce hysteresis H. The availability of this statement was examined and confirmed on structured surfaces. Therefore, advancing contact angle became the main parameter being discussed in this section. The study of advancing contact angle on structured surfaces was mentioned in section 5.3.1, in which

* Part of this section is reprinted with permission from "Empirical study and prediction of liquids retention on structured polymer surfaces" by Chung-Han Chiou, Sheng-Jen Hsieh, Surface and Interface Analysis, 48, 3, 146-163, Copyright (2016) by Wiley.

data obtained from various combinations of liquids, plastics, surface inclined angle α, and contact length ratio σ was reported.

Liquids' retention on inclined surfaces is another major topic in this section. In section 5.2, the author formulated his own model of liquids' critical retention volume which adopts the new perspective of retention force. The proposed model was compared with previous ones and discussed in section 5.3.2. Observations of liquids' critical retention volume under various conditions of plastics, surface inclined angle α, and contact length ratio σ were also reported. In the same section, the comprehensive discussion of liquids' critical retention volume and advancing contact angles were also included.

Similar with the result obtain from previous section, surface structures were also found to have linear effect on advancing contact angles. The linear model of liquids' advancing contact angle estimations was proposed in section 5.3.3. The predicted advancing contact angle was used as a main input parameter of liquids' retention model. The predicted critical retention volumes were compared with experiment data, and the low error validated the prediction of advancing contact angles. Predicted results of advancing contact angles and critical retention volumes were reported in the same section.

5.1 Material and Methods

5.1.1 Design of Experiments

There are two major experiments processed in the present study, which will be done sequentially followed the process chart. The first one is contact angle experiment, which

was designed to build up the foundation of the present study. To understand how surface structures affect liquids' contact angle hysteresis and sliding behaviors on polymers, it is necessary to investigate how surface structures affect the wettability and surface free energy of plastics in advance. Measuring contact angle is the most intuitive approach to understand plastics' wettability and surface free energy. In order to understand the effect of surface structures, contact angle data obtained from non-structured plastics' surfaces was classified as the control group. On the other hand, contact angle data obtained from plastics' surfaces with surface structures was classified as the treatment group. For each plastic-liquid combination, the surface structure was the only independent variable, and the contact length ratio σ, was the parameter of the surface fraction. For cross-materials comparisons, plastics and testing liquids could be independent variables. All contact angle data was obtained from surfaces of plastic samples which were placed horizontally, i.e. the tilting angle of testing rig was 0º. While measuring contact angles, the volume of each liquid droplet dispensed onto plastics' surfaces was controlled to be 10μL. Therefore, the droplet volume and tilting angle of testing rig were control variables. Measured contact angles and calculated surface free energy were dependent variables of preliminary experiments. Overall, there were fifteen plastic-liquid combinations composed by five plastics and three testing liquids. For each plastic-liquid combination, contact angle and surface free energy were measured and calculated at four surface fractions. By such experiment designs, outcomes could be compared at various surface fractions for the same plastic-liquid combination. In addition, outcomes could also be compared cross-materials. All experiment variables are listed in Table 4.

The second major experiment's purpose is to understand the effect of surface structures on liquids' contact angle hysteresis and onset of sliding behaviors on polymers, which both happen if samples placed non-horizontally. Data of liquids' contact angle hysteresis and critical retention volumes obtained from non-structured polymer surfaces is classified to control group. Data of both measurements obtained from structured polymer surfaces is classified to treatment group.

For each plastic sample with specific contact length ratio σ, contact angle hysteresis will be measured at a series of tilting angles between 45º ~ 90º, 15º per increment. Control variables include plastic and liquid materials, liquid dispensed volume, and contact length ratio σ. Independent and dependent variables are tilting angle of testing rig and contact angle hysteresis respectively. This design of experiment allows the author to obtain a series of advancing and receding contact angle data at various σ for each plastic-liquid combination. Effects of surface structure on contact angle hysteresis can thus be determined by comparing the data obtained at various σ.

There is a more specific definition of onset of liquids' sliding behavior. In the present study, studying the onset of sliding behavior refers to studying the condition when the droplet starts to move downward on an inclined plastic surface. Due to the gravity effect, a liquid droplet will eventually leave its original location on an inclined plastic surface if its volume keeps increasing and exceeds a critical value. The critical value is thus defined as the critical retention volume V_C, and it would be the dependent variable of the experiment. For each plastic sample with specific contact length ratio σ, critical

retention volume V_C, will be measured when the testing rig is tilted to a series angles. To acquire obvious V_C, tilting angle would be set between 45º ~ 90º, 15º per increment. Tilting angle of testing rig thus becomes the independent variable of the experiment. Control variables include plastic, liquid materials, and contact length ratio σ. This design of experiment allows the author to obtain a series of critical retention volume V_C, at various σ for each plastic-liquid combination. Effects of surface structures on V_C can thus be determined by comparing the data obtained at various σ. Details of all variables of contact angle hysteresis and critical retention volume experiments are listed in Table 13 and Table 14.

Table 13. Variable lists of contact angle hysteresis experiments.

Variable	**Value**	**Type**
Plastics	PET, PP, HDPE, LDPE, ABS	Control variable
Testing liquids	DI Water, Ethylene Glycol	Control variable
Surface inclined angle	45º ~ 90º, 15º per increment	Independent variable
Droplet volume	5μL / ea.	Control variable
Surface structure parameter	σ=1, flat surface (Control group)	Control variable
	σ between 1.1~1.6 structured surface (Treatment group)	
Contact angle hysteresis	0º ~ 90º	Dependent variable

Table 14. Variable lists of liquids' critical retention volume experiments.

Variable	Value	Type
Plastics	PET, PP, HDPE, LDPE, ABS	Control variable
Testing liquids	DI Water, Ethylene Glycol	Control variable
Surface inclined angle	45º ~ 90º, 15º per increment	Independent variable
Surface structure parameter	σ=1, flat surface (Control group)	Control variable
	σ between 1.1~1.6 structured surface (Treatment group)	
Critical retention volume V_C	More than 0μL	Dependent variable

5.1.2 Materials and Surface Fabrication

In the present study, five commonly used plastics were selected as testing solids which include Polyethylene terephthalate (PETE), High-density polyethylene (HDPE), Low-density polyethylene (LDPE), Polypropylene (PP), and Acrylonitrile Butadiene Styrene (ABS). These selections are based on their extensive applications in industry and daily life. To efficiently fabricate symmetrically arranged structures on these plastics' surfaces, laser engraving method were adopted. Laser engraver (CO_2 Laser Engraving Cutting Machine 3020 Laser Engraver equipped with one 40W water cooling laser tube) was used to engrave chevron-shaped grooves on samples' surfaces orthogonally. Samples thus have symmetrically square frustum-like structures on their surfaces, see Figure 18.

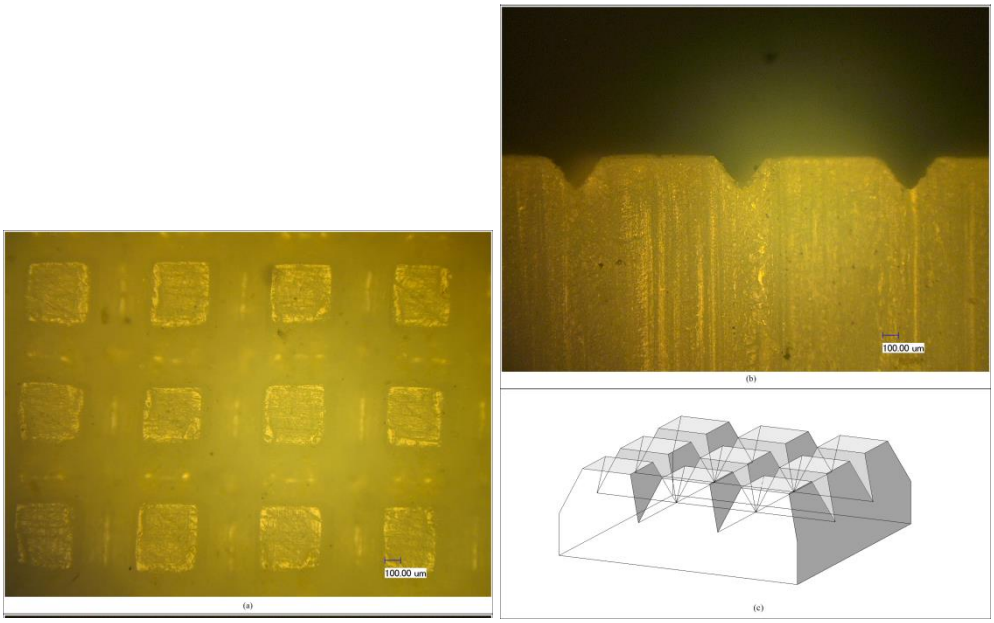

Figure 18. The symmetric square frustum-like structure was found on PETE surfaces (a) top view (b) side view (c) 3-D model.

Because polymers have various thermal properties such as heat capacity and melting point, the dimension of chevron-shaped groove on each plastic surface would be different under the same laser intensity. In this study, the laser intensity was controlled by current regulation and fixed at 10mA for all polymer samples. Various specifications of square frustum-like structures were designed by setting different spacing of chevron-shaped grooves. According to previous studies [64], [83], [84], [85], [86], [87], [88], fully impaled Wenzel state is common in many systems with microscale structures, where Wenzel state would cause the extension of liquid and solid's contact line length. Note a droplet in the Wenzel state if the structure groove is fully wet within the contact region. In the present study, surface structures are in the hundred-micrometer scale. It is

also observed that droplets displayed Wenzel state on surfaces with square frustum-like structures, Figure 19.

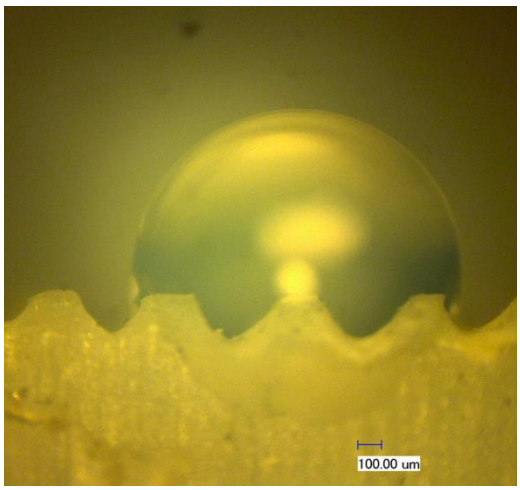

Figure 19. DI water's droplet was found staying in the Wenzel state on ABS surface with frustum-like structure in hundred-micrometer scale.

The contact length ratio σ is thus defined as the contact line length of a liquid droplet sitting on a structured solid surface divided by the contact line length of a liquid droplet sitting on a solid surface without structure. The contact length ratio σ was proposed as a parameter of surface fraction which could be formulated as:

$$\sigma = (W + 2L)/(W + G) \tag{36}$$

where W, L, and G are dimensions of the square frustum-like structure, illustrated in Figure 20. (Note σ =1 for the non-structured surface). Table 15 lists specifications of all

polymers with square frustum-like structure and their corresponding contact length ratio σ.

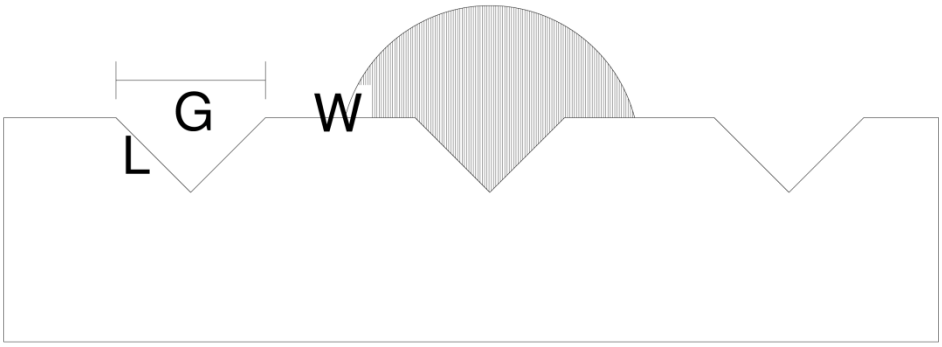

Figure 20. Dimensions of the frustum-like structure. The contact length ratio σ is in terms of W, L, and G.

Di-ionized (DI) water, ethylene glycol (EG), and formamide were testing liquids to study polymers' surface free energy and liquid-solid interaction. [31] These liquids were selected because they are representative to various polarities (Table 16). To study liquids' contact angle hysteresis and critical retention volume on inclined polymer surface, samples were placed on a tiltable stage, and droplet images were captured by the high performance CCD camera (VH-310G2-M/C 264) made by Vieworks with 640×480 resolution and 264 fps frame rate. There are two methods to quantify liquids' contact angle hysteresis and critical retention volume. One method is carried out by dispensing fixed-volume liquid onto a horizontal plastic surface first, and then keeping tilting the

solid surface until the liquid droplet starts to leave its original location. At the moment that liquid droplet starts to move, the stage tilting angle is recorded as the critical inclined angle. By applying this method, one can obtain a series data of critical inclined angles corresponding to various liquid volumes. However, this method is not appropriate because the tilting process often causes solid surface's vibration which highly increases the complexity of the force balance and results in inaccuracy. The other method is carried out by tilting the solid surface to a fixed angle in advance, and then keeping dispensing fixed-volume testing liquid droplets until the droplet starts to leave its original location. At the moment that a liquid droplet starts to move, the total dispensed volume is recorded as critical retention volume. Pierce et al. [89] compared with both methods and stated that the latter method has lower sensitivity to the perturbation. Therefore, the latter method was adopted in the present study which allows the authors obtain a series data of contact angle hysteresis and critical retention volumes corresponding to various surface inclined angles. To obviously distinguish the gravity effect on various inclined angles, in the present study, the sample stage was tilted from 0 to 90 degree, 15 degree per interval, and, the volume increment of each dispensing droplet was fixed between 4 to 20μL. It is considered the measurement on a fixed inclined angle is more practicable because it avoids the vibration problem. Furthermore, as long as the liquid dispensed volume is large enough to overcome the friction force of solid surface, one can always obtain the critical retention volume from an inclined surface. On the contrary, a small-volume liquid droplet might stick on an inclined

surface without sliding even if the solid surface is tilted to vertical.

5.2 Model Formulation

5.2.1 Critical Retention Model

The force balance diagram of a liquid droplet sitting on an inclined surface is shown on Figure 21 (b). Due to the gravity effect, the profile of the asymmetric droplet in the x-z plane displays contact angle phenomenon. The sliding force is formulated by droplet's density ρ, volume V, and surface inclined angle α.

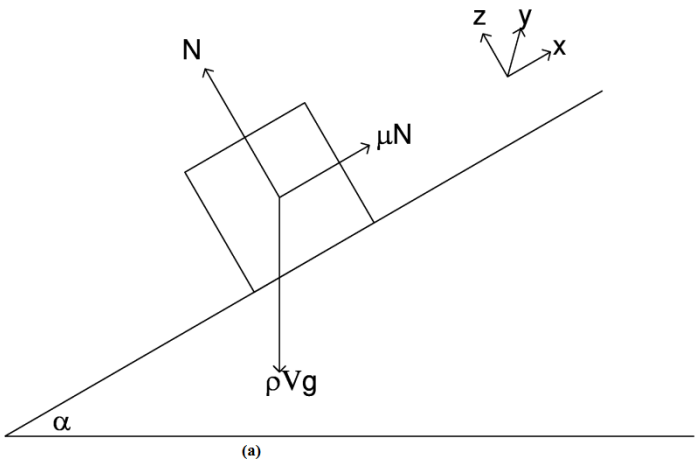

Figure 21 (a) The free body diagram of a rigid body, where N is the normal force and μ is the coefficient of friction. (b) The force balance diagram of a droplet sitting on the inclined surface. Gravity effect makes its profile asymmetric in the x-z plane.

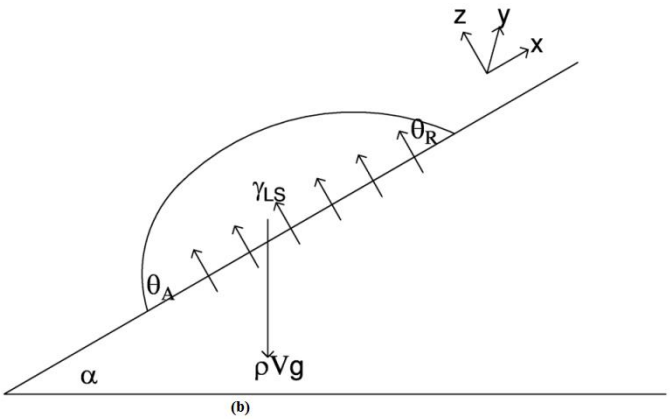

Figure 21. Continued

Extrand and Kumagi [58] pointed out that droplet's contour could be a circular drop, a parallel-sided drop, or a drop with front-to back asymmetry. Several models [38], [39], [40] have been proposed to estimate the contact line length, retention force, and the volume of the critical drop on non-structured surfaces. They all indicated that retention force of the droplet comes from the liquid-vapor surface tension, contact angle hysteresis, and contour of the droplet in the x-y plane. Surface structures would cause the liquid and solid contact line length change and hence affects the droplet's retention force. From the perspective of the unit, surface tension has its unit as the force per unit length. Therefore, instead of the liquid-solid contact area, the liquid-solid contact line in the x-y plane is one key factor which determines droplet's retention force. A static droplet displays contact angle hysteresis phenomenon on an inclined surface. It was stated that such a static droplet stays in the metastable state [23] which keeps its shape unchanged until a change in its volume, surface inclined angle, or external force.

Consider a free body diagram of a rigid body shown in Figure 21 (a), where the friction force equals to the coefficient of friction μ times the normal force N. The friction force exists at the interface of the rigid body and the surface of slope. Although a liquid droplet is not a rigid body, its retention force must exist at the liquid-solid interface. Therefore, we can consider the force balance diagram of a static droplet on an inclined surface as Figure 21 (b), where we treat the retention force as a form of the friction force. Because the friction force exists between liquid and solid interface, we further claim that the retention force comes from the liquid-solid interaction γ_{LS} over the contour of the droplet in the x-y plane.

Liquid-solid interaction is composed by apolar cohesion, polar cohesion, and polar adhesion. It determines liquid's contact angle and hence believed dominated the contact angle hysteresis. [7], [8] Therefore, the droplet's sliding force and retention force at critical condition can be balanced as

$$F = \rho\, V\, g\, sin\alpha = \gamma_{LS}\, C \tag{37}$$

where C is the contact line length of the droplet in the x-y plane. For estimation and prediction purposes, it is necessary to express C as a function of the liquid's volume and apparent contact angles. For a parallel-sided drop, or a drop with front-to back asymmetry, the analytical expressions of the contact line length are either complex or not existed. For simple estimation, the contour of a droplet can be simplified as a circle if the shape of a droplet is considered as a spherical-cap. As shown in Equation (38), the

volume of the spherical-cap can be formulated as a part of spherical integral minus the volume of the cone,

$$V = \int_{\varphi=0}^{2\pi} \int_{\vartheta=0}^{\theta} \int_{r=0}^{R} r^2 \, sin\vartheta \, dr \, d\vartheta \, d\varphi - \frac{1}{3}\pi r^2 h \tag{38}$$

where R is the radius of the sphere, r is the radius of the contour, h is the height of the cone, and θ is the contact angle, illustrated in Figure 22. The result is

$$V = \frac{\pi r^3}{3 \, sin^3\theta}(2 - 3cos\theta + \, cos^3\theta), \tag{39}$$

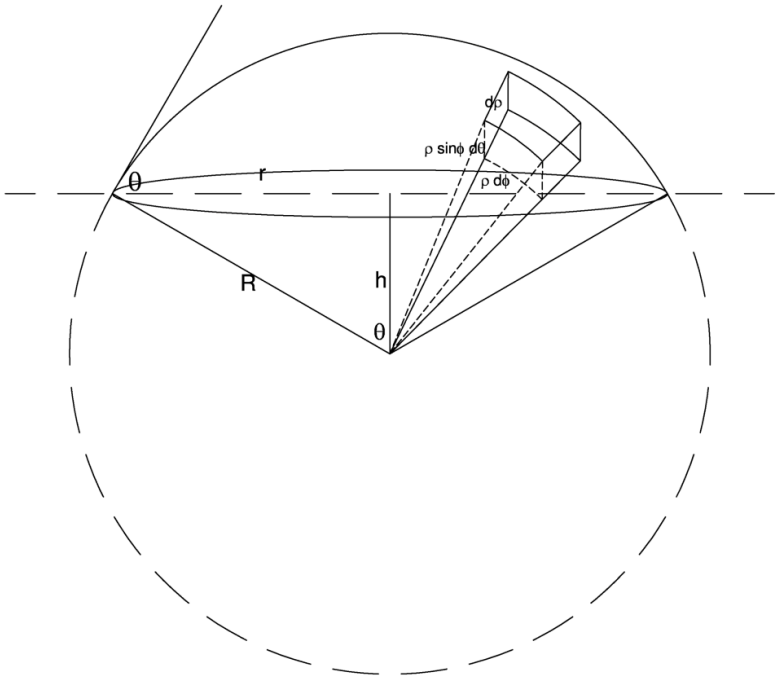

Figure 22. A spherical-cap-shaped droplet.

Under the circular drop assumption, the contact line length C is 2πr, which makes the droplet's volume to be expressed from Equation (37) as:

$$V = \frac{2\pi r\, \gamma_{LS}}{\rho g\, sin\alpha} \tag{40}$$

The radius of the contour r can be derived from Equation (39) and (40) and expressed as:

$$r = \sqrt{\frac{6\, \gamma_{LS}\, sin^3\theta}{\rho g\, sin\alpha\, (2 - 3cos\theta + cos^3\theta)}} \tag{41}$$

Since a droplet performs contact angle hysteresis phenomenon on an inclined surface, its contact angles at two ends would not be the same. We hereby follow previous studies [40] to use average contact angle θ_{av} to substitute θ in Equation (41). Substituting Equation (41) into Equation (40), the droplet's volume at critical condition can be obtained as:

$$V = \frac{2\pi\, \gamma_{LS}\, (6\, \gamma_{LS}\, sin^3\theta_{av})^{1/2}}{(\rho g\, sin\alpha)^{3/2}\, (2 - 3cos\theta_{av} + cos^3\theta_{av})^{1/2}} \tag{42}$$

where $\theta_{av} = (\theta_{max} + \theta_{min})/2$.

Equation (42) reveals the droplet's volume as a function of surface inclined angle α, liquid-solid surface tension γ_{LS}, and average contact angle θ_{av}. Extrand and Kumagai [25], [58] have proposed reduced hysteresis H, defined in Equation (4).

$$H = (\theta_A - \theta_R)/\theta_A \tag{4}$$

They found each solid has a unique H for various contact liquids at critical conditions, i.e. H value is independent of liquids, and surface inclined angles. Therefore, they claimed that H represents an intrinsic parameter which describes liquid-solid interaction. The ratio of θ_R to θ_A of a critical droplet can be derived from Equation (4) as:

$$\frac{\theta_R}{\theta_A} = 1 - H \tag{4}$$

Since H is claimed as an intrinsic parameter of solids, each solid should also have a unique θ_R / θ_A for any contact liquid at critical condition. ElSherbini and Jacobi [40] proposed that θ_{max} and θ_{min} are close to θ_A and θ_R, respectively. Therefore, substituting Equation (4) into Equation (42), the volume of a critical droplet can be further expressed as:

$$V = \frac{2\pi\,\gamma_{LS}\,(6\,\gamma_{LS}\,sin^3((1-H/2)\theta_A))^{1/2}}{(\rho g\,sin\alpha)^{3/2}\,(2-3cos((1-H/2)\theta_A)+\,cos^3((1-H/2)\theta_A))^{1/2}} \tag{43}$$

The proposed model for critical retention volume estimation can be seen as a function of liquid's density ρ, solid's reduce hysteresis H, surface inclined angle α, liquid-solid interfacial tension γ_{LS}, and liquid's advancing contact angle θ_A. When the liquid and solid material selections are fixed, at a certain surface inclined angle α, the proposed model can be reduced to a function of two variables: γ_{LS} and θ_A. In the later section, it would be addressed that solid's reduce hysteresis H is independent of contacting liquid and its surface structure. As mentioned before, it is addressed that surface structure alters solid's surface polarity and hence changes liquid-solid interfacial tension γ_{LS}. Therefore, even the solid selection is fixed, the γ_{LS} is still a variable corresponding to various

surface structure. It would also be addressed in the later section that θ_A is changed due to surface structure. Sum up, Equation (43) can be used to form tables (ex: Table 17) which list liquid's critical retention volume for various γ_{LS} and θ_A combinations under the condition of fixed liquid and solid selections at a certain surface inclined angle.

5.2.2 Liquid-Plastic Contact Line Length

The liquid-plastic contact line length is an important parameter for critical retention volume estimation and study of contact angle hysteresis. As mentioned in the previous study, contact angle hysteresis is attributed to three-phase contact line change [30] and a droplet's contour could be a circular drop, a parallel-sided drop, or a drop with front-to back asymmetry. [58] For a circular drop, its liquid-plastic contact line length can be analytically expressed by the average contact angle which has been shown in Equation (41) and (42). However, in the most cases, a droplet's contour displays front-to back asymmetry. In addition to previous studies, [40], [58] a large drop with front-to back asymmetry was also found in the present study, shown in Figure 23.

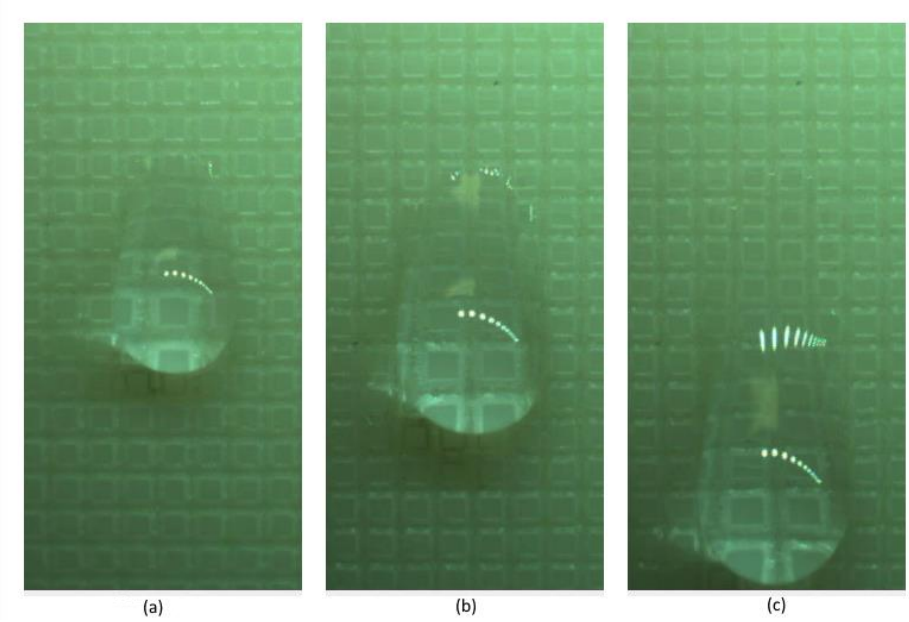

Figure 23. A DI water droplet attaches on a structured and vertical ABS surface. The contour displays front-to back asymmetry when the droplet is (a) just dispensed (b) reaching the critical retention volume (c) sliding down.

To estimate the liquid-plastic contact line length of a drop with front-to back asymmetry, the two-circle method was introduced. [40] This method approximates the profile of a drop displaying contact angle hysteresis phenomenon as the composition of two arcs where each arc is part of a circle. As shown in Figure 24, both circles are truncated by a horizontal line which represents the front view of the plastic surfaces. Two circles have different centers and radii where the larger circle is associated with the smaller truncated angle θ_1 which stands for receding contact angle θ_R, and the smaller circle is associated with the larger truncated angle θ_2 which stands for advancing contact angle θ_A. A droplet's contour can be approximated by the rotation of its profile around the truncate line to the plane surface, illustrated in Figure 25. Although ElSherbini and Jacobi [40]

have proposed their calculation, the author aims to propose another expression in the following content. As the assumption that half of a droplet's contour in the plane surface is its profile in the front view, a droplet's volume can be consider as upper half of a solid of revolution. While using the solid of revolution method, the plane curve is a droplet's profile and the axis is the truncate line. As mentioned above, the profile is composed by two arcs. Therefore, a droplet's volume is the summation of volumes obtained respectively from two arcs rotating around the same truncate line. As shown in Figure 26, the profile of the larger arc is expressed as Equation (44).

$$y = f(x) = \sqrt{R^2 - x^2},\ -Rsin\beta_1 \leq x \leq Rsin\theta_1 \tag{44}$$

where R is the radius of the larger circle.

The truncate line, which represents the rotating axis, is formulated as Equation (45).

$$y = R\ cos\theta_1 \tag{45}$$

Applying the solid of revolution method, the volume V_1 is

$$V_1 = \frac{\pi}{2}\int_{-Rsin\beta_1}^{Rsin\theta_1} (\sqrt{R^2 - x^2} - Rcos\theta_1)^2 dx \tag{46}$$

Solving Equation (46), one can obtained the volume as

$$V_1 = \frac{\pi}{2}\left(R^2(1+cos^2\theta_1)\, x - \frac{x^3}{3} - 2Rcos\theta_1\left(\frac{x}{2}\sqrt{R^2-x^2} + \frac{R^2}{2}sin^{-1}\frac{x}{R}\right)\right)\Big|_{x=-Rsin\beta_1}^{x=Rsin\theta_1} \tag{47}$$

Equation (47) expresses the rotation volume in which the larger arc as the plane curve. Applying the same calculation, the rotation volume V_2, illustrated in Figure 27, in which the smaller arc as the plane curve can be expressed as

$$V_2 = \frac{\pi}{2}\left(r^2(1+cos^2\theta_2)\, x - \frac{x^3}{3} - 2rcos\theta_2\left(\frac{x}{2}\sqrt{r^2-x^2} + \frac{r^2}{2}sin^{-1}\frac{x}{r}\right)\right)\Big|_{x=-rsin\beta_2}^{x=rsin\theta_2} \tag{48}$$

where r stands for the radius of the smaller circle. The summation of Equation (47) and (48) is the total volume of a drop with front-to back asymmetry, shown in Figure 28. Although it is an analytic expression, the volume can no longer obtained without knowing the radii of both arcs (referring to Equation (42)). Therefore, four additional parameters R, r, β_1 and β_2 become necessary information which must be acquired with advancing and receding contact angles. Surprisingly, this brings a simple expression of the liquid-plastic contact line length C as

$$C = 2R(\theta_1 + \beta_1) + 2r(\theta_2 - \beta_2) \tag{49}$$

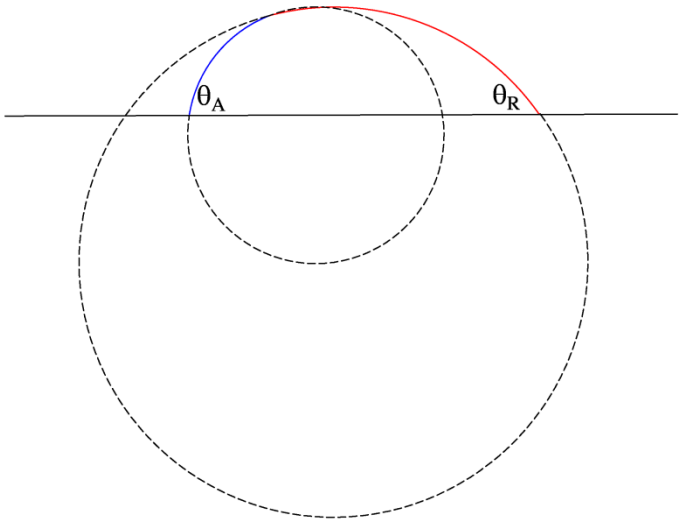

Figure 24. A droplet's asymmetric profile in the front view, composed by blue and red arcs, can be approximated by two circles. [40] The advancing contact angle exists in between the intersection of smaller arc (in blue) and the horizontal line, while the receding contact angle exists in between the intersection of larger arc (in red) and the horizontal line.

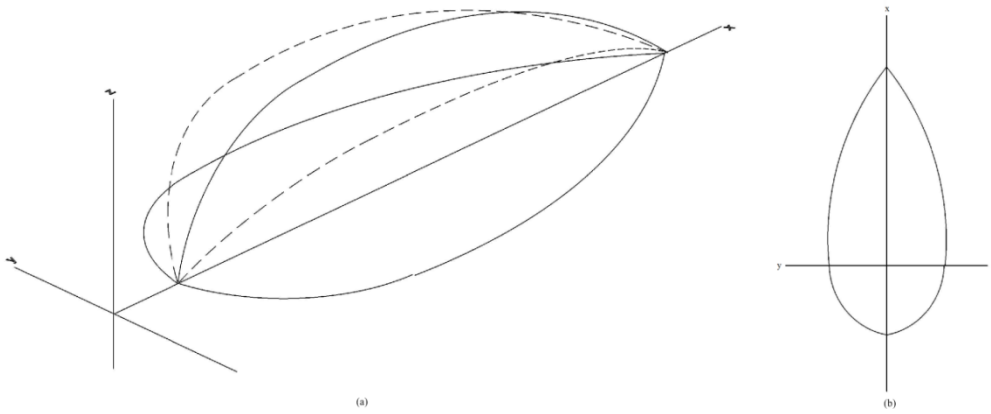

Figure 25. (a) A droplet's contour can be approximated by rotating its profile from the x-z plane to the x-y plane. (b) In the x-y plane, the contour displays the front-to back asymmetry.

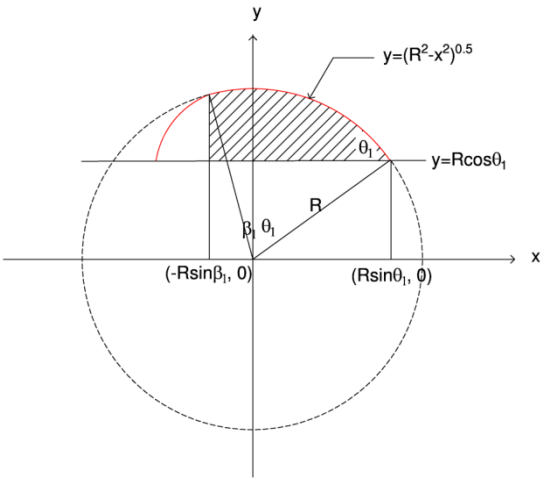

Figure 26. Continuing from Figure 25, a droplet's volume can be approximated by the solid of revolution, where the plane curve is its profile and the center line is the truncate line. The larger arc is formulated as Equation (45) and the center line is formulated as Equation (44). Hatched portion stands for the result of the solid of revolution.

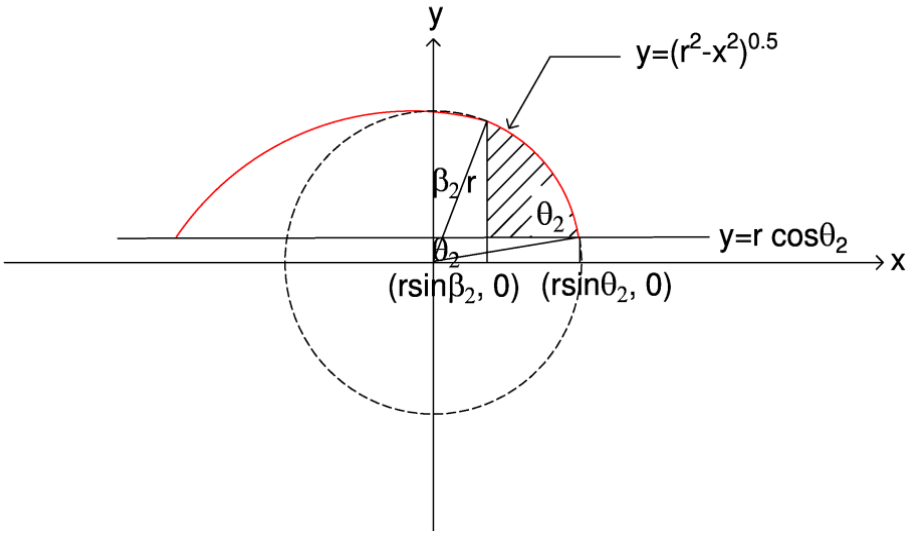

Figure 27. For the purpose of simple calculation, the droplet's profile is mirrored by the y-axis. Similar with Figure 26, hatched portion stands for the result of the solid of revolution, in which the plane curve is the smaller arc.

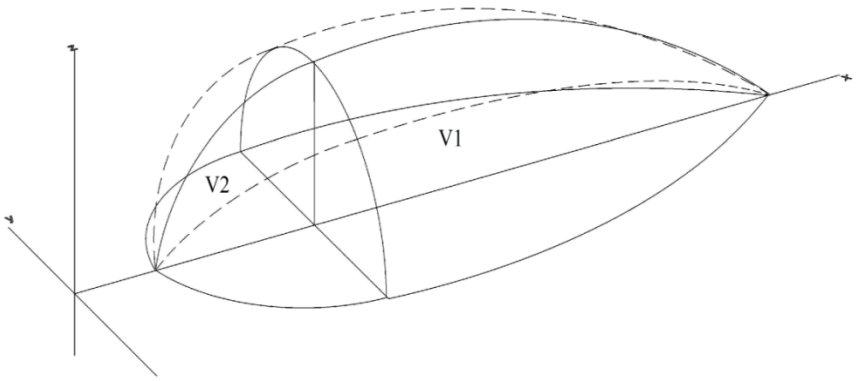

Figure 28. A droplet's volume can be obtained by summation of two hatched portions V1 and V2 shown in Figure 26 and Figure 27.

The volume and circumference can be obtained by Equation (47), (48), (49), and results are different from the original study. [40] Their work and the difference from the present study are excerpted and discussed in the following.

ElSherbini and Jacobi proposed the two-circle method which coordinated and illustrated in Figure 29 and Figure 30. According to figures, one can observe that they claimed that the contour is an ellipse, Figure 30(b), which is the major difference from the present study. Our measurement has shown that the contour is close to front-to back asymmetry, Figure 23. Therefore, the assumption of ellipse contour is not appropriate to apply for the present study. This difference brings various results of the volume and circumference of a droplet shown in the below.

The length of the cross section is 2ζ which can be the summation of L_1 and L_2 as

$$L_1 = \frac{2\zeta L_f}{1+L_f} \text{ and } L_2 = \frac{2\zeta}{1+L_f} \tag{50}$$

where L_f is the ratio of L_1 to L_2 as

$$L_f = \frac{L_1}{L_2} = \frac{sin\theta_1}{sin\theta_2}\frac{(1-cos\theta_2)}{(1-cos\theta_1)} \tag{51}$$

Similar with the present calculation, the droplet's volume is composed with two parts V_1 and V_2 shown in Figure 30. V_1 and V_2 are not distinguished by circles C_1 and C_2, instead, they have the same project length of the cross section ζ in the x-y plane. Simplifying triple integrals in the cylindrical coordinate system, volumes V_1 and V_2 are shown as

$$\begin{aligned} V_1 = \int_0^{\pi/2} [&\frac{(y_b - Y_0)^3}{3}(2 - 3cos\theta_1 + cos^3\theta_1) \\ &+X_0(y_b - Y_0)^2\theta_1 - X_0(y_b - Y_0)(y_a - Y_0)\, sin\theta_1 \\ &+{X_0}^2(y_b - y_a) - \frac{2}{3}{y_b}^3 + \frac{2}{3}{y_b}^2 y_c - {X_0}^2 y_b + \frac{{X_0}^2}{3} y_c \\ &+X_0{y_b}^2(\frac{\pi}{2} - sin^{-1}\left(\frac{y_c}{y_b}\right))]d\phi \end{aligned} \tag{52}$$

and

$$V_2 = \int^{3\pi/2} [y_c\left(\frac{2}{3}{y_b}^2 + \frac{{X_0}^2}{3}\right) - {y_b}^2 y_a \tag{53}$$

$$-X_0 {y_b}^2 (sin^{-1}\left(\frac{y_c}{y_b}\right) - \frac{\pi}{2} + \theta_2)]d\phi$$

where

$$y_a = \frac{L_2}{sin\theta_2} cos\theta_2 = Y_0 + \frac{L_1}{sin\theta_1} cos\theta_1 \tag{54}$$

$$y_b = \frac{L_2}{sin\theta_2} = Y_0 + \frac{L_1}{sin\theta_1} \tag{55}$$

$$y_c = \sqrt{\frac{{L_2}^2}{sin^2\theta_2} - {X_0}^2} \tag{56}$$

$$X_0 = \zeta - L_1 \tag{57}$$

Consider Equations (50) and (51) and substitute Equations (54) (55) (56) (57) into Equations (52) (53), one can find that V_1 and V_2 are functions of ζ, θ_1, and θ_2. In other words, as long as the length of the cross section ζ, advancing and receding contact angles θ_1 and θ_2 are measured and known, the droplet's volume can be derived. This conclusion is similar with the present study which R and r have to be measured as well for the purpose of droplet's volume calculation.

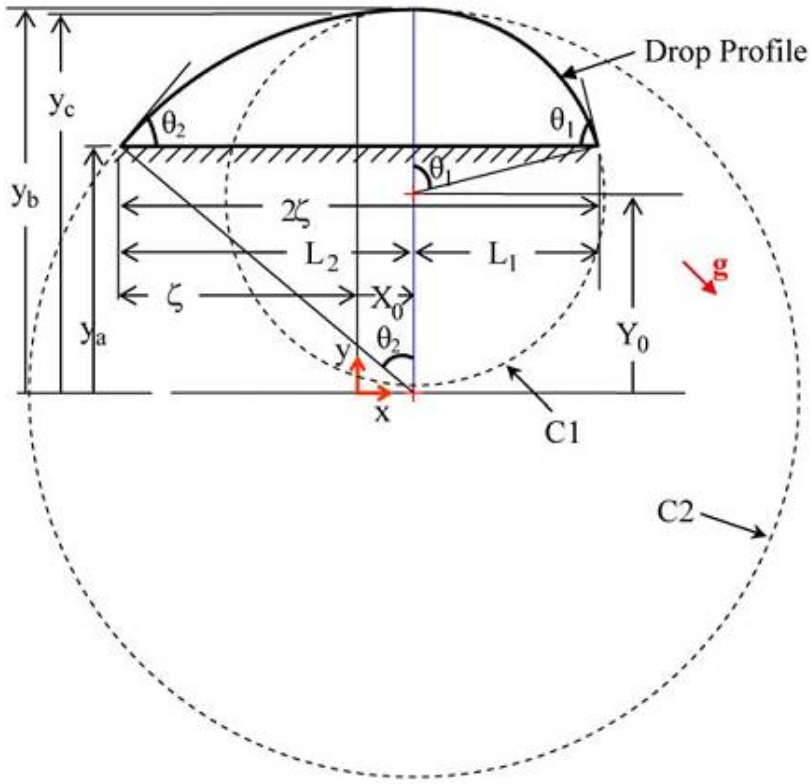

Figure 29. The original two-circle method proposed by ElSherbini and Jacobi. [40]

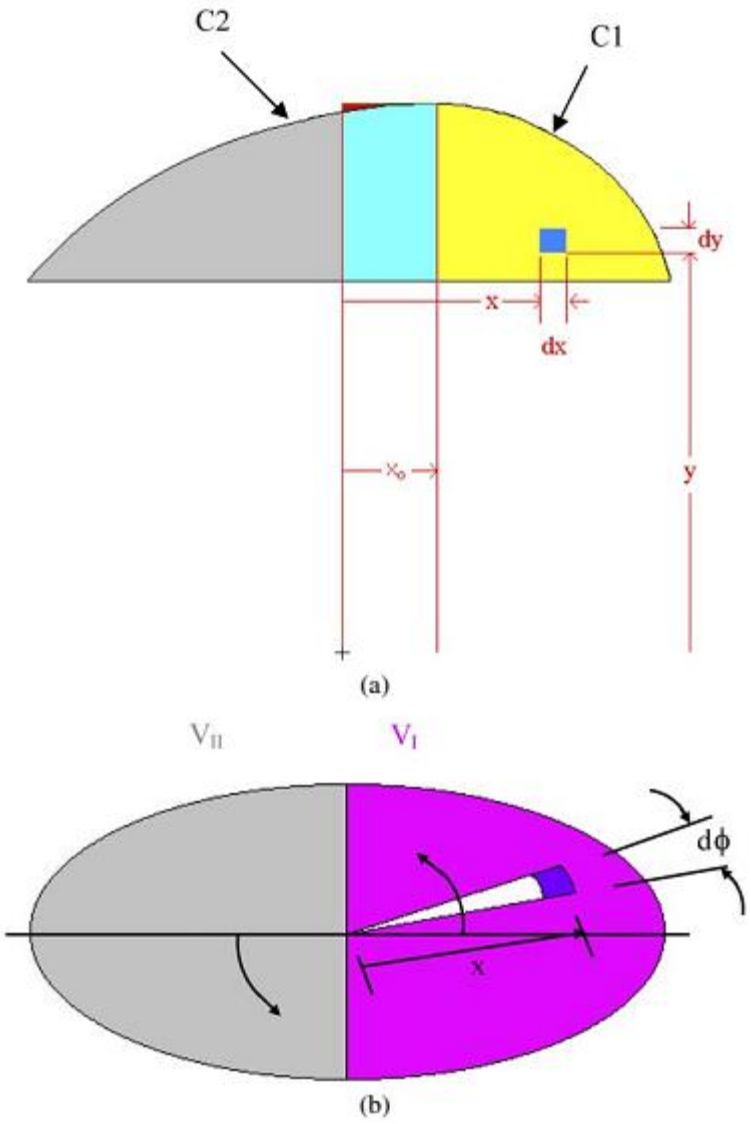

Figure 30. (a) The front view and (b) top view of a droplet which is coordinated and modeled for two-circle method. [40]

5.3 Result and Discussion

The present study focuses on droplets' θ_A and θ_R and sizes at the onset of droplets' movement on inclined surfaces. The following contents mainly discuss these data recorded at critical conditions.

5.3.1 Contact Angle Hysteresis

Advancing and receding contact angles of DI water and EG on polymer surfaces at various inclined angles α were recorded and reported in Table 18. The data indicates that DI water's θ_A ranges from 85º to 129º, whereas EG's θ_A ranges from 75º to 101º. For almost every polymer-α-σ combination, DI water has higher θ_A than EG does. This phenomenon can be explained by the difference of liquids' surface free energy and their interactions with polymers. It was also observed that both liquids' θ_A increase with α increased, no matter contacting non-structured or structured surfaces. Surface structure was also found to affect liquids' θ_A. The trends of structure effects classify selected polymers into three groups. ABS and both PEs have similar trends that both liquids' θ_A decrease, whereas PP has opposite trend that both liquids' θ_A increase along with σ increased. Different from others, DI water's and EG's θ_A have contrary trends on structured PETE surfaces that the former increases but the later decreases as σ increased. Various θ_A trends could be related to polymers' apolar and polar surface free energy change due to structure effects mentioned in the previous paper [31].

Reduced hysteresis H, and the ratio of θ_R to θ_A data list in Table 19, it was found a good agreement with the statement of Extrand and Kumagai [25] that H is independent of contact liquids, and every polymer' H is unique. The data also shows that every polymer, no matter structured or not, maintains its H value at all inclined angles. Therefore, the statement can be extended to that every solid has a unique H which is independent of contacting liquids and its surface structure. Table 19 also lists each polymer's H value in average. It was found that PETE has the highest H value and ABS has the lowest. Note that it doesn't mean PETE has the highest contact angle hysteresis at the critical condition. Since θ_R / θ_A equals to 1-H, it also reflects that PETE has the lowest θ_R / θ_A and ABS has the highest. Besides, it was not surprising to find that both PEs have close H and θ_R / θ_A. Since it is aforementioned that H is an intrinsic parameter which describes liquid-solid interaction, θ_R / θ_A should also be another intrinsic parameter which describes the θ_A and θ_R at critical conditions.

It has been mentioned that θ_A and θ_R are affected by contacting solids, surface inclined angle, and surface structure. To further understand the droplet at critical condition, it is necessary to discuss the critical retention volume coupled with contact angle hysteresis results.

5.3.2 Critical Retention Volume

Measured critical retention volume data is listed in Table 18. It was found that critical retention volume decays along with α increased, illustrated in Figure 31. High

correlation coefficients of nonlinear regression analysis confirm the proposed and all previous models that critical retention volume is inverse proportional to $(sin\,\alpha)^{3/2}$. This result applies to both liquids contacting non-structured and structured surfaces. The proposed model was found to have a good fit to experiment data, reported and illustrated in Table 20 and Figure 32, in which most estimation values stay within error bars of measurement data. Errors of the present and previous models could originate from the inaccuracy of the liquid-solid contact length estimations, because all models were built and simplified based on circular drop assumption. Several studies have stated that on inclined surfaces, circular drop shape only happens for the small drop, and the large drop is often associated with front-to back asymmetry. This statement was also found in the present study, in which average estimation error on DI water's critical retention volume (4.81μL) is larger than EG's (3.05μL). The result is attributable to that DI water always has larger critical retention volume then EG does under the identical surface condition. This statement could also explain the critical retention volume's error at 45º surface inclined angle is relatively larger than steeper surfaces because the steeper surface is associated with smaller critical retention volume.

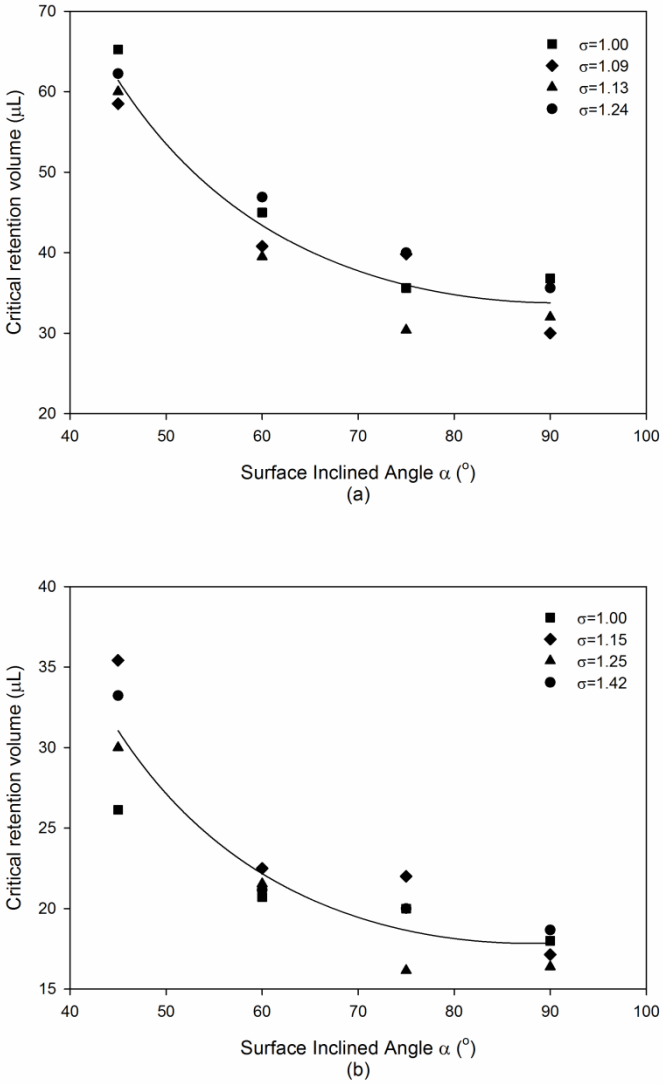

Figure 31. Critical retention volume (a) DI Water on HDPE (b) EG on ABS versus surface at 45° ,60° ,75°, and 90° inclined angles.

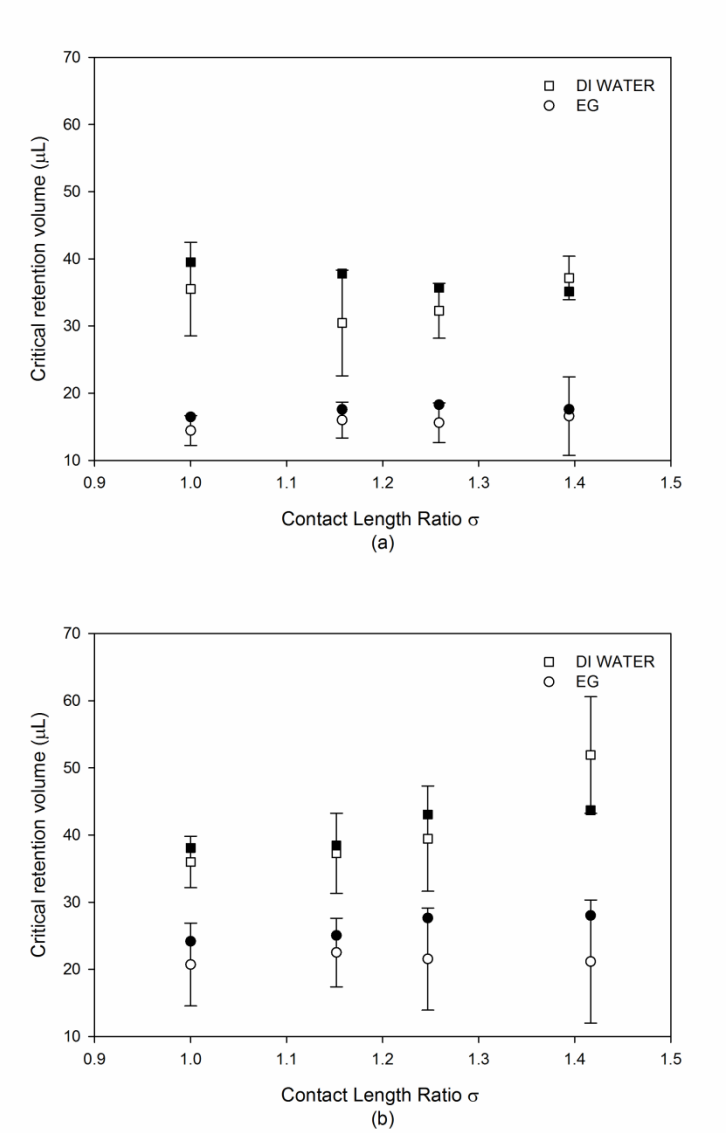

Figure 32. Liquids' critical retention volume on (a) PETE at 90° inclined angle (b) ABS at 60° inclined angle. White and black symbols stand for experimental values and estimation values from Equation (13) respectively.

It is aforementioned that the authors treat retention force as the friction force between droplets and surfaces, and the friction force comes from liquid-solid interaction γ_{LS} at contact line. This statement becomes the major difference between the present and previous models, Equation (5), (6), and (7). While previous models focus on bond number B_0 derivation, the proposed model pays attention to liquid-solid surface tension γ_{LS} calculation. In the present study, average contact angles of three liquids on non-structured and structured surfaces were taken and used to derive liquid-solid surface tensions. The calculation was first proposed by van Oss et al. [7], where the detail of selected liquid-solid combinations have been reported in the previous paper [31] and the result lists in Table 21.

To estimate liquids' critical retention volumes on solids' surfaces with any condition, in addition to α and γ_{LS}, θ_A and θ_R are essential parameters. It is aforementioned that reduce hysteresis H links θ_A and θ_R. Therefore, θ_A becomes the key factor which determines the result. Steep surface is often associated with large θ_A, therefore, it was found that critical retention volume decreases with θ_A increased, which fits the proposed model shown in Figure 33. It was observed that θ_A changes due to surface structure effect, therefore, it was claimed that surface structure also changes critical retention volume and the trend depends on how θ_A changes. This statement found the best example on DI water's critical retention volume change when it contacts structured HDPE and PP surfaces. Figure 34 illustrates that HDPE and PP have opposite changing trends of DI water's critical retention volume at various σ. The phenomenon can be explained by opposite changing of DI water's θ_A while contacting these two structured polymers. Similar

examples can be also found at most liquid-polymer combinations, although minor disagreements exist. Those sporadic counterexamples were originated from the turbulence of θ_R which made confusion of average contact angles. However, from the perspective of average reduce hysteresis H, θ_R stably link with θ_A; which eventually maintains the statement. The result implies the predictability of liquids' critical retention volumes on structured surfaces based on Equation (43), where θ_A is the main input corresponding to various σ.

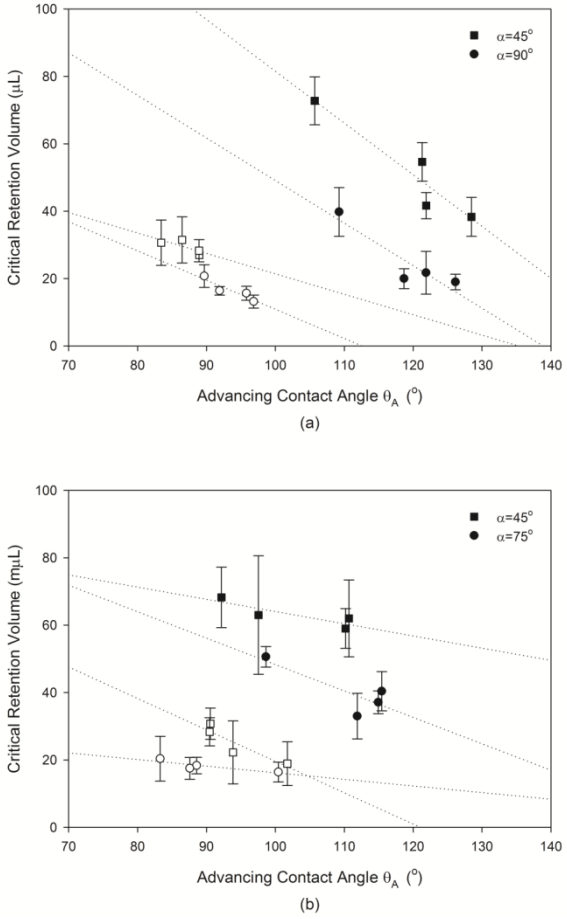

Figure 33. Liquids' critical retention volumes decay as advancing contact angle increased. (a) PP at 45° and 90° inclined angles, (b) PETE at 45° and 75° inclined angles. White and black symbols stand for DI water and EG respectively.

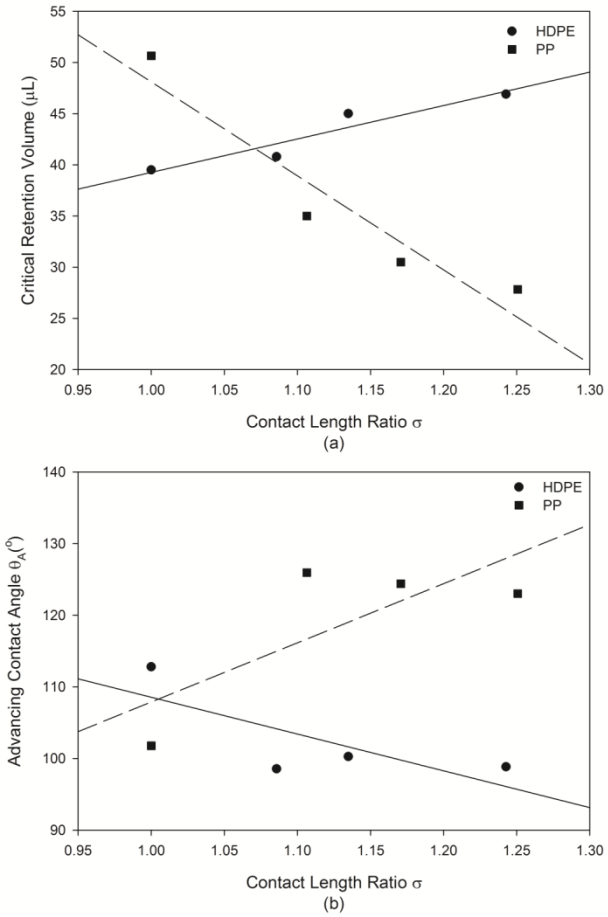

Figure 34. DI water's (a) critical retention volumes and (b) advancing contact angles on structured HDPE (solid line) and PP (dash line) surfaces.

5.3.3 Model Evaluation

According to data reported in Table 21, we can calculate the mean squared error (MSE) of proposed model for all plastics-α-σ combinations, reported in Table 22. The overall MSE of DI water and EG are 6.67μL and 3.76 μL, respectively. The proposed model found its lowest MSE of both DI water and EG on HDPE surfaces. To compare the V_C estimation on structured surfaces by proposed and previous models, we can firstly compare mean of residue errors of each model, where residue error is defined as the difference between measured and estimated values. To determine whether the proposed and previous models have statistically significant difference of the mean of residue errors, T-test was used for hypothesis testing. Following are steps of T-test of the proposed and previous models.

1. Set the null hypothesis H_0: both models have the same mean of residue errors. Alternative hypothesis H_1: both models don't have the same mean of residue errors.
2. Set the significant interval as 0.05.
3. Do three sets of T-test: Chiou(proposed)/ElSherbini, Chiou/Dussan, and Chiou/Extrand.
4. Using P value to accept or reject the null hypothesis H_0.

Results of three sets of T-test are:

- Chiou/ElSherbini: $P=1.26\times10^{-8} < 0.05$

  Since $P<0.05$, the null hypothesis H_0 is rejected. In other words, two models have statistically significant difference of mean of residue errors.

- Chiou/Dussan: $P=0.0014 < 0.05$

  Since $P<0.05$, the null hypothesis H0 is rejected. In other words, two models have statistically significant difference of mean of residue errors.

- Chiou/Extrand: $P=1.73\times10^{-14} < 0.05$

  Since $P<0.05$, the null hypothesis H_0 is rejected. In other words, two models have statistically significant difference of mean of residue errors.

According to above T-test results, we can tell the proposed model has statistically significant difference of the mean of residue errors from previous models'.

F-test was also used to determine whether the proposed and previous models have statistically significant difference of variance. Following are steps of F-test of the proposed and previous models.

1. Set the null hypothesis H_0: both models have the same variance.

   Alternative hypothesis H_1: both models don't have the same variance.
2. Set the significant interval as 0.05.
3. Do three sets of T-test: Chiou(proposed)/ElSherbini, Chiou/Dussan, and Chiou/Extrand.
4. Using P value to accept or reject the null hypothesis H_0.

Results of three sets of F-test are:

- Chiou/ElSherbini: $P=3.25\times10^{-14} < 0.05$

  Since $P<0.05$, the null hypothesis H_0 is rejected. In other words, two models have statistically significant difference of variance.

- Chiou/Dussan: $P=0.000998 < 0.05$

  Since $P<0.05$, the null hypothesis H0 is rejected. In other words, two models have statistically significant difference of variance.

- Chiou/Extrand: $P=4.56\times10^{-13} < 0.05$

  Since $P<0.05$, the null hypothesis H_0 is rejected. In other words, two models have statistically significant difference of variance.

According to above F-test results, we can tell the proposed model has statistically significant difference of variance from previous models'.

Results of T-test and F-test have demonstrated that the proposed model is statistically significant different from previous models. However, which one is the most accurate? To answer this question, standard error of the mean (SEoM) needs to be addressed. SEoM is standard deviation of the error in the sample mean with respect to the true mean, which can tell how accurate the estimate of the mean is likely to be. [90] SEoM is defined as the sample standard deviation divided by square root of the size of the sample. SEoM results show that the proposed model has the lowest SEoM (0.2893) compared with ElSherbini (0.5922), Dussan (0.3851), and Extrand (0.5711). This indicates that the proposed model has the most accurate estimation among all models.

We can also compare proposed models with previous ones by mean squared error (MSE). Reported in Table 23, it was found that proposed model has lowest MSE in DI water and EG on overall plastics while comparing with previous models. This result once again demonstrates the superiority of proposed method over previous ones.

5.3.4 Prediction

The proposed model for critical retention volume estimation has been confirmed by hypothesis testing. To apply the proposed model for prediction, liquids' θ_A must be predictable. Previous study has concluded that contact angle is predictable on structured polymer surfaces when placed horizontally. The study indicated that there exists linear relationship between contact angles and σ. In the present study, the authors applied the same analysis and found that θ_A also has linear distribution with σ on inclined surfaces. Figure 35 illustrates selected examples of both liquids' θ_A on various structured polymer surfaces when placed vertically, where lines and scatter dots represent predictions and experiment data, respectively. The slope of each line was obtained from the linear regression of each data set; and each line was set to pass the data point at σ =1. The correctness was examined by errors calculation and results are listed in Table 24. The data indicates that approximate 80% of data points have less than 6 percent error, and a quarter data points even have less than 1 percent error. In terms of average, almost every liquid-solid combination has less than 5 degree error. These results validated the accuracy of θ_A prediction based on linear regression analysis.

Predicted θ_A were then applied into the proposed model to estimate critical retention volumes with various α and σ combinations, and results list in Table 25. Compared with experiment data, it was found that DI water has 4.48μL and EG has 2.79μL errors of average critical retention volumes among all structured surfaces. To be more specific, DI water has the largest error (6.42μL) on ABS and the smallest error on HDPE (2.55μL), while EG has the largest error (3.48μL) on PP and the smallest error on LDPE (1.71μL). In addition to average errors, most predicted values stay within the error bars of each liquid-solid-α-σ combination, Figure 36. Low errors of predicted critical retention volumes verify the robustness of the proposed model and further confirm the accuracy of θ_A predictions on structured surfaces.

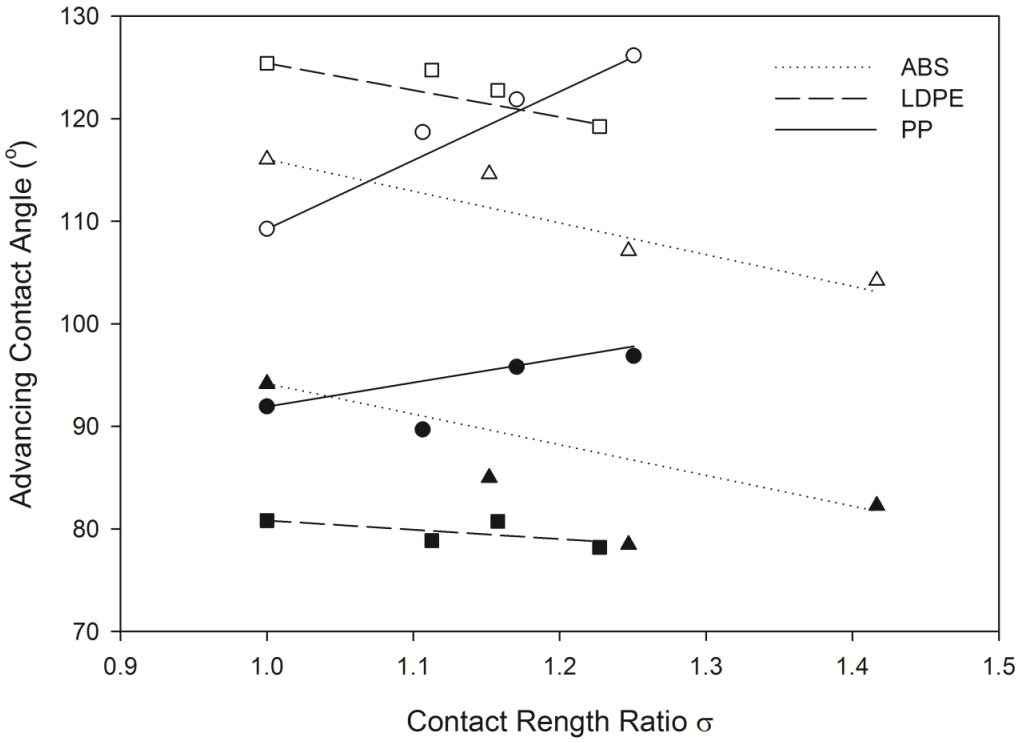

Figure 35. Liquids' advancing contact angles on structured ABS (triangle), LDPE (square), and PP (circle) surfaces at 90° inclined angle. White and black symbols stand for DI water and EG respectively.

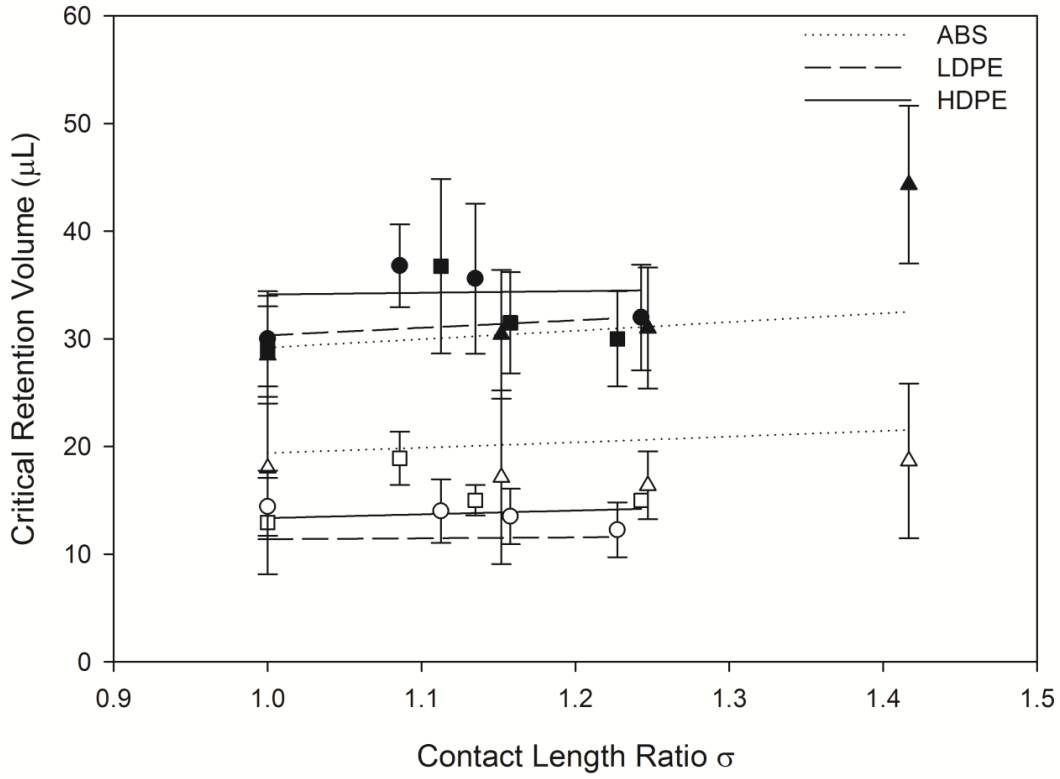

Figure 36. Predicted (lines) and experiment (scatter dots) critical retention volume on structured ABS (dot line, triangle), LDPE (dash line, square), and HDPE (solid line, circle) surfaces at 90° inclined angle. White and black symbols stand for DI water and EG respectively.

5.4 Summary and Conclusion

Based on circular drop assumption, a new model of liquids' critical retention volume estimation was established. The model originated from the balance of retention force on inclined surfaces. Different from previous studies, liquid-solid surface tension γ_{LS} along the contour of liquid drop was considered as the source of retention force. The model was then examined by several liquid-solid combinations, where liquids include DI water and EG, and solids include ABS, HDPE, LDPE, PETE, and PP. Symmetrically arranged frustum-like structures were fabricated on polymers' surfaces by the laser engraver, where various specifications were represented by σ. Both liquids' contact angle hysteresis on inclined surfaces with various σ were studied. It was found that θ_A and θ_R were linked by reduced hysteresis H, which was claimed as an intrinsic parameter of solids in previous studies. Our result confirms and extends this statement on structured polymer surfaces. Surface structures can affect liquids' contact angle hysteresis. As σ increased, liquids' θ_A would have different changing trends on various polymers which were believed to depend on liquid-solid interactions γ_{LS} and natures of polymers. Although these liquid-solid combinations could have opposite changing trends of θ_A, those trends all display that θ_A and σ have linear relationships. θ_A were predicted based on linear regression analysis. Predicted results, as inputs, were then applied into the proposed model for critical retention volumes prediction. Compared with experiment data, low errors of predicted results proved the correctness of both the proposed model and advancing contact angles prediction. The results provide the industry a chance to easily control liquids' storage and repellency on commonly used plastics surfaces. The

study also left spaces for further researches on various materials, such as metals. The research could also be extended to study contact angle hysteresis and liquids' retentions on surfaces with finer scale structures.

Table 15. Specifications of square frustum-like structures on polymers' surfaces and their corresponding contact length ratio σ, where G, L, and W are illustrated in Figure 20.

Samples	G (μm)	L (μm)	W (μm)	σ
ABS-I	302.50	228.12	710.46	1.15
ABS-II	296.65	240.79	451.97	1.25
ABS-III	297.63	241.88	149.03	1.42
HDPE-I	318.26	203.31	711.65	1.09
HDPE-II	326.78	212.42	400.36	1.13
HDPE-III	316.09	218.28	180.18	1.24
LDPE-I	208.44	161.95	817.16	1.11
LDPE-II	187.35	151.92	551.08	1.16
LDPE-III	192.65	153.96	314.47	1.23
PETE-I	298.55	229.62	720.32	1.16
PETE -II	314.43	227.36	227.77	1.26
PETE -III	308.29	240.82	131.53	1.39
PP-I	278.97	190.64	682.18	1.11
PP-II	270.77	201.55	504.36	1.17
PP-III	273.06	199.65	230.41	1.25

Table 16. Surface free energy of testing liquids and their polarity.

Testing liquids	Total γ^{Total} (mN/m)	Apolar γ^{LW} (mN/m)	Lewis Acid γ^{+} (mN/m)	Lewis Base γ^{-} (mN/m)	Polarity
Di-ionized (DI) Water	72.8	21.8	25.5	25.5	Bipolar
Ethylene Glycol (EG)	48	29	1.92	47	Monopolar
Formamide	58	39	2.28	39.6	Monopolar

Table 17. DI water's (ρ=1000 kg/m^3) critical retention volumes (μL) on ABS (H=0.6) surface at 90° surface inclined angle. Units of θ_A and γ_{LS} are ° and mN/m, respectively.

θ_A / γ_{LS}	80	85	90	95	100	105	110
0.01	16.96	16.25	15.58	14.94	14.33	13.74	13.18
0.011	19.56	18.74	17.97	17.23	16.53	15.86	15.20
0.012	22.29	21.36	20.47	19.64	18.84	18.07	17.32
0.013	25.13	24.08	23.09	22.14	21.24	20.37	19.53
0.014	28.09	26.91	25.80	24.75	23.74	22.77	21.83
0.015	31.15	29.85	28.61	27.44	26.32	25.25	24.21
0.016	34.32	32.88	31.52	30.23	29.00	27.82	26.67
0.017	37.58	36.01	34.52	33.11	31.76	30.46	29.21
0.018	40.95	39.23	37.61	36.08	34.60	33.19	31.82
0.019	44.41	42.55	40.79	39.12	37.53	35.99	34.51
0.02	47.96	45.95	44.05	42.25	40.53	38.87	37.27
0.021	51.60	49.44	47.40	45.46	43.61	41.82	40.10
0.022	55.33	53.01	50.82	48.75	46.76	44.85	43.00
0.023	59.14	56.67	54.33	52.11	49.98	47.94	45.97
0.024	63.04	60.40	57.91	55.54	53.28	51.10	49.00
0.025	67.02	64.22	61.57	59.05	56.64	54.33	52.09
0.026	71.08	68.11	65.30	62.63	60.07	57.62	55.25
0.027	75.22	72.07	69.10	66.27	63.57	60.97	58.46
0.028	79.44	76.12	72.97	69.99	67.14	64.39	61.74

Table 18. Liquids' critical retention volumes, advancing and receding contact angles on polymers with various conditions.

Polymer-Inclined Angle α - Liquid	Contact Length Ratio σ	Critical Retention Volume (μL)	Advancing Contact Angle θ_A(°)	Receding Contact Angle θ_R(°)
ABS-45°-DI water	1.00	40.5±6.07	94.66±8.06	37.87±4.3
	1.15	43.71±5.97	90.19±4.69	41.9±5.93
	1.25	54.64±11.95	89.21±6.02	36±6
	1.42	68.54±18.2	85.01±5.96	33.8±3.73
ABS-60°-DI water	1.00	36±3.84	110.93±6.31	42.02±5.29
	1.15	37.29±5.97	108.5±6.72	42.9±4.89
	1.25	39.46±7.83	97.26±5.23	35.18±5.33
	1.42	51.92±8.68	95.96±7.67	33.95±5.68
ABS-75°-DI water	1.00	28.5±5.2	113.38±6.99	44.35±4.44
	1.15	31±6.69	113.14±7.14	43.95±6
	1.25	32.31±10.55	103.68±13.41	38.41±5.81
	1.42	56±6.48	102.51±12.88	36.95±4.42
ABS-90°-DI water	1.00	28.5±4.52	116.03±6.62	45.74±3.66
	1.15	30.43±5.98	114.62±5.89	49.53±7.65
	1.25	31±5.62	107.13±12.06	39.18±7.3
	1.42	44.33±7.33	104.22±7.02	38.09±3.92
PETE-45°-DI water	1.00	68.25±8.97	92.17±4.29	27.35±7.15
	1.16	63±17.59	97.54±7.82	29.91±7.63
	1.26	59±5.91	110.18±5.67	29.86±5.76
	1.39	62±11.42	110.68±6.13	28.22±2.27
PETE -60°-DI water	1.00	46.29±5.71	93.15±4.53	27.46±6.19
	1.16	43.5±9.97	98.97±7.43	30.54±5.13
	1.26	40.25±4.35	109.95±5.28	32.66±3.23
	1.39	41.42±3.6	110.34±3.47	33.6±4.33
PETE -75°-DI water	1.00	50.62±3.07	98.62±8.97	28.8±6.44
	1.16	33±6.75	111.88±8.57	30.93±2.98
	1.26	37.1±3.38	114.93±4.69	36.62±6.89
	1.39	40.38±5.82	115.44±8.67	32.76±4.09
PETE -90°-DI water	1.00	35.5±6.98	100.04±8.48	30.33±9.95
	1.16	30.45±6.88	105.54±5.6	32.19±4.55
	1.26	32.27±4.1	111.45±5.85	36.12±3.65
	1.39	37.17±3.24	114.36±7.5	35.75±2.45

Table 18. Continued

Polymer-Inclined Angle α - Liquid	Contact Length Ratio σ	Critical Retention Volume (µL)	Advancing Contact Angle θ_A(°)	Receding Contact Angle θ_R(°)
HDPE-45°-DI water	1.00	65.25±4.07	107.02±5.23	37.25±7.06
	1.09	58.5±11.78	110.5±24.69	42.14±12.36
	1.13	60±5.86	93.69±6.1	37±3.09
	1.24	62.25±8.97	97.36±5.37	35.95±7.55
HDPE-60°-DI water	1.00	39.5±4.01	112.77±3.92	36.29±9.03
	1.09	40.8±7.38	98.54±8.59	39±5.97
	1.13	45±4.05	100.24±4.72	36.08±7.77
	1.24	46.91±7.5	98.82±7.52	34.36±6.59
HDPE-75°-DI water	1.00	35.6±6.98	109.78±8.81	35.53±6.9
	1.09	39.82±4.85	91.74±6.5	34.27±3.92
	1.13	30.38±5.57	98.93±5.05	38.36±9.03
	1.24	40±5.91	100.57±8.29	35.41±6.6
HDPE-90°-DI water	1.00	30±4.43	110.65±6.49	35.21±5.85
	1.09	36.8±3.84	88.89±4.68	34.5±6.82
	1.13	35.6±6.98	102.18±5.25	37.25±7.3
	1.24	32±4.9	105.43±8.92	35.82±5.28
PP-45°-DI water	1.00	72.78±7.12	105.7±6.45	31.97±7.59
	1.11	54.64±5.71	121.32±6.55	41.42±8.22
	1.17	41.67±3.89	121.91±5.6	45.24±5.78
	1.25	38.33±5.77	128.46±3.8	47.57±7.45
PP-60°-DI water	1.00	50.67±8.84	101.77±7.59	32.19±7.37
	1.11	35±5.22	125.93±6.97	42.4±3.91
	1.17	30.5±3.09	124.38±5.93	45.62±5
	1.25	27.83±4.3	123.01±5.18	48.82±4.43
PP-75°-DI water	1.00	40.5±8.14	106.29±11.34	32.89±8.97
	1.11	26.5±3.09	120.61±7.05	41.38±5.41
	1.17	25±2.34	129.19±4.47	48.43±3.01
	1.25	22.5±2.71	127.7±6.52	51.14±5.13
PP-90°-DI water	1.00	39.82±7.24	109.26±11.21	33.06±5.47
	1.11	20±2.95	118.68±5.54	40.15±5.04
	1.17	21.75±6.36	121.87±6.58	45.02±8.28
	1.25	19±2.34	126.15±6.2	50.14±5.86

Table 18. Continued

Polymer-Inclined Angle α - Liquid	Contact Length Ratio σ	Critical Retention Volume (µL)	Advancing Contact Angle θ_A(°)	Receding Contact Angle θ_R(°)
LDPE-45°-DI water	1.00	42.75±5.59	104.34±4.32	37.2±5.95
	1.11	67.5±9	101.17±5.36	30.33±6.12
	1.16	59.25±8.97	99.12±4.38	37.43±5.77
	1.23	48.75±6.02	97.21±4.71	39.88±7.19
LDPE-60°-DI water	1.00	43.5±6.46	116.48±6.88	37.67±6.46
	1.11	45±6.65	111.19±4.32	39.89±7.7
	1.16	44.18±6.31	107.69±4.85	41.08±8.35
	1.23	35.25±7.14	106.51±2.71	42.02±6.58
LDPE-75°-DI water	1.00	32.25±6.02	121.94±4	43.76±5.33
	1.11	39.6±8.69	119.55±5.53	42.39±9.4
	1.16	31.5±7.65	114.09±7.81	45.01±8.74
	1.23	31.09±7.38	112.81±3.24	45.26±6.78
LDPE-90°-DI water	1.00	29±5.01	125.42±6.01	46.77±7.78
	1.11	36.75±8.1	124.74±5.11	46.01±10.3
	1.16	31.5±4.7	122.77±4.69	45.33±6.72
	1.23	30±4.43	119.25±3.97	47.09±6.66
ABS-45°-EG	1.00	26.14±8.23	92.98±9.47	35.35±3.43
	1.15	30±3.02	92.36±6.94	39.73±8.31
	1.25	35.43±9.26	77.69±3.64	31.26±1.86
	1.42	33.23±9.15	81.14±7.48	32.41±8.98
ABS-60°-EG	1.00	20.71±6.16	92.62±7.81	38.71±3.17
	1.15	22.5±11.12	87.31±9.41	38.04±3.51
	1.25	21.54±2.6	76.74±3.97	32.48±2.57
	1.42	21.15±9.16	76.53±6.68	30.59±4.94
ABS-75°-EG	1.00	16.15±2.3	98.18±8.59	38.16±4.81
	1.15	22±6.49	96.29±6.23	37.62±4.74
	1.25	20±5.48	75.87±3.39	34.03±2.83
	1.42	20±7.91	81.74±8.92	32.41±3.4
ABS-90°-EG	1.00	18±6.61	94.17±8.62	32.23±4.51
	1.15	17.14±8.07	84.99±11.73	32.26±4.58
	1.25	16.38±3.15	78.46±7.99	31.37±6.43
	1.42	18.67±7.2	82.27±5.51	35.53±4.86

Table 18. Continued

Polymer-Inclined Angle α - Liquid	Contact Length Ratio σ	Critical Retention Volume (µL)	Advancing Contact Angle θ_A(°)	Receding Contact Angle θ_R(°)
	1.00	18.9±6.49	101.73±7.24	30.5±9.01
PETE-45°-EG	1.16	30.75±4.63	90.55±6.88	26.99±6.31
	1.26	28.33±4.19	90.46±5.11	22.18±2.19
	1.39	22.21±9.33	93.84±7.85	23.11±5.62
	1.00	16.5±3.67	99.16±10.26	27.65±4.04
PETE -60°-EG	1.16	20.33±2.97	92.46±3.85	27.38±4.15
	1.26	17.86±2.57	84.66±4.56	23.58±2.26
	1.39	15.45±6.88	91.5±6.55	23.7±3.84
	1.00	16.4±2.97	100.43±5.47	32.02±8.09
PETE -75°-EG	1.16	18.33±2.44	88.56±3.23	29.77±4.32
	1.26	17.5±3.25	87.58±5.76	24.13±2.79
	1.39	20.36±6.64	83.28±14.1	29.89±5.42
	1.00	14.44±1.21	97.89±3.21	28.7±4.19
PETE -90°-EG	1.16	16±2.67	88.81±7.81	26.97±3.63
	1.26	15.6±2.95	84.2±4.65	25.15±3.05
	1.39	16.57±5.84	86.76±9.84	28.77±4.37
	1.00	30.36±3.67	82.15±3.74	26.28±2.76
LDPE-45°-EG	1.11	21.29±3.1	72.16±4.65	21.97±2.3
	1.16	19±1.81	77.34±4.32	24.14±2.87
	1.23	20±0	75.49±3.92	22.77±3.09
	1.00	19.67±2.06	77.55±4.82	26.69±4.31
LDPE-60°-EG	1.11	17.23±1.92	74.86±5.71	23.35±2.09
	1.16	14.86±1.88	77.02±5.23	26.32±2.27
	1.23	16±1.71	76.89±3.94	23.77±2.36
	1.00	16±2.17	80.94±5.83	29.1±4.05
LDPE-75°-EG	1.11	15.64±2.41	80.62±6.19	27.24±2.98
	1.16	14±2.09	81.74±4.54	27.46±2.92
	1.23	15.64±1.21	75.58±4.73	23.82±4.03
	1.00	14.4±2.68	80.82±4.15	30.4±4.06
LDPE-90°-EG	1.11	14±2.95	78.86±3.92	29.68±6.6
	1.16	13.5±2.57	80.73±6.58	28.61±3.45
	1.23	12.25±2.54	78.21±6.75	28.18±3.93

Table 18. Continued

Polymer-Inclined Angle α - Liquid	Contact Length Ratio σ	Critical Retention Volume (µL)	Advancing Contact Angle θ_A(°)	Receding Contact Angle θ_R(°)
	1.00	26.4±2.07	86.26±6.11	22.94±2.78
HDPE-45°-EG	1.09	24.73±2.41	90.28±8.32	31.13±7.45
	1.13	33.45±3.7	80.57±4.81	26.31±1.99
	1.24	34.5±5.59	81.31±3.16	22.26±1.73
	1.00	22.13±2.07	88.69±2.96	27.21±2.72
HDPE-60°-EG	1.09	22.5±6.33	81.32±7.02	29.31±5.46
	1.13	17.6±2.03	82.11±3.62	28.05±4.25
	1.24	20.36±2.8	80.68±4.61	25.59±3.35
	1.00	16.8±1.69	92.9±7.22	31.03±5.05
HDPE-75°-EG	1.09	17.6±4.97	84.32±15.86	32.57±6.92
	1.13	18.4±2.8	86.29±2.85	31.36±3.05
	1.24	18.8±1.93	83.94±5.06	30.06±5.11
	1.00	12.94±4.8	98.87±7.34	32.69±3.55
HDPE-90°-EG	1.09	18.9±2.47	77.55±15.12	31.01±6.28
	1.13	15±1.41	85.08±3.48	32.47±3.87
	1.24	15±0	88.13±3.06	28.15±1.88
	1.00	30.67±6.73	83.41±14.74	25.13±7.07
PP-45°-EG	1.11	27±0	88.96±7.24	28.65±4.06
	1.17	28.29±3.27	88.92±4.62	27.21±4.1
	1.25	31.5±6.84	86.46±4.71	26.27±2.55
	1.00	29.33±5.48	92.17±6.2	29.86±3.48
PP-60°-EG	1.11	24.6±4.12	92.86±7.58	32.61±5.87
	1.17	22±2.95	93.44±4.46	29.02±3.39
	1.25	19.93±3.25	96.68±11.33	35.04±7.85
	1.00	19.92±3.97	80.27±6.09	28.61±4.02
PP-75°-EG	1.11	20.31±1.97	98±6.49	32.32±3.55
	1.17	15.67±2.67	89.79±3.96	29.65±4.32
	1.25	16.67±1.56	92.44±3.46	31.06±3.1
	1.00	16.4±1.26	91.91±9.99	33.12±4.66
PP-90°-EG	1.11	20.77±3.35	89.68±2.66	30.1±2.31
	1.17	15.67±2.06	95.79±7.9	34.49±4.99
	1.25	13.2±1.93	96.85±7.66	34.09±4

Table 19. Reduce hysteresis H and θ_R / θ_A of various liquid-polymer combinations.

	Contact Length Ratio σ	**surface inclined angle α=45°**	**surface inclined angle α=60°**	**surface inclined angle α=75°**	**surface inclined angle α=90°**
		H/(θ_R / θ_A)	**H/(θ_R / θ_A)**	**H/(θ_R / θ_A)**	**H/(θ_R / θ_A)**
ABS-DI water	1	0.6/0.4	0.64/0.36	0.63/0.37	0.63/0.37
	1.15	0.54/0.46	0.62/0.38	0.61/0.39	0.61/0.39
	1.25	0.6/0.4	0.6/0.4	0.61/0.39	0.57/0.43
	1.42	0.6/0.4	0.65/0.35	0.64/0.36	0.63/0.37
HDPE-DI water	1	0.62/0.38	0.6/0.4	0.63/0.37	0.61/0.39
	1.09	0.65/0.35	0.68/0.32	0.68/0.32	0.68/0.32
	1.13	0.61/0.39	0.64/0.36	0.61/0.39	0.64/0.36
	1.24	0.63/0.37	0.65/0.35	0.65/0.35	0.66/0.34
LDPE-DI water	1	0.64/0.36	0.68/0.32	0.64/0.36	0.63/0.37
	1.11	0.7/0.3	0.64/0.36	0.65/0.35	0.63/0.37
	1.16	0.62/0.38	0.62/0.38	0.61/0.39	0.63/0.37
	1.23	0.59/0.41	0.61/0.39	0.6/0.4	0.61/0.39
PETE-DI water	1	0.7/0.3	0.71/0.29	0.71/0.29	0.7/0.3
	1.16	0.73/0.27	0.7/0.3	0.68/0.32	0.68/0.32
	1.26	0.75/0.25	0.7/0.3	0.72/0.28	0.69/0.31
	1.39	0.69/0.31	0.69/0.31	0.72/0.28	0.69/0.31
PP-DI water	1	0.7/0.3	0.68/0.32	0.69/0.31	0.7/0.3
	1.11	0.66/0.34	0.66/0.34	0.66/0.34	0.66/0.34
	1.17	0.63/0.37	0.63/0.37	0.63/0.37	0.63/0.37
	1.25	0.63/0.37	0.6/0.4	0.6/0.4	0.6/0.4

Table 19. Continued

	Contact Length Ratio σ	**surface inclined angle α=45°**	**surface inclined angle α=60°**	**surface inclined angle α=75°**	**surface inclined angle α=90°**
		H/(θ_R / θ_A)	**H/(θ_R / θ_A)**	**H/(θ_R / θ_A)**	**H/(θ_R / θ_A)**
ABS-EG	1	0.6/0.4	0.58/0.42	0.55/0.45	0.6/0.4
	1.15	0.62/0.38	0.58/0.42	0.61/0.39	0.66/0.34
	1.25	0.57/0.43	0.56/0.44	0.61/0.39	0.62/0.38
	1.42	0.6/0.4	0.6/0.4	0.6/0.4	0.57/0.43
HDPE-EG	1	0.73/0.27	0.69/0.31	0.67/0.33	0.67/0.33
	1.09	0.66/0.34	0.64/0.36	0.61/0.39	0.6/0.4
	1.13	0.67/0.33	0.66/0.34	0.64/0.36	0.62/0.38
	1.24	0.73/0.27	0.68/0.32	0.64/0.36	0.68/0.32
LDPE-EG	1	0.68/0.32	0.66/0.34	0.64/0.36	0.62/0.38
	1.11	0.7/0.3	0.69/0.31	0.66/0.34	0.62/0.38
	1.16	0.69/0.31	0.66/0.34	0.66/0.34	0.65/0.35
	1.23	0.7/0.3	0.69/0.31	0.68/0.32	0.64/0.36
PETE-EG	1	0.7/0.3	0.72/0.28	0.68/0.32	0.71/0.29
	1.16	0.7/0.3	0.7/0.3	0.66/0.34	0.7/0.3
	1.26	0.75/0.25	0.72/0.28	0.72/0.28	0.7/0.3
	1.39	0.75/0.25	0.74/0.26	0.64/0.36	0.67/0.33
PP-EG	1	0.7/0.3	0.64/0.36	0.64/0.36	0.64/0.36
	1.11	0.68/0.32	0.65/0.35	0.67/0.33	0.66/0.34
	1.17	0.69/0.31	0.69/0.31	0.67/0.33	0.64/0.36
	1.25	0.7/0.3	0.68/0.32	0.66/0.34	0.65/0.35
	ABS	HDPE	LDPE	PETE	PP
H/(θ_R / θ_A)	0.6/0.4	0.65/0.35	0.65/0.35	0.7/0.3	0.66/0.34
	±0.028	±0.034	±0.032	±0.025	±0.029

Table 20. Liquids' critical retention volumes on polymers with various conditions. Comparisons of experiment data with the present and previous models.

Polymer-Inclined Angle α	Contact Length Ratio σ	Critical Retention Volume (μL)	The proposed model (μL)	ElSherbini [40] model (μL)	Dussan [38] model (μL)	Extrand [39] model (μL)
			Ave. / Error	Ave. / Error	Ave. / Error	Ave. / Error
ABS-45°-DI water	1.00	40.5±6.07	58.32/17.82	49.38/8.88	50.94/10.44	36.83/3.67
	1.15	43.71±5.97	58.48/14.76	39.39/4.32	43.03/0.68	29.38/14.33
	1.25	54.64±11.95	60.93/6.29	45.02/9.63	47.8/6.84	33.58/21.07
	1.42	68.54±18.2	63.33/5.21	42.35/26.19	45.65/22.89	31.59/36.95
ABS-60°-DI water	1.00	36±3.84	38.09/2.09	45.81/9.81	41.69/5.69	34.17/1.83
	1.15	37.29±5.97	38.45/1.17	43.1/5.81	40.47/3.19	32.15/5.14
	1.25	39.46±7.83	43.05/3.59	41.12/1.66	40.9/1.43	39.11/0.35
	1.42	51.92±8.68	43.71/8.21	41.06/10.85	40.96/10.95	30.63/21.29
ABS-75°-DI water	1.00	28.5±5.2	31.42/2.92	38.38/9.88	34.46/5.96	28.63/0.13
	1.15	31±6.69	31.54/0.54	38.59/7.59	34.65/3.65	28.78/2.22
	1.25	32.31±10.55	34.51/2.2	37.05/4.74	35.52/3.21	34.02/1.71
	1.42	56±6.48	35.06/20.94	37.4/18.6	35.92/20.08	27.89/28.11
ABS-90°-DI water	1.00	28.5±4.52	29.1/0.6	36.74/8.24	32.22/3.72	27.41/1.09
	1.15	30.43±5.98	28.67/1.76	32.86/2.44	30.01/0.42	24.51/5.92
	1.25	31±5.62	31.95/0.95	36.82/5.82	34.3/3.3	33.27/2.27
	1.42	44.33±7.33	32.72/11.61	35.78/8.56	34.06/10.27	26.69/17.65
PETE-45°-DI water	1.00	68.25±8.97	70.92/2.67	58.55/9.7	57.78/10.47	43.67/24.58
	1.16	63±17.59	67.63/4.63	62.46/0.54	60.05/2.95	46.59/16.41
	1.26	59±5.91	62.74/3.74	77.56/18.56	66.18/7.18	57.85/1.15
	1.39	62±11.42	63.17/1.17	80.24/18.24	67.43/5.43	59.85/2.15
PETE -60°-DI water	1.00	46.29±5.71	51.99/5.7	44.04/2.24	43.18/3.1	32.85/13.43
	1.16	43.5±9.97	49.28/5.78	46.83/3.33	44.66/1.16	34.93/8.57
	1.26	40.25±4.35	45.59/5.34	54.34/14.09	47.26/7.01	40.53/0.28
	1.39	41.42±3.6	45.23/3.81	53.73/12.32	46.8/5.39	40.08/1.34
PETE -75°-DI water	1.00	50.62±3.07	42.36/8.25	40.79/9.82	38.62/12	30.43/20.19
	1.16	33±6.75	38.65/5.65	48.87/15.87	41.18/8.18	36.45/3.45
	1.26	37.1±3.38	36.69/0.41	46.03/8.93	38.7/1.6	34.33/2.77
	1.39	40.38±5.82	37.43/2.95	49.65/9.27	40.54/0.16	37.04/3.35
PETE -90°-DI water	1.00	35.5±6.98	39.52/4.02	38.68/3.18	36.51/1.01	28.85/6.65
	1.16	30.45±6.88	37.82/7.37	41.2/10.75	37.4/6.94	30.73/0.28
	1.26	32.27±4.1	35.67/3.4	42/9.72	36.68/4.41	31.32/0.95
	1.39	37.17±3.24	35.13/2.04	44.07/6.9	37.12/0.04	32.87/4.3

Table 20. Continued

Polymer-Inclined Angle α	Contact Length Ratio σ	Critical Retention Volume (µL)	The proposed model (µL) Ave. / Error	ElSherbini [40] model (µL) Ave. / Error	Dussan [38] model (µL) Ave. / Error	Extrand [39] model (µL) Ave. / Error
HDPE-45°-DI water	1.00	65.25±4.07	59.6/5.65	64.11/1.14	59.1/6.15	47.82/17.43
	1.09	58.5±11.78	56.68/1.82	61.22/2.72	56.03/2.47	45.67/12.83
	1.13	60±5.86	64.61/4.61	49.05/10.95	50.72/9.28	36.59/23.41
	1.24	62.25±8.97	63.61/1.36	54.69/7.56	54.6/7.65	40.8/21.45
HDPE-60°-DI water	1.00	39.5±4.01	42.73/3.23	52.74/13.24	45.41/5.91	39.34/0.16
	1.09	40.8±7.38	45.77/4.97	38.59/2.21	38.85/1.95	28.79/12.01
	1.13	45±4.05	46.1/1.1	42.74/2.26	41.68/3.32	31.88/13.12
	1.24	46.91±7.5	46.97/0.06	43.07/3.84	42.08/4.83	32.13/14.78
HDPE-75°-DI water	1.00	35.6±6.98	37.1/1.5	43.45/7.85	38.52/2.92	32.41/3.19
	1.09	39.82±4.85	41.62/1.8	31.25/8.57	32.25/7.56	23.31/16.51
	1.13	30.38±5.57	38.91/8.53	33.55/3.17	33.53/3.16	25.02/5.35
	1.24	40±5.91	39.22/0.78	37.05/2.95	35.88/4.12	27.64/12.36
HDPE-90°-DI water	1.00	30±4.43	35.1/5.1	42.05/12.05	36.85/6.85	31.37/1.37
	1.09	36.8±3.84	40.13/3.33	27.44/9.36	28.94/7.86	20.47/16.33
	1.13	35.6±6.98	36.47/0.87	34.9/0.7	33.69/1.91	26.03/9.57
	1.24	32±4.9	36.08/4.08	38.19/6.19	35.45/3.45	28.48/3.52
PP-45°-DI water	1.00	72.78±7.12	52/20.78	69.76/3.02	63.13/9.65	52.03/20.75
	1.11	54.64±5.71	44.72/9.92	72.52/17.88	57.65/3.01	54.09/0.55
	1.17	41.67±3.89	43.52/1.85	67.5/25.83	54.47/12.81	50.35/8.68
	1.25	38.33±5.77	41.13/2.8	68.84/30.51	50.7/12.37	51.35/13.02
PP-60°-DI water	1.00	50.67±8.84	39.22/11.44	47.85/2.82	44.98/5.68	35.69/14.98
	1.11	35±5.22	31.87/3.13	55.11/20.11	41.02/6.02	41.1/6.1
	1.17	30.5±3.09	31.54/1.04	50.8/20.3	39.57/9.07	37.89/7.39
	1.25	27.83±4.3	31.17/3.34	46.63/18.8	37.86/10.03	34.78/6.95
PP-75°-DI water	1.00	40.5±8.14	32.28/8.22	43.38/2.88	39.25/1.25	32.36/8.14
	1.11	26.5±3.09	28.14/1.64	45.08/18.58	36.2/9.7	33.63/7.13
	1.17	25±2.34	25.5/0.5	42.61/17.61	31.15/6.15	31.78/6.78
	1.25	22.5±2.71	25.3/2.8	39.54/17.04	30.21/7.71	29.49/6.99
PP-90°-DI water	1.00	39.82±7.24	30.08/9.74	43.03/3.21	37.8/2.02	32.09/7.73
	1.11	20±2.95	27.24/7.24	42.85/22.85	35.07/15.07	31.96/11.96
	1.17	21.75±6.36	25.92/4.17	40.31/18.56	32.5/10.75	30.07/8.32
	1.25	19±2.34	24.42/5.42	37.79/18.79	29.44/10.44	28.19/9.19

Table 20. Continued

Polymer-Inclined Angle α	Contact Length Ratio σ	Critical Retention Volume (µL)	The proposed model (µL) Ave. / Error	ElSherbini [40] model (µL) Ave. / Error	Dussan [38] model (µL) Ave. / Error	Extrand [39] model (µL) Ave. / Error
LDPE-45° DI water	1.00	42.75±5.59	61.38/18.63	61.21/18.46	57.9/15.15	45.66/2.91
	1.11	67.5±9	65.16/2.34	66.15/1.35	61.84/5.66	49.34/18.16
	1.16	59.25±8.97	63.23/3.98	54.94/4.31	54.53/4.72	40.98/18.27
	1.23	48.75±6.02	63.03/14.28	49.7/0.95	50.84/2.09	37.07/11.68
LDPE-60° DI water	1.00	43.5±6.46	41.99/1.51	54.02/10.52	44.84/1.34	40.29/3.21
	1.11	45±6.65	42.78/2.22	47.94/2.94	42.95/2.05	35.76/9.24
	1.16	44.18±6.31	43.37/0.81	44.09/0.09	41.3/2.89	32.89/11.3
	1.23	35.25±7.14	43.44/8.19	42.25/7	40.28/5.03	31.52/3.73
LDPE-75° DI water	1.00	32.25±6.02	33.22/0.97	43.45/11.2	34.73/2.48	32.41/0.16
	1.11	39.6±8.69	34/5.6	43.43/3.83	35.62/3.98	32.4/7.2
	1.16	31.5±7.65	34.6/3.1	38.08/6.58	34.03/2.53	28.4/3.1
	1.23	31.09±7.38	34.81/3.72	37.1/6.01	33.71/2.62	27.67/3.42
LDPE-90° DI water	1.00	29±5.01	30.28/1.28	40.23/11.23	31.05/2.05	30.01/1.01
	1.11	36.75±8.1	30.55/6.2	40.6/3.85	31.52/5.23	30.28/6.47
	1.16	31.5±4.7	31.07/0.43	40.3/8.8	32.12/0.62	30.06/1.44
	1.23	30±4.43	31.41/1.41	37.12/7.12	31.47/1.47	27.69/2.31
LDPE-45°-EG	1.00	30.36±3.67	21.15/9.21	22.17/8.19	15.78/14.58	19.08/11.28
	1.11	21.29±3.1	17.13/4.15	18.48/2.8	12.78/8.51	20.92/0.36
	1.16	19±1.81	19.26/0.26	20.49/1.49	14.37/4.63	19.94/0.94
	1.23	20±0	18.75/1.25	19.97/0.03	13.98/6.02	20.36/0.36
LDPE-60°-EG	1.00	19.67±2.06	13.5/6.17	14.58/5.09	10.07/9.6	14.45/5.21
	1.11	17.23±1.92	13.39/3.84	14.37/2.87	9.98/7.25	15.02/2.21
	1.16	14.86±1.88	13.39/1.47	14.47/0.38	9.99/4.87	14.54/0.32
	1.23	16±1.71	14.13/1.87	15.03/0.97	10.54/5.46	14.79/1.21
LDPE-75°-EG	1.00	16±2.17	12/4	12.9/3.1	8.95/7.05	11.83/4.17
	1.11	15.64±2.41	12.42/3.23	13.22/2.43	9.26/6.38	11.99/3.65
	1.16	14±2.09	12.76/1.24	13.51/0.49	9.52/4.48	11.89/2.11
	1.23	15.64±1.21	11.51/4.13	12.34/3.3	8.58/7.05	12.66/2.98
LDPE-90°-EG	1.00	14.4±2.68	10.99/3.41	11.92/2.48	8.2/6.2	11.15/3.25
	1.11	14±2.95	10.54/3.46	11.51/2.49	7.86/6.14	11.34/2.66
	1.16	13.5±2.57	11.46/2.04	12.29/1.21	8.55/4.95	11.28/2.22
	1.23	12.25±2.54	10.71/1.54	11.64/0.61	7.99/4.26	11.49/0.76

Table 20. Continued

Polymer-Inclined Angle α	Contact Length Ratio σ	Critical Retention Volume (µL)	The proposed model (µL)	ElSherbini [40] model (µL)	Dussan [38] model (µL)	Extrand [39] model (µL)
			Ave. / Error	Ave. / Error	Ave. / Error	Ave. / Error
ABS-45°-EG	1.00	26.14±8.23	22.86/3.28	23.53/2.61	17.05/9.09	33.35/7.21
	1.15	30±3.02	20.17/9.83	21.41/8.59	15.04/14.96	32.62/2.62
	1.25	35.43±9.26	16.35/19.07	18.16/17.27	12.2/23.23	37.52/2.09
	1.42	33.23±9.15	17.73/15.5	19.43/13.8	13.23/20	36.47/3.24
ABS-60°-EG	1.00	20.71±6.16	15.39/5.32	16.2/4.51	11.48/9.23	24.17/3.46
	1.15	22.5±11.12	13.54/8.96	14.75/7.75	10.1/12.4	25.05/2.55
	1.25	21.54±2.6	11.28/10.25	12.7/8.84	8.42/13.12	27.64/6.1
	1.42	21.15±9.16	11.81/9.34	13.15/8	8.81/12.34	28/6.85
ABS-75°-EG	1.00	16.15±2.3	15.11/1.04	15.18/0.97	11.27/4.88	19.92/3.76
	1.15	22±6.49	14.67/7.33	14.92/7.08	10.94/11.06	20.21/1.79
	1.25	20±5.48	8.86/11.14	10.11/9.89	6.61/13.39	23.36/3.36
	1.42	20±7.91	11.32/8.68	12.35/7.65	8.44/11.56	22.76/2.76
ABS-90°-EG	1.00	18±6.61	14.98/3.02	15/3	11.17/6.83	20.06/2.06
	1.15	17.14±8.07	11.87/5.27	12.68/4.46	8.85/8.29	21.2/4.06
	1.25	16.38±3.15	9.95/6.44	11/5.38	7.42/8.97	22.19/5.81
	1.42	18.67±7.2	10.03/8.63	11.12/7.54	7.48/11.18	21.13/2.46
PETE-45°-EG	1.00	18.9±6.49	30.37/11.47	28.28/9.38	22.65/3.75	26.76/7.86
	1.16	30.75±4.63	25.8/4.95	25.71/5.04	19.25/11.5	29.23/1.52
	1.26	28.33±4.19	28.08/0.26	27.18/1.16	20.94/7.39	30.11/1.78
	1.39	22.21±9.33	29.69/7.48	28.21/5.99	22.15/0.07	29.33/7.12
PETE -60°-EG	1.00	16.5±3.67	22.5/6	21.06/4.56	16.78/0.28	20.39/3.89
	1.16	20.33±2.97	19.72/0.61	19.43/0.91	14.71/5.62	21.26/0.93
	1.26	17.86±2.57	17.62/0.24	17.88/0.02	13.14/4.71	22.83/4.98
	1.39	15.45±6.88	20.65/5.19	20.03/4.57	15.4/0.05	21.87/6.42
PETE -75°-EG	1.00	16.4±2.97	18.04/1.64	17.15/0.75	13.46/2.94	16.74/0.34
	1.16	18.33±2.44	14.56/3.77	14.96/3.37	10.86/7.47	18.22/0.12
	1.26	17.5±3.25	15.91/1.59	15.9/1.6	11.87/5.63	18.97/1.47
	1.39	20.36±6.64	12.61/7.75	13.42/6.93	9.41/10.95	18.8/1.56
PETE -90°-EG	1.00	14.44±1.21	17.37/2.93	16.53/2.09	12.95/1.48	16.46/2.02
	1.16	16±2.67	14.73/1.27	14.85/1.15	10.99/5.01	17.56/1.56
	1.26	15.6±2.95	13.61/1.99	13.99/1.61	10.15/5.45	18.27/2.67
	1.39	16.57±5.84	13.49/3.08	13.95/2.63	10.06/6.51	17.59/1.02

Table 20. Continued

Polymer-Inclined Angle α	Contact Length Ratio σ	Critical Retention Volume (µL)	The proposed model (µL)	ElSherbini [40] model (µL)	Dussan [38] model (µL)	Extrand [39] model (µL)
			Ave. / Error	Ave. / Error	Ave. / Error	Ave. / Error
Polymer-HDPE-45°-EG	1.00	26.4±2.07	25.14/1.26	25.16/1.24	18.75/7.65	25.82/0.58
	1.09	24.73±2.41	23.55/1.18	24.1/0.63	17.56/7.16	23.97/0.76
	1.13	33.45±3.7	20.21/13.24	21.4/12.06	15.08/18.38	26.2/7.25
	1.24	34.5±5.59	22.43/12.07	23.04/11.46	16.73/17.77	26.76/7.74
HDPE-60°-EG	1.00	22.13±2.07	18.14/3.99	18.33/3.8	13.53/8.6	18.28/3.85
	1.09	22.5±6.33	14.23/8.27	15.27/7.23	10.61/11.89	18.88/3.62
	1.13	17.6±2.03	14.99/2.61	15.89/1.71	11.18/6.42	18.94/1.34
	1.24	20.36±2.8	15.2/5.17	16/4.36	11.34/9.03	19.41/0.96
HDPE-75°-EG	1.00	16.8±1.69	15.72/1.08	15.78/1.02	11.73/5.07	14.78/2.02
	1.09	17.6±4.97	12.18/5.42	13.09/4.51	9.08/8.52	15.43/2.17
	1.13	18.4±2.8	13.25/5.15	13.95/4.45	9.88/8.52	15.35/3.05
	1.24	18.8±1.93	12.8/6	13.58/5.22	9.54/9.26	15.7/3.1
HDPE-90°-EG	1.00	12.94±4.8	16.39/3.45	15.85/2.91	12.23/0.71	13.41/0.47
	1.09	18.9±2.47	9.74/9.16	10.81/8.09	7.27/11.63	15.42/3.48
	1.13	15±1.41	11.84/3.16	12.66/2.34	8.83/6.17	14.59/0.41
	1.24	15±0	14.15/0.85	14.44/0.56	10.55/4.45	14.7/0.3
PP-45°-EG	1.00	30.67±6.73	22.43/8.24	23.16/7.51	16.73/13.94	35.33/4.67
	1.11	27±0	24.04/2.96	24.46/2.54	17.93/9.07	33.42/6.42
	1.17	28.29±3.27	24.72/3.56	24.95/3.34	18.44/9.84	33.72/5.43
	1.25	31.5±6.84	23.71/7.79	24.19/7.31	17.69/13.81	34.43/2.93
PP-60°-EG	1.00	29.33±5.48	18.66/10.67	18.7/10.64	13.92/15.41	24/5.33
	1.11	24.6±4.12	17.89/6.71	18.13/6.47	13.34/11.26	23.51/1.09
	1.17	22±2.95	19.53/2.47	19.28/2.72	14.57/7.43	23.94/1.94
	1.25	19.93±3.25	18.49/1.44	18.46/1.47	13.79/6.14	22.65/2.72
PP-75°-EG	1.00	19.92±3.97	11.9/8.02	12.8/7.12	8.88/11.05	22.08/2.16
	1.11	20.31±1.97	17.09/3.21	16.61/3.7	12.75/7.56	19.39/0.92
	1.17	15.67±2.67	15.05/0.62	15.31/0.35	11.22/4.44	20.7/5.03
	1.25	16.67±1.56	15.55/1.12	15.66/1	11.6/5.07	20.2/3.53
PP-90°-EG	1.00	16.4±1.26	13.94/2.46	14.27/2.13	10.4/6	19/2.6
	1.11	20.77±3.35	14.11/6.66	14.41/6.36	10.52/10.25	19.61/1.16
	1.17	15.67±2.06	14.79/0.87	14.83/0.84	11.03/4.63	18.41/2.75
	1.25	13.2±1.93	15.27/2.07	15.14/1.94	11.39/1.81	18.34/5.14

Table 21. Average liquid-solid surface tension, unit in mN/m.

	ABS	HDPE	LDPE	PETE	PP
DI water	17.59	18.63	18.77	18.93	16.55
EG	13.22	10.28	8.39	11.57	12.66

Table 22. MSE of proposed model for all plastics-α-σ combinations: [unit in μL]

	Overall	ABS	HDPE	LDPE	PETE	PP
DI water	6.67	8.94	3.77	6.82	4.66	7.77
EG	3.76	4.13	3.39	3.78	3.70	3.76

Table 23. MSE of proposed and previous models in overall. [unit in μL]

	Proposed	ElShernini	Dussan	Extrand
DI water	6.67	11.65	7.24	11.68
EG	3.76	6.25	5.54	9.31

Table 24. Liquids' advancing contact angles on structured polymers at various inclined angles. Comparisons of experiment with predicted values.

Polymer-Inclined Angle α	**Contact Length Ratio σ**	**Measured θ_A (°)**	**Predicted θ_A /error (°)**	**Error %**
ABS-45°-DI water	1.00	94.66±8.06	-	-
	1.15	90.19±4.69	91.25/1.05	1.17
	1.25	89.21±6.02	89.11/0.1	0.11
	1.42	85.01±5.96	85.29/0.28	0.33
ABS-60°-DI water	1.00	110.93±6.31	-	-
	1.15	108.5±6.72	104.87/3.63	3.34
	1.25	97.26±5.23	101.07/3.81	3.92
	1.42	95.96±7.67	94.3/1.66	1.73
ABS-75°-DI water	1.00	113.38±6.99	-	-
	1.15	113.14±7.14	108.87/4.28	3.78
	1.25	103.68±13.41	106.03/2.35	2.27
	1.42	102.51±12.88	100.99/1.52	1.49
ABS-90°-DI water	1.00	116.03±6.62	-	-
	1.15	114.62±5.89	111.34/3.28	2.86
	1.25	107.13±12.06	108.4/1.27	1.19
	1.42	104.22±7.02	103.16/1.06	1.02
PETE-45°-DI water	1.00	92.17±4.29	-	-
	1.16	97.54±7.82	100.38/2.84	2.91
	1.26	110.18±5.67	105.63/4.55	4.13
	1.39	110.68±6.13	112.68/2	1.81
PETE -60°-DI water	1.00	93.15±4.53	-	-
	1.16	98.97±7.43	100.71/1.74	1.76
	1.26	109.95±5.28	105.55/4.41	4.01
	1.39	110.34±3.47	112.04/1.7	1.54
PETE -75°-DI water	1.00	98.62±8.97	-	-
	1.16	111.88±8.57	105.36/6.52	5.83
	1.26	114.93±4.69	109.67/5.26	4.58
	1.39	115.44±8.67	115.45/0.01	0.01
PETE -90°-DI water	1.00	100.04±8.48	-	-
	1.16	105.54±5.6	106/0.46	0.44
	1.26	111.45±5.85	109.82/1.62	1.45
	1.39	114.36±7.5	114.94/0.58	0.51

Table 24. Continued

Polymer-Inclined Angle α	Contact Length Ratio σ	Measured θ_A (°)	Predicted θ_A /error (°)	Error %
HDPE-45°-DI water	1.00	107.02±5.23	-	-
	1.09	110.5±24.69	102.6/7.89	7.14
	1.13	93.69±6.1	100.08/6.39	6.82
	1.24	97.36±5.37	94.53/2.83	2.9
HDPE-60°-DI water	1.00	112.77±3.92	-	-
	1.09	98.54±8.59	108.37/9.83	9.98
	1.13	100.24±4.72	105.85/5.61	5.59
	1.24	98.82±7.52	100.31/1.49	1.51
HDPE-75°-DI water	1.00	109.78±8.81	-	-
	1.09	91.74±6.5	107.46/15.72	17.13
	1.13	98.93±5.05	106.13/7.2	7.28
	1.24	100.57±8.29	103.22/2.64	2.63
HDPE-90°-DI water	1.00	110.65±6.49	-	-
	1.09	88.89±4.68	110.18/21.28	23.94
	1.13	102.18±5.25	109.91/7.73	7.57
	1.24	105.43±8.92	109.31/3.88	3.68
PP-45°-DI water	1.00	105.7±6.45	-	-
	1.11	121.32±6.55	114.97/6.35	5.23
	1.17	121.91±5.6	120.57/1.34	1.1
	1.25	128.46±3.8	127.54/0.93	0.72
PP-60°-DI water	1.00	101.77±7.59	-	-
	1.11	125.93±6.97	110.56/15.37	12.21
	1.17	124.38±5.93	115.87/8.5	6.84
	1.25	123.01±5.18	122.48/0.53	0.43
PP-75°-DI water	1.00	106.29±11.34	-	-
	1.11	120.61±7.05	115.98/4.63	3.84
	1.17	129.19±4.47	121.83/7.36	5.7
	1.25	127.7±6.52	129.11/1.41	1.1
PP-90°-DI water	1.00	109.26±11.21	-	-
	1.11	118.68±5.54	116.38/2.3	1.94
	1.17	121.87±6.58	120.68/1.19	0.98
	1.25	126.15±6.2	126.04/0.11	0.09

Table 24. Continued

Polymer-Inclined Angle α	Contact Length Ratio σ	Measured θ_A (°)	Predicted θ_A /error (°)	Error %
LDPE-45° DI water	1.00	104.34±4.32	-	-
	1.11	101.17±5.36	100.75/0.42	0.41
	1.16	99.12±4.38	99.32/0.2	0.2
	1.23	97.21±4.71	97.1/0.11	0.11
LDPE-60° DI water	1.00	116.48±6.88	-	-
	1.11	111.19±4.32	111.3/0.11	0.1
	1.16	107.69±4.85	109.23/1.54	1.43
	1.23	106.51±2.71	106.03/0.48	0.45
LDPE-75° DI water	1.00	121.94±4	-	-
	1.11	119.55±5.53	117.11/2.44	2.04
	1.16	114.09±7.81	115.17/1.08	0.94
	1.23	112.81±3.24	112.18/0.63	0.56
LDPE-90° DI water	1.00	125.42±6.01	-	-
	1.11	124.74±5.11	122.47/2.27	1.82
	1.16	122.77±4.69	121.29/1.48	1.21
	1.23	119.25±3.97	119.47/0.22	0.18
LDPE-45°-EG	1.00	82.15±3.74	-	-
	1.11	72.16±4.65	79.15/6.99	9.69
	1.16	77.34±4.32	77.95/0.61	0.79
	1.23	75.49±3.92	76.1/0.61	0.8
LDPE-60°-EG	1.00	77.55±4.82	-	-
	1.11	74.86±5.71	77.33/2.47	3.3
	1.16	77.02±5.23	77.24/0.22	0.29
	1.23	76.89±3.94	77.1/0.21	0.28
LDPE-75°-EG	1.00	80.94±5.83	-	-
	1.11	80.62±6.19	78.8/1.83	2.26
	1.16	81.74±4.54	77.93/3.81	4.66
	1.23	75.58±4.73	76.61/1.02	1.35
LDPE-90°-EG	1.00	80.82±4.15	-	-
	1.11	78.86±3.92	79.79/0.93	1.18
	1.16	80.73±6.58	79.38/1.35	1.67
	1.23	78.21±6.75	78.75/0.54	0.7

Table 24. Continued

Polymer-Inclined Angle α	Contact Length Ratio σ	Measured θ_A (°)	Predicted θ_A /error (°)	Error %
	1.00	92.98±9.47	-	-
ABS-45°-EG	1.15	92.36±6.94	87.76/4.6	4.98
	1.25	77.69±3.64	84.48/6.79	8.74
	1.42	81.14±7.48	78.63/2.5	3.08
	1.00	92.62±7.81	-	-
ABS-60°-EG	1.15	87.31±9.41	86.26/1.05	1.2
	1.25	76.74±3.97	82.26/5.52	7.19
	1.42	76.53±6.68	75.15/1.38	1.8
	1.00	98.18±8.59	-	-
ABS-75°-EG	1.15	96.29±6.23	90.94/5.35	5.55
	1.25	75.87±3.39	86.39/10.52	13.86
	1.42	81.74±8.92	78.29/3.44	4.21
	1.00	94.17±8.62	-	-
ABS-90°-EG	1.15	84.99±11.73	89.64/4.65	5.47
	1.25	78.46±7.99	86.79/8.33	10.62
	1.42	82.27±5.51	81.72/0.55	0.67
	1.00	101.73±7.24	-	-
PETE-45°-EG	1.16	90.55±6.88	98.92/8.36	9.24
	1.26	90.46±5.11	97.25/6.79	7.51
	1.39	93.84±7.85	94.32/0.48	0.51
	1.00	99.16±10.26	-	-
PETE -60°-EG	1.16	92.46±3.85	95.81/3.35	3.62
	1.26	84.66±4.56	93.82/9.15	10.81
	1.39	91.5±6.55	90.31/1.19	1.3
	1.00	100.43±5.47	-	-
PETE -75°-EG	1.16	88.56±3.23	94.18/5.62	6.34
	1.26	87.58±5.76	90.48/2.9	3.32
	1.39	83.28±14.1	83.95/0.67	0.81
	1.00	97.89±3.21	-	-
PETE -90°-EG	1.16	88.81±7.81	93.53/4.72	5.32
	1.26	84.2±4.65	90.96/6.75	8.02
	1.39	86.76±9.84	86.4/0.36	0.41

Table 24. Continued

Polymer-Inclined Angle α	Contact Length Ratio σ	Measured θ_A (°)	Predicted θ_A /error (°)	Error %
HDPE-45°-EG	1.00	86.26±6.11	-	-
	1.09	90.28±8.32	83.87/6.41	7.1
	1.13	80.57±4.81	82.51/1.93	2.4
	1.24	81.31±3.16	79.5/1.81	2.22
HDPE-60°-EG	1.00	88.69±2.96	-	-
	1.09	81.32±7.02	86.12/4.8	5.9
	1.13	82.11±3.62	84.66/2.55	3.1
	1.24	80.68±4.61	81.44/0.76	0.94
HDPE-75°-EG	1.00	92.9±7.22	-	-
	1.09	84.32±15.86	90.1/5.77	6.85
	1.13	86.29±2.85	88.5/2.2	2.55
	1.24	83.94±5.06	84.97/1.04	1.24
HDPE-90°-EG	1.00	98.87±7.34	-	-
	1.09	77.55±15.12	96.12/18.57	23.95
	1.13	85.08±3.48	94.56/9.47	11.14
	1.24	88.13±3.06	91.11/2.98	3.38
PP-45°-EG	1.00	83.41±14.74	-	-
	1.11	88.96±7.24	84.78/4.18	4.7
	1.17	88.92±4.62	85.61/3.31	3.72
	1.25	86.46±4.71	86.64/0.18	0.21
PP-60°-EG	1.00	92.17±6.2	-	-
	1.11	92.86±7.58	93.96/1.1	1.19
	1.17	93.44±4.46	95.04/1.6	1.71
	1.25	96.68±11.33	96.39/0.29	0.29
PP-75°-EG	1.00	80.27±6.09	-	-
	1.11	98±6.49	84.58/13.43	13.7
	1.17	89.79±3.96	87.17/2.62	2.92
	1.25	92.44±3.46	90.41/2.03	2.2
	1.00	91.91±9.99	-	-
PP-90°-EG	1.11	89.68±2.66	94.42/4.74	5.29
	1.17	95.79±7.9	95.94/0.15	0.15
	1.25	96.85±7.66	97.82/0.97	1

Table 25. Liquids' critical retention volumes on polymers with various conditions. Comparisons of experiment data with predicted values.

Polymer-liquid-Inclined Angle α	Contact Length Ratio σ	Critical Retention Volume (μL)	Predicted Volume / Error (μL)	Polymer-liquid-Inclined Angle α	Contact Length Ratio σ	Critical Retention Volume (μL)	Predicted Volume / Error (μL)
ABS-DI WATER-45°	1.00	40.5±6.07	-	**HDPE- DI WATER-45°**	1.00	65.25±4.07	-
	1.15	43.71±5.97	60.37/16.66		1.09	58.5±11.78	61.28/2.78
	1.25	54.64±11.95	61.46/6.82		1.13	60±5.86	62.55/2.55
	1.42	68.54±18.2	63.46/5.08		1.24	62.25±8.97	65.42/3.17
ABS-DI WATER-60°	1.00	36±3.84	-	**HDPE- DI WATER-60°**	1.00	39.5±4.01	-
	1.15	37.29±5.97	39.79/2.51		1.09	40.8±7.38	43.15/2.35
	1.25	39.46±7.83	41.07/1.61		1.13	45±4.05	44.04/0.96
	1.42	51.92±8.68	43.43/8.49		1.24	46.91±7.5	46.06/0.85
ABS-DI WATER-75°	1.00	28.5±5.2	-	**HDPE- DI WATER-75°**	1.00	35.6±6.98	-
	1.15	31±6.69	32.68/1.68		1.09	39.82±4.85	36.9/2.91
	1.25	32.31±10.55	33.46/1.15		1.13	30.38±5.57	37.3/6.93
	1.42	56±6.48	34.89/21.11		1.24	40±5.91	38.19/1.81
ABS-DI WATER-90°	1.00	28.5±4.52	-	**HDPE- DI WATER-90°**	1.00	30±4.43	-
	1.15	30.43±5.98	30.39/0.04		1.09	36.8±3.84	34.27/2.53
	1.25	31±5.62	31.15/0.15		1.13	35.6±6.98	34.34/1.26
	1.42	44.33±7.33	32.53/11.8		1.24	32±4.9	34.51/2.51
ABS-EG-45°	1.00	26.14±8.23	-	**HDPE-EG-45°**	1.00	26.4±2.07	-
	1.15	30±3.02	34.39/4.39		1.09	24.73±2.41	25.34/0.62
	1.25	35.43±9.26	35.36/0.07		1.13	33.45±3.7	25.63/7.82
	1.42	33.23±9.15	37.18/3.95		1.24	34.5±5.59	26.28/8.22
ABS-EG-60°	1.00	20.71±6.16	-	**HDPE-EG-60°**	1.00	22.13±2.07	-
	1.15	22.5±11.12	25.7/3.2		1.09	22.5±6.33	18.41/4.09
	1.25	21.54±2.6	26.59/5.05		1.13	17.6±2.03	18.58/0.98
	1.42	21.15±9.16	28.29/7.13		1.24	20.36±2.8	19.08/1.28
ABS-EG-75°	1.00	16.15±2.3	-	**HDPE-EG-75°**	1.00	16.8±1.69	-
	1.15	22±6.49	20.97/1.03		1.09	17.6±4.97	15.09/2.51
	1.25	20±5.48	21.79/1.79		1.13	18.4±2.8	15.28/3.12
	1.42	20±7.91	23.36/3.36		1.24	18.8±1.93	15.73/3.07
ABS-EG-90°	1.00	18±6.61	-	**HDPE-EG-90°**	1.00	12.94±4.8	-
	1.15	17.14±8.07	20.13/2.98		1.09	18.9±2.47	13.65/5.25
	1.25	16.38±3.15	20.62/4.23		1.13	15±1.41	13.82/1.18
	1.42	18.67±7.2	21.53/2.86		1.24	15±0	14.21/0.79

Table 25. Continued

Polymer-liquid-Inclined Angle α	Contact Length Ratio σ	Critical Retention Volume (μL)	Predicted Volume / Error (μL)	Polymer-liquid-Inclined Angle α	Contact Length Ratio σ	Critical Retention Volume (μL)	Predicted Volume / Error (μL)
LDPE- DI WATER-45°	1.00	42.75±5.59	-	**PETE- DI WATER-45°**	1.00	68.25±8.97	-
	1.11	67.5±9	62.68/4.82		1.16	63±17.59	66.53/3.53
	1.16	59.25±8.97	63.42/4.17		1.26	59±5.91	63.89/4.89
	1.23	48.75±6.02	64.58/15.83		1.39	62±11.42	60.51/1.49
LDPE- DI WATER-60°	1.00	43.5±6.46	-	**PETE- DI WATER-60°**	1.00	46.29±5.71	-
	1.11	45±6.65	42.42/2.58		1.16	43.5±9.97	48.96/5.46
	1.16	44.18±6.31	43.15/1.03		1.26	40.25±4.35	47.17/6.92
	1.23	35.25±7.14	44.3/9.05		1.39	41.42±3.6	44.86/3.45
LDPE- DI WATER-75°	1.00	32.25±6.02	-	**PETE- DI WATER-75°**	1.00	50.62±3.07	-
	1.11	39.6±8.69	34.32/5.28		1.16	33±6.75	40.1/7.1
	1.16	31.5±7.65	34.88/3.38		1.26	37.1±3.38	38.79/1.69
	1.23	31.09±7.38	35.75/4.66		1.39	40.38±5.82	37.09/3.29
LDPE- DI WATER-90°	1.00	29±5.01	-	**PETE- DI WATER-90°**	1.00	35.5±6.98	-
	1.11	36.75±8.1	31.13/5.62		1.16	30.45±6.88	37.88/7.43
	1.16	31.5±4.7	31.45/0.05		1.26	32.27±4.1	36.78/4.51
	1.23	30±4.43	31.94/1.94		1.39	37.17±3.24	35.35/1.82
LDPE-EG-45°	1.00	30.36±3.67	-	**PETE-EG-45°**	1.00	18.9±6.49	-
	1.11	21.29±3.1	19.41/1.87		1.16	30.75±4.63	27.43/3.32
	1.16	19±1.81	19.61/0.61		1.26	28.33±4.19	27.78/0.55
	1.23	20±0	19.92/0.08		1.39	22.21±9.33	28.42/6.21
LDPE-EG-60°	1.00	19.67±2.06	-	**PETE-EG-60°**	1.00	16.5±3.67	-
	1.11	17.23±1.92	14.55/2.68		1.16	20.33±2.97	20.73/0.4
	1.16	14.86±1.88	14.56/0.3		1.26	17.86±2.57	21.05/3.2
	1.23	16±1.71	14.57/1.43		1.39	15.45±6.88	21.64/6.19
LDPE-EG-75°	1.00	16±2.17	-	**PETE-EG-75°**	1.00	16.4±2.97	-
	1.11	15.64±2.41	12.2/3.45		1.16	18.33±2.44	17.82/0.51
	1.16	14±2.09	12.29/1.71		1.26	17.5±3.25	18.35/0.85
	1.23	15.64±1.21	12.43/3.21		1.39	20.36±6.64	19.33/1.03
LDPE-EG-90°	1.00	14.4±2.68	-	**PETE-EG-90°**	1.00	14.44±1.21	-
	1.11	14±2.95	11.48/2.52		1.16	16±2.67	17.01/1.01
	1.16	13.5±2.57	11.52/1.98		1.26	15.6±2.95	17.35/1.75
	1.23	12.25±2.54	11.58/0.67		1.39	16.57±5.84	17.99/1.42

Table 25. Continued

Polymer-liquid-Inclined Angle α	Contact Length Ratio σ	Critical Retention Volume (μL)	Predicted Volume / Error (μL)	Polymer-liquid-Inclined Angle α	Contact Length Ratio σ	Critical Retention Volume (μL)	Predicted Volume / Error (μL)
PETE- DI WATER-45°	1.00	72.78±7.12	-	**PETE-EG-45°**	1.00	30.67±6.73	-
	1.11	54.64±5.71	46.75/7.9		1.11	27±0	34.35/7.35
	1.17	41.67±3.89	44.64/2.97		1.17	28.29±3.27	34.12/5.83
	1.25	38.33±5.77	42.08/3.75		1.25	31.5±6.84	33.84/2.34
PETE- DI WATER-60°	1.00	50.67±8.84	-	**PETE-EG-60°**	1.00	29.33±5.48	-
	1.11	35±5.22	35.75/0.75		1.11	24.6±4.12	23.53/1.07
	1.17	30.5±3.09	34.24/3.74		1.17	22±2.95	23.33/1.33
	1.25	27.83±4.3	32.41/4.58		1.25	19.93±3.25	23.08/3.15
PETE- DI WATER-75°	1.00	40.5±8.14	-	**PETE-EG-75°**	1.00	19.92±3.97	-
	1.11	26.5±3.09	29.04/2.54		1.11	20.31±1.97	21.55/1.24
	1.17	25±2.34	27.66/2.66		1.17	15.67±2.67	21.1/5.43
	1.25	22.5±2.71	26/3.5		1.25	16.67±1.56	20.55/3.89
PETE- DI WATER-90°	1.00	39.82±7.24	-	**PETE-EG-90°**	1.00	16.4±1.26	-
	1.11	20±2.95	27.48/7.48		1.11	20.77±3.35	18.9/1.87
	1.17	21.75±6.36	26.52/4.77		1.17	15.67±2.06	18.67/3
	1.25	19±2.34	25.34/6.34		1.25	13.2±1.93	18.39/5.19

6 TEST OF PROPOSED MODEL ON EXTENSIVE SOLIDS

Present study provides methodologies of studies on contact angle, contact angle hysteresis, solids' surface free energy, and liquids' retention. According to research objectives and assumptions, these studies were processed on plastics' surfaces with symmetrically arranged structures. Based on measurement results, some empirical formula and models were proposed and detailed in section 4 and 5. In this section, the author aims to evaluate proposed methodologies by comprehensive experiment results. The main outcome being evaluated would be liquid's retention model on various solids' surfaces.

6.1 Applicability of Proposed Model for Solids with Nanostructures

Listed in section 1.4, one important research assumption is that the effect of surface roughness on study objects is neglected. This assumption was made based on surface roughness measurement results and scales of designed surface structures. Surface roughness undoubtedly has certain effect on contact angle and contact angle hysteresis, and therefore on solids' surface free energy and liquids' retention. [24], [27], [44], [57], [64] Two concepts regarding to surface roughness and structure must be clarified:

- Unless a surface is polished to atomic flat, a surface must have roughness no matter this surface is structured or not.
- Microstructures also carry surface roughness on their surfaces.

Results of surface roughness measurement (Table 2) tell us that average surface roughness R_a ranges in the hundred-nanometer scale. However, scales of designed surface structures range in the hundred-micrometer scale. A-thousand-time difference of both scales allows the author to neglect effect of surface roughness and focus on effect of surface structures only. In addition to structures' scale, this assumption was also based on the dispensed volume of probed liquids. As stated in the section 1.5.1, the volume of dispensed liquid can only reach as smallest as 0.1 µL, which makes the circumference of the droplet far beyond nanometer scale.

This assumption brings a question: can proposed methodologies apply to solids' surfaces with nanoscale surface structures? The answer is no, which could be explained theoretically and experimentally. Here we start to answer theoretically. If the scale of surface structures is in the same range with the scale of surface roughness, both effects (surface structures and surface roughness) would couple with each other. This result doesn't allow us to determine which effect dominates outcomes. Recall the definition of the contact length ratio σ in Equation (36), σ can be modified if the effect of surface roughness is considered as:

$$\sigma' = \frac{(W + W') + 2(L + L')}{(W + W') + G} \tag{58}$$

where W', and L'are R_a (or another roughness parameter) readings from several sampling lengths within each region. If values of W and L are in the same order with values of W' and L', σ' would not necessarily equal to σ. Therefore, it is unable to

isolate the effect of surface structures in this scenario. On the contrary, if the scale of surface structures is obviously larger than the scale of surface roughness, then Equation (58) can be expressed as

$$\sigma' = \frac{(1 + \frac{W'}{W}) + 2(\frac{L}{W} + \frac{L'}{W})}{\left(1 + \frac{W'}{W}\right) + \frac{G}{W}} \tag{59}$$

Consider W'<<W and L'<<W, ratios of W' to W and L' to W can be simplified to zero. Equation (59) can thus be simplified as

$$\sigma' = \frac{(1 + 0) + 2\left(\frac{L}{W} + 0\right)}{(1 + 0) + \frac{G}{W}} = \frac{W + 2L}{W + G} = \sigma \tag{60}$$

which results σ' equals to σ when W'<<W and L'<<W. Therefore, if the scale of surface structures is obviously larger than the scale of surface roughness, then the effect of surface roughness could be neglected. This statement is the foundation of the research assumption.

To explain the negative answer experimentally, the author adopted Anodic Aluminum Oxide (AAO) as the material of the probed solid. Although the material selection is out of scope of polymers, it is a good chance to test proposed methodologies on materials in different categories. AAO was fabricated from high or general-purity aluminum to obtain nano-structured surfaces. The fabrication process undergoes anodization at certain voltage and current density. Commonly used electrolytes in the anodization process include chromic acid (CrO3), sulfuric acid (H2SO4), oxalic acid (C2H2O4), boric acid

(H3BO3), phosphoric acid (H3PO4), and perchloric acid (HClO4). [91] Depending on the electrolyte selection and current/voltage regulation, various sizes of structures in nanoscale and aspect ratios can be reached. AAO's pores display honeycomb-like structure and self-organized in uniform and parallel arrays. [92] AAO has the most popular applications in nanowires and nanotubes with adjustable wire/tube diameter. [93], [94], [95], [96] In the present study, the usage focuses on reverse sides of AAO membranes. This side is also known as barrier layer which has at most 2% thickness of the membrane. [97]Since the barrier layer, shown in Figure 37(a), has convex structures in nanoscale, AAO becomes a good selection for us to evaluate proposed methodologies on surfaces with submicron or nanoscale structures. As shown in Figure 37(b), AAO barrier layer can be controlled to have symmetrically arranged structures.

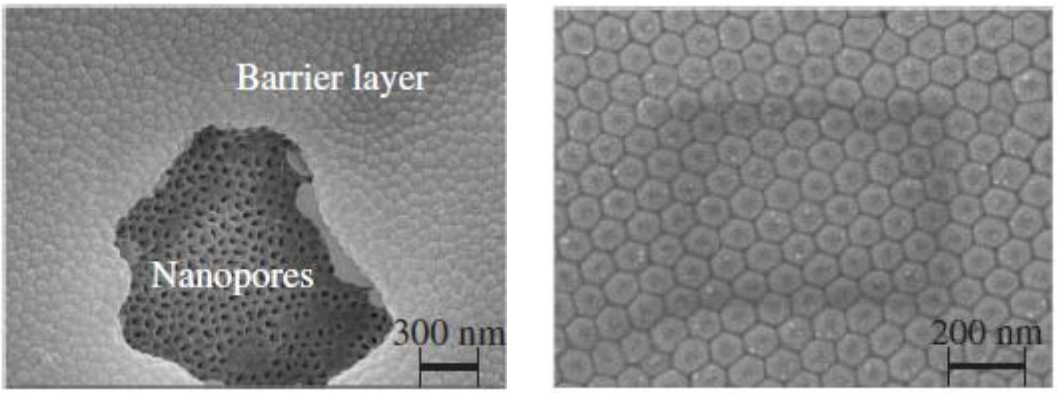

(a) (b)

Figure 37. SEM images of (a) AAO barrier layer and (b) bottom view, which shows AAO barrier layer is composed of hexagonally packed structures. [91]

The DI water's contact angles were measured on polished aluminum surface and AAO barrier layers with various specifications. Results are listed and illustrated in Table 26 and Figure 38. Comparing contact angles obtained from polished aluminum surface with anyone AAO barrier layer, one can see that nanostructures does affect the result. However, within the range in the nano scale (i.e. 70nm and 20nm), the local changing trend cannot maintain the same with the global one. As explained above, this inconsistent result might originate from roughness effect which couples with structure effect within the same scale. Therefore, it is not applicable to apply proposed methodologies for solids with nanostructures.

Table 26. DI water's contact angle on polished aluminum surface and AAO barrier layer.

Sample and structure size	**DI water's contact angle (°)**
Polished aluminum surface	76.75±4.40
AAO I, structure diameter 20nm	65.14±10.44
AAO II, structure diameter 70nm	45.64±13.36
AAO III, structure diameter 200nm	44.64±8.79
AAO IV, structure diameter 300nm	52.30±11.28

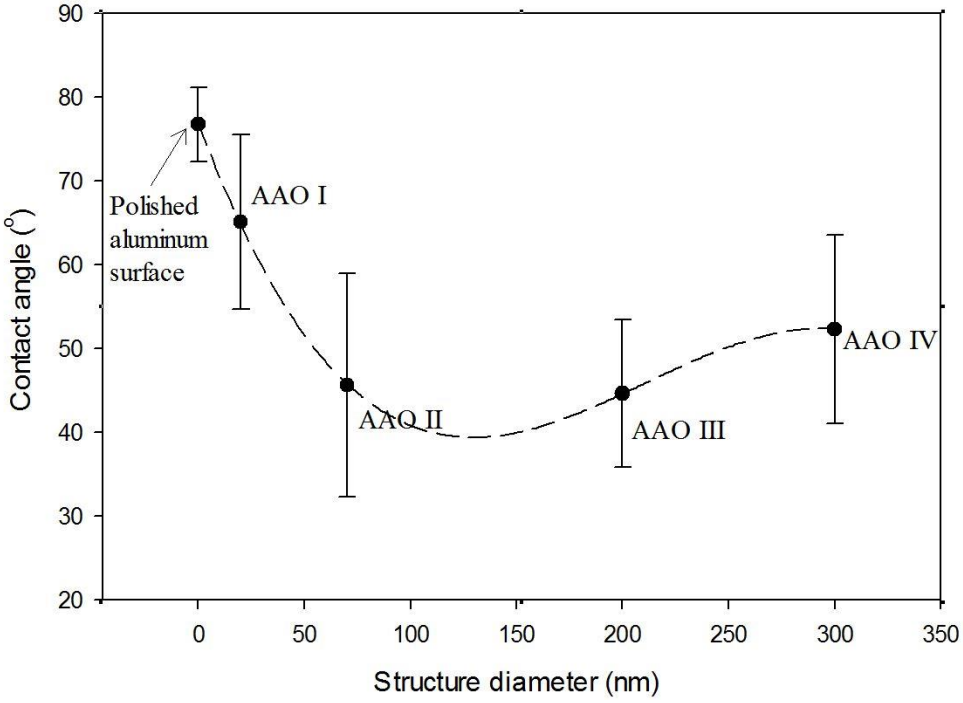

Figure 38. DI water's contact angle on polished aluminum surface and AAO barrier layer. Nanostructures decrease the contact angle, however, roughness effect could alter the changing trend.

6.2 Test of Proposed Model on Various Solids

Liquid retention model is the main outcome of the present study. In this section, the author aims to use solids which were not used in section 5.3.2 for retention model evaluations. Those solids include Polycarbonates (PC), Polyvinyl chloride (PVC), and aluminum (Al). Testing liquids were still de-ionized (DI) water and ethylene glycol (EG). To highlight the most critical scenario, most measurements were undergone at vertical surfaces. (α=90°) It is indicated in Table 25 that θ_A increase as surface inclined angle α increased. This phenomenon was found at both DI water's and EG's θ_A on PC surfaces. This finding is consistent with aforementioned discussion in section 5.3.1. Low

mean square error of proposed model and measured critical retention volume demonstrates the applicability of proposed model on extensive solids.

Reduce hysteresis H is another major topic discussed in section 5.3.1. In this section, the statement of H was examined again by advancing and receding contact angles at critical conditions listed in Table 27. From the listed H data, we found H values of PC-DI water and PC-EG combinations in average are 0.433±0.01 and 0.433±0.02, respectively. It was found that the proposed statement of H remains effective no matter contacting liquids and surface structures.

It is surprised to see the proposed model is also applicable to aluminum surfaces. This result could be explained by approximate wettability of aluminum and some plastic surfaces (ex: Al and PP have close CA of DI water and EG). Consider tests of proposed model by using extensive solids mentioned above, we can imply that the proposed model is applicable for most polymers and other solids which have similar wetting behavior with polymers.

Table 27. Various solid-liquid combinations for proposed methodology evaluations.

Solid-liquid combination **Surface inclined angle α (°)**	**σ**	**Advancing contact angle θ_A (°)**	**Receding contact angle θ_R (°)**	**Reduce hysteresis H**	**Measured critical retention volume V_C (µL)**	**Estimated critical retention volume V_C (µL)**
PC-DI water-60°	1	82.58±4.06	46.91±5.68	0.432	27.75±5.50	30.04
PC-DI water-60°	1.09	96.12±6.18	54.38±5.97	0.434	25.94±3.37	26.50
PC-DI water-60°	1.14	99.47±8.79	55.01±6.24	0.447	25.15±4.16	25.87
PC-DI water-90°	1	86.84±3.44	50.19±4.18	0.422	20.63±1.77	23.15
PC-DI water-90°	1.09	105.27±4.62	61.49±5.74	0.416	18.30±1.92	19.34
PC-DI water-90°	1.14	113.95±5.63	62.84±7.31	0.449	17.43±2.06	18.15
PC-EG-60°	1	64.33±4.56	35.19±4.97	0.453	16.33±1.20	12.71
PC- EG -60°	1.09	77.91±7.94	44.25±5.87	0.432	14.67±2.82	11.05
PC- EG -60°	1.14	84.09±9.73	46.39±5.79	0.448	13.56±1.97	10.51
PC- EG -90°	1	71.53±6.47	41.02±3.85	0.427	10.34±2.11	9.44
PC- EG -90°	1.09	80.01±6.87	45.61±5.98	0.430	10.57±1.29	8.72
PC- EG -90°	1.14	83.12±7.54	49.27±6.14	0.407	8.29±1.42	8.37
PVC- DI water-90°	1	82.81±2.68	30.48±1.91	0.632	34.14±2.85	33.39
PVC- EG-90°	1	63.38±5.38	23.83±2.40	0.624	10.89±1.76	7.57
Al-DI water-90°	1	81.14±5.89	37.28±3.95	0.541	22.36±6.05	27.74
Al-EG-90°	1	63.64±4.92	26.85±2.31	0.578	9.67±1.97	11.49

7 CONCLUSIONS AND FUTURE DIRECTIONS

7.1 Conclusion

The present research was studied in two stages. The first stage was carried out on horizontal surfaces. Three probed liquids, including DI water, EG, α-BN were selected to study their contact angles on five commonly used plastics. Those plastics include PET, PP, HDPE, LDPE, and PVC. Pillar-like structures with various aspect ratios were fabricated on those plastics' surfaces. Based on contact angle results, plastics' surface free energy and their interfacial tensions with contacting liquids were characterized. A change in liquid droplets' three-phase contact line due to surface structures has been proposed in literatures. In this article, contact length ratio σ, was used as a parameter corresponding to a specific dimension of the pillar-like structure. The effects of pillar-like structures on liquids' contact angles and plastics' surface free energy were studied. Major achievements in the first stage include:

- It was found that pillar-like structure, represented by contact length ratio σ, has linear effect on liquids' contact angles in the range of σ=1.0 to 1.96.
- Linear regression models are hence proposed to predict liquids' contact angles, and accuracies are confirmed by less than 6% error for most plastic-liquid combinations.

- It was found that the polarity of plastics' surfaces could be altered by surface structures. For examples, with structures on their surfaces, PE' polarity tends to become bipolar while PET's and PP's tend to become monopolar.

- Surface free energy of structured plastics can be estimated by predicted contact angles. The outcomes were validated by study of plastic-liquid interfacial tensions.

The second stage of the present research was carried out on inclined surfaces. This part is the extending research from stage one. DI water's and EG's contact angle hysteresis and critical retention volumes on five commonly used plastics with square frustum-like structures were studied. The chevron-like groove structures, which are orthogonally arranged, make the liquid-solid contact line elongated while the droplet found staying in the Wenzel state. The effects of surface structure on liquids' contact angle hysteresis and critical retention volumes were studied. Major achievements in the second stage include:

- Reduced hysteresis H, which links between advancing and receding contact angles, was also studied and found to extend its availability on structured and/or inclined surfaces.

- The research found that surface structures, represented by σ, have linear effects on advancing contact angles in the range of σ=1.0 to 1.42 for all plastic-liquid combinations.

- Predictions of advancing contact angles were progressed by the linear regression model. Low errors found in most data points confirm the accuracy of the prediction.

- An empirical model which adopts liquid-solid interfacial tension as the source of liquids' retention force was proposed to estimate liquids' critical retention volumes on inclined surfaces. The proposed model found low mean squared error with existing experiment data which demonstrates its superiority over previous ones.

- Predicted advancing contact angles, as an input variable, was applied into the proposed liquids' retention model to predict critical retention volumes. Compared with experiment data, low errors of predicted results proved the correctness of the proposed model.

The comprehensive results provide the industry a chance to efficiently control wettability and liquids' storage and repellency of commonly used plastics by fabricating surface structures.

7.2 Future Work

The potential works could be explored to get the full insight from the present study.

- The symmetrically arranged structure allows the proposed methodologies to have extensive applicability for liquids dispensing from various directions. The

present study only focused on pillar-like and square frustum-like structures. Although those structures are symmetrically arranged, there are still many structure shapes within this category. For example: cylindrical or hexagonal. Therefore, surface structures can be extended to other shapes. Since the type of shape corner is believed to affect wettability, the comparison of effects due to various shapes becomes a potential research direction. For a special need, the asymmetrically arranged structure, for example: 1-D groove, is another choice of structure shape.

- Proposed methodologies were studied on commonly used plastic surfaces. To examine the extensive applicability, it is recommended to include metals and ceramics as probed solids. Most polymers have moderate polar surface free energy and therefore have moderate interfacial tension with contacting liquids. However, this may or may not be the same case with metals and ceramics.

- The present study only considers the liquids' retention. The future work can extend the research to liquids' sliding. Although this topic has been investigated by many previous studies, the research processed on structured surfaces are rarely seen. Therefore, it could be another future direction.

- Proposed liquids' retention model is based on assumption of the circular drop shape. However, it is also found the droplet displaying other shapes. Therefore, the numerical method or finite element would be a practical approach which can estimate the drop shape closely to the fact.

REFERENCES

1. Eral, H. and J. Oh, *Contact angle hysteresis: a review of fundamentals and applications.* Colloid and Polymer Science, 2013. **291**(2): p. 247-260.
2. Ahmed, G., et al., *Modeling the effects of contact angle hysteresis on the sliding of droplets down inclined surfaces.* European Journal of Mechanics - B/Fluids, 2014. **48**: p. 218-230.
3. Callister, W.D., *Materials science and engineering: An introduction*. 2007: John Wiley & Sons.
4. Hayat, M.A., *Principles and techniques of scanning electron microscopy. Biological applications. Volume 1*. 1974: Van Nostrand Reinhold Company.
5. Bigelow, W.C., D.L. Pickett, and W.A. Zisman, *Oleophobic monolayers: I. Films adsorbed from solution in non-polar liquids.* Journal of Colloid Science, 1946. **1**(6): p. 513-538.
6. Young, T., *An essay on the cohesion of fluids.* Philosophical Transactions of the Royal Society of London, 1805. **95**: p. 65-87.
7. Van Oss, C.J., M.K. Chaudhury, and R.J. Good, *Interfacial Lifshitz-van der Waals and polar interactions in macroscopic systems.* Chemical Reviews, 1988. **88**(6): p. 927-941.
8. Van Oss, C.J., R.J. Good, and M.K. Chaudhury, *Additive and nonadditive surface tension components and the interpretation of contact angles.* Langmuir, 1988. **4**(4): p. 884-891.

9. Neumann, A.W., et al., *An equation-of-state approach to determine surface tensions of low-energy solids from contact angles.* Journal of Colloid and Interface Science, 1974. **49**(2): p. 291-304.

10. Fowkes, F.M., *Attractive forces at interfaces.* Industrial & Engineering Chemistry, 1964. **56**(12): p. 40-52.

11. Owens, D.K. and R. Wendt, *Estimation of the surface free energy of polymers.* Journal of Applied Polymer Science, 1969. **13**(8): p. 1741-1747.

12. Wu, S. *Calculation of interfacial tension in polymer systems*. in *Journal of Polymer Science Part C: Polymer Symposia*. 1971. Wiley Online Library.

13. Wu, S., *Polymer Interface and Adhesion*. 1982: Taylor & Francis.

14. Overbeek, J.T.G. and M.J. Sparnaay, *Experiments on long-range attractive forces between macroscopic objects.* Journal of Colloid Science, 1952. **7**(3): p. 343-345.

15. Fowkes, F.M., in *Physicochemical aspects of polymer surfaces*, K.L. Mittal, Editor. 1983, Plenum: New York. p. 583.

16. Lifshitz, E.M., *The theory of molecular attractive forces between solids.* Soviet Physics, 1955. **2**(1): p. 73-83.

17. Van Oss, C.J., R.J. Good, and M.K. Chaudhury, *Determination off the hydrophobia interaction energy-application to separation processes.* Separation Science and Technology, 1987. **22**(1): p. 1-24.

18. Ohki, S., *Molecular mechanisms of membrane fusion*. 1988, Plenum Press.

19. Van Oss, C.J., M.K. Chaudhury, and R.J. Good, *Monopolar surfaces.* Advances in Colloid and Interface Science, 1987. **28**(0): p. 35-64.

20. Good, R.J. and L.A. Girifalco, *A theory for estimation of surface and interfacial energies. III. Estimation of surface energies of solids from contact angle data.* The Journal of Physical Chemistry, 1960. **64**(5): p. 561-565.

21. Eral, H.B., D.J.C.M. 't Mannetje, and J.M. Oh, *Contact angle hysteresis: A review of fundamentals and applications.* Colloid and Polymer Science, 2013. **291**(2): p. 247-260.

22. Yuan, Y. and T.R. Lee, *Contact angle and wetting properties*, in *Surface Science Techniques*, G. Bracco and B. Holst, Editors. 2013, Springer Berlin Heidelberg. p. 3-34.

23. Johnson, R.E. and R.H. Dettre, *Contact angle hysteresis. III. Study of an idealized heterogeneous surface.* The Journal of Physical Chemistry, 1964. **68**(7): p. 1744-1750.

24. Dettre, R.H. and R.E. Johnson, *Contact angle hysteresis. IV. Contact angle measurements on heterogeneous surfaces.* The Journal of Physical Chemistry, 1965. **69**(5): p. 1507-1515.

25. Extrand, C.W. and Y. Kumagai, *An experimental study of contact angle hysteresis.* Journal of Colloid and Interface Science, 1997. **191**(2): p. 378-383.

26. McHale, G., N.J. Shirtcliffe, and M.I. Newton, *Contact angle hysteresis on super-hydrophobic surfaces.* Langmuir, 2004. **20**(23): p. 10146-10149.

27. Wenzel, R.N., R*esistance of solid surfaces to wetting by water.* Industrial & Engineering Chemistry, 1936. **28**(8): p. 988-994.

28. Cassie, A.B.D. and S. Baxter, *Wettability of porous surfaces.* Transactions of the Faraday Society, 1944. **40**(0): p. 546-551.

29. David, Q., L. Aurélie, and B. José, *Slippy and sticky microtextured solids.* Nanotechnology, 2003. **14**(10): p. 1109.

30. Gao, L. and T.J. McCarthy, *Contact angle hysteresis explained.* Langmuir, 2006. **22**(14): p. 6234-6237.

31. Chiou, C.-H. and S.-J. Hsieh, *Empirical study and prediction of contact angle and surface free energy of commonly used plastics with pillar-like structure.* Surface and Interface Analysis, 2015. **47**(1): p. 45-55.

32. Milionis, A., et al., *Control of the water adhesion on hydrophobic micropillars by spray coating technique.* Colloid and Polymer Science, 2013. **291**(2): p. 401-407.

33. Marmur, A., *The Lotus Effect: Superhydrophobicity and metastability.* Langmuir, 2004. **20**(9): p. 3517-3519.

34. Extrand, C.W., *Designing for optimum liquid repellency.* Langmuir, 2006. **22**(4): p. 1711-1714.

35. Bouteau, M., et al., *Sliding behavior of liquid droplets on tilted Langmuir–Blodgett surfaces.* Journal of Colloid and Interface Science, 2008. **317**(1): p. 247-254.

36. Kim, H.-Y., H.J. Lee, and B.H. Kang, *Sliding of liquid drops down an inclined solid surface.* Journal of Colloid and Interface Science, 2002. **247**(2): p. 372-380.

37. Sakai, M., et al., *Relationship between sliding acceleration of water droplets and dynamic contact angles on hydrophobic surfaces.* Surface Science, 2006. **600**(16): p. L204-L208.

38. Dussan V., E.B., *On the ability of drops or bubbles to stick to non-horizontal surfaces of solids. Part 2. Small drops or bubbles having contact angles of arbitrary size.* Journal of Fluid Mechanics, 1985. **151**: p. 1-20.

39. Extrand, C.W. and A.N. Gent, *Retention of liquid drops by solid surfaces.* Journal of Colloid and Interface Science, 1990. **138**(2): p. 431-442.

40. ElSherbini, A.I. and A.M. Jacobi, *Retention forces and contact angles for critical liquid drops on non-horizontal surfaces.* Journal of Colloid and Interface Science, 2006. **299**(2): p. 841-849.

41. Dettre Robert, H. and E. Johnson Rulon, *Contact angle hysteresis*, in *Contact angle, wettability, and adhesion*. 1964, American Chemical Society. p. 136-144.

42. Patankar, N.A., *Transition between superhydrophobic states on rough surfaces.* Langmuir, 2004. **20**(17): p. 7097-7102.

43. Marmur, A., *Wetting on hydrophobic rough surfaces: To be heterogeneous or not to be?* Langmuir, 2003. **19**(20): p. 8343-8348.

44. Patankar, N.A., *Mimicking the lotus effect: Influence of double roughness structures and slender pillars.* Langmuir, 2004. **20**(19): p. 8209-8213.

45. Nakajima, A., *Design of hydrophobic surfaces for liquid droplet control.* NPG Asia Mater, 2011. **3**: p. 49-56.

46. Gao, L. and T.J. McCarthy, *How wenzel and cassie were wrong.* Langmuir, 2007. **23**(7): p. 3762-3765.

47. Bartell, F.E. and J.W. Shepard, *Surface roughness as related to hysteresis of contact angles. II. The systems paraffin–3 molar calcium chloride solution–air and paraffin–glycerol–air.* The Journal of Physical Chemistry, 1953. **57**(4): p. 455-458.

48. Extrand, C.W., *Contact angles and hysteresis on surfaces with chemically heterogeneous islands.* Langmuir, 2003. **19**(9): p. 3793-3796.

49. Sasaki, M., et al., *Processing and properties of transparent super-hydrophobic polymer film with low surface electric resistance.* Journal of Materials Science, 2004. **39**(11): p. 3717-3722.

50. Yoshimitsu, Z., et al., *Effects of surface structure on the hydrophobicity and sliding behavior of water droplets.* Langmuir, 2002. **18**(15): p. 5818-5822.

51. Promraksa, A. and Chen, L-J., *Modeling contact angle hysteresis of a liquid droplet sitting on a cosine wave-like pattern surface.* Journal of Colloid and Interface Science, 2012. **384**(1): p. 172-181.

52. Zhu, L., et al., *Tuning wettability and getting superhydrophobic surface by controlling surface roughness with well-designed microstructures.* Sensors and Actuators A: Physical, 2006. **130–131**(0): p. 595-600.

53. Kang, C., et al., *Superhydrophilicity/superhydrophobicity of nickel micro-arrays fabricated by electroless deposition on an etched porous aluminum template.* Chemical Engineering Journal, 2012. **203**(0): p. 1-8.

54. Akovali, G., et al., *Mechanical properties and surface energies of low density polyethylene-poly(vinyl chloride) blends.* Polymer, 1998. **39**(6–7): p. 1363-1368.

55. Kim, J.S., R.H. Friend, and F. Cacialli, *Surface energy and polarity of treated indium–tin–oxide anodes for polymer light-emitting diodes studied by contact-angle measurements.* Journal of Applied Physics, 1999. **86**(5): p. 2774-2778.

56. McHale, G., *Cassie and Wenzel: Were they really so wrong?* Langmuir, 2007. **23**(15): p. 8200-8205.

57. Choi, W., et al., *A modified Cassie–Baxter relationship to explain contact angle hysteresis and anisotropy on non-wetting textured surfaces.* Journal of Colloid and Interface Science, 2009. **339**(1): p. 208-216.

58. Extrand, C.W. and Y. Kumagai, *Liquid drops on an inclined plane: The relation between contact angles, drop shape, and retentive force.* Journal of Colloid and Interface Science, 1995. **170**(2): p. 515-521.

59. ElSherbini, A. and A. Jacobi, *Retention forces and contact angles for critical liquid drops on non-horizontal surfaces.* Journal of Colloid and Interface Science, 2006. **299**(2): p. 841-849.

60. Ahmed, G., et al., *Modeling the effects of contact angle hysteresis on the sliding of droplets down inclined surfaces.* European Journal of Mechanics - B/Fluids, 2014. **48**(0): p. 218-230.

61. Hirvi, J.T. and T.A. Pakkanen, *Nanodroplet impact and sliding on structured polymer surfaces.* Surface Science, 2008. **602**(10): p. 1810-1818.

62. Yeh, K.-Y., Chen, L.-J., and Chang, J.-Y., *Contact angle hysteresis on regular pillar-like hydrophobic surfaces.* Langmuir, 2008. **24**(1): p. 245-251.

63. Xiu, Y., et al., *Relationship between work of adhesion and contact angle hysteresis on superhydrophobic surfaces.* The Journal of Physical Chemistry C, 2008. **112**(30): p. 11403-11407.

64. Marmur, A. and E. Bittoun, *When Wenzel and Cassie are right: Reconciling local and global considerations.* Langmuir, 2009. **25**(3): p. 1277-1281.

65. Chiou, C.-H. and S.-J. Hsieh, *Empirical study and prediction of liquids retention on structured polymer surfaces.* Surface and Interface Analysis, 2016. **48**(3): p. 146-163.

66. Kusumaatmaja, H. and J. Yeomans, *Modeling contact angle hysteresis on chemically patterned and superhydrophobic surfaces.* Langmuir, 2007. **23**(11): p. 6019-6032.

67. Ruiz-Cabello, F.J.M., M.A. Rodríguez-Valverde, and M.A. Cabrerizo-Vílchez, *Equilibrium contact angle or the most-stable contact angle?* Advances in Colloid and Interface Science, 2014. **206**(0): p. 320-327.

68. W. A, Z., *Relation of the equilibrium contact angle to liquid and solid constitution*, in *Contact angle, wettability, and adhesion*. 1964, American Chemical Society. p. 1-51.

69. Rulison, C., *So you want to measure surface energy.* Charlotte NC (cf. p. 99), 1999.

70. Kwok, D.Y. and A.W. Neumann, *Contact angle measurement and contact angle interpretation.* Advances in Colloid and Interface Science, 1999. **81**(3): p. 167-249.

71. Owens, D.K. and R.C. Wendt, *Estimation of the surface free energy of polymers.* Journal of Applied Polymer Science, 1969. **13**(8): p. 1741-1747.

72. Wu, S., *Calculation of interfacial tension in polymer systems.* Journal of Polymer Science Part C: Polymer Symposia, 1971. **34**(1): p. 19-30.

73. Wu, S., *Polar and nonpolar interactions in adhesion.* The Journal of Adhesion, 1973. **5**(1): p. 39-55.

74. Hejda, F., P. Solar, and J. Kousal. *Surface free energy determination by contact angle measurements – A comparison of various approaches*. in *WDS*. 2010.

75. Siboni, S., et al., *The solid surface free energy calculation: II. The limits of the Zisman and of the "equation-of-state" approaches.* Journal of colloid and interface science, 2004. **271**(2): p. 454-472.

76. Douillard, J.M. and V. Médout-Marère, *A new interpretation of contact angle variations in view of a recent analysis of immersion calorimetry*. Journal of Colloid and Interface Science, 2000. **223**(2): p. 255-260.

77. Żenkiewicz, M., *Comparative study on the surface free energy of a solid calculated by different methods.* Polymer Testing, 2007. **26**(1): p. 14-19.

78. Della Volpe, C., et al., *The solid surface free energy calculation: I. In defense of the multicomponent approach.* Journal of Colloid and Interface Science, 2004. **271**(2): p. 434-453.

79. Furuta, T., et al., *Wetting mode transition of nanoliter scale water droplets during evaporation on superhydrophobic surfaces with random roughness structure.* Applied Surface Science, 2012. **258**(7): p. 2378-2383.

80. Wang, S., et al., *Fabrication of superhydrophobic wood surface by a sol–gel process.* Applied Surface Science, 2011. **258**(2): p. 806-810.

81. Feng, X., J. Zhai, and L. Jiang, *The fabrication and switchable superhydrophobicity of TiO_2 nanorod films.* Angewandte Chemie International Edition, 2005. **44**(32): p. 5115-5118.

82. Zhang, J. and Y. Han, *Shape-gradient composite surfaces: Water droplets move uphill.* Langmuir, 2007. **23**(11): p. 6136-6141.

83. Wolansky, G. and A. Marmur, *Apparent contact angles on rough surfaces: The Wenzel equation revisited.* Colloids and Surfaces A: Physicochemical and Engineering Aspects, 1999. **156**(1–3): p. 381-388.

84. Boreyko, J.B. and C.P. Collier, *Dewetting transitions on superhydrophobic surfaces: When are Wenzel drops reversible?* The Journal of Physical Chemistry C, 2013. **117**(35): p. 18084-18090.

85. Lafuma, A. and D. Quéré, *Superhydrophobic states.* Nature Materials, 2003. **2**(7): p. 457-460.

86. Afferrante, L. and G. Carbone, *Microstructured superhydrorepellent surfaces: effect of drop pressure on fakir-state stability and apparent contact angles.* Journal of Physics: Condensed Matter, 2010. **22**(32): p. 325107.

87. Narhe, R. and D. Beysens, *Nucleation and growth on a superhydrophobic grooved surface.* Physical Review Letters, 2004. **93**(7): p. 076103.

88. Wier, K.A. and T.J. McCarthy, *Condensation on ultrahydrophobic surfaces and its effect on droplet mobility: Ultrahydrophobic surfaces are not always water repellant.* Langmuir, 2006. **22**(6): p. 2433-2436.

89. Pierce, E., F. Carmona, and A. Amirfazli, *Understanding of sliding and contact angle results in tilted plate experiments.* Colloids and Surfaces A: Physicochemical and Engineering Aspects, 2008. **323**(1): p. 73-82.

90. McDonald, J.H., *Handbook of biological statistics*. Vol. 2. 2009: Sparky House Publishing Baltimore, MD.

91. Chien Chon, C., C. Jung Husan, and C. Chuen Guang, *Post-treatment method of producing ordered array of anodic aluminum oxide using general purity commercial (99.7%) aluminum.* Japanese Journal of Applied Physics, 2005. **44**(3R): p. 1529.

92. Md Jani, A.M., D. Losic, and N.H. Voelcker, *Nanoporous anodic aluminium oxide: Advances in surface engineering and emerging applications.* Progress in Materials Science, 2013. **58**(5): p. 636-704.

93. Chen, S.H., C.C. Chen, and C.G. Chao, *Novel morphology and solidification behavior of eutectic bismuth–tin (Bi–Sn) nanowires.* Journal of Alloys and Compounds, 2009. **481**(1–2): p. 270-273.

94. Chen, S.-H., et al., *Fabrication and characterization of eutectic bismuth–tin (Bi–Sn) nanowires.* Materials Letters, 2009. **63**(13–14): p. 1165-1168.

95. Chen, S.-H., et al., *Fabrication of pure aluminum nanowires by using injection molding process in ambient air.* Materials Letters, 2015. **148**: p. 30-33.

96. Chen, S.-H., et al., *Fabrication of bismuth oxide–tin oxide nanowires by direct thermal oxidation of Bi–Sn eutectic nanowires.* Materials Letters, 2010. **64**(22): p. 2502-2504.

97. Tajima, S., *Anodic oxidation of aluminum*, in *Advances in corrosion science and technology*. 1970, Springer. p. 229-362.